Fast responders: uncovering immediate early splicing events following lymphocyte activation

Inaugural-Dissertation

to obtain the academic degree

Doctor rerum naturalium (Dr. rer. nat.)

submitted to the Department of Biology, Chemistry, Pharmacy

of Freie Universität Berlin

by

Mateusz Dróżdż

Berlin, 2024

DECLARATION

This work was carried out in the period between September 2020 and September 2024 under the supervision of Prof. Dr. Florian Heyd at the Institute of Chemistry and Biochemistry, Freie Universität Berlin, Germany.

First reviewer: Prof. Dr. Florian Heyd

RNA Biochemistry

Institute for Chemistry and Biochemistry

Freie Universität Berlin

Takustraße 6

14195 Berlin, Germany

Second reviewer: Prof. Dr. Markus Wahl

Structural Biochemistry

Institute for Chemistry and Biochemistry

Freie Universität Berlin

Takustraße 6

14195 Berlin, Germany

Date of defense: 25.11.2024

Acknowledgements:

First and foremost, I would like to thank Prof. Florian Heyd for giving me the opportunity to work on this exciting project, and for trusting that a microbiologist could become an RNA biochemist.

I thank the members of my thesis advisor committee for their time, effort and thoughtful advice. Prof. Markus Wahl, I want to thank additionally for reviewing this thesis and joining my defense committee.

I would like to thank Dr. Marco Preußner, Dr. Bruna Los and Luiza Zuvanov for their support on many levels of this project. The RNA sequencing presented in this work was only possible with their help and experience. Apart from that I also thank for all their advice and friendship.

Gopika Sasikumar, I thank for all her help on the hnRNPC side of the project. I am grateful for her hard work and support in every stage of this journey. It was great fun working with her.

I would also like to thank all current and former members of the Prof. Florian Heyd's group for their friendship and support. Especially, I would like to thank Mary and Silvia for believing in me, giving me motivation and enthusiasm to work. I would also like to express my gratitude to Tom for maintaining a great atmosphere in the lab, especially in the evenings when we can enjoy a beer together, my roommate Felix for giving me food when there was no time to cook, and Ann-Katrin, Ioana and Stefan for answering all my scientific questions during my PhD life.

I also want to thank Antje and Bobby for preparing all required reagents, always being ready to help and suggest ideas for me to be more efficient while working in the lab.

This list would not be complete without expressing my gratitude to my dear friend Sebastian Makuch for his support and friendship since our school day. It wouldn't have been done without his help.

Furthermore, I would like to thank my parents and my sister Kornelia for their unconditional love and support, understanding that I am not always available for their life.

Last but not least, I would like to thank my amazing wife, Aleksandra, for her incredible understanding of my current priorities and her love and support in every stage of my life, both scientific and private.

Declaration of Independence

Herewith I certify that I have prepared and written my thesis independently and that I have not used any sources and aids other than those indicated by me. The thesis in the same or similar form has not been submitted to any examination body.

ABSTRACT

Lymphocytes require a certain time frame (24-48 hours) after their activation to fully develop effector functions. Hence, most studies have focused on characterizing splicing switches after this period. However, shortly after lymphocyte activation (0h to 4 hours), rapid gene expression changes occur, resulting in cytokines production and their secretion, as well as the initiation of cell proliferation, and differentiation. The expression of immediate early genes (IEG) is transiently induced upon T cell activation, with regulation being independent of *de novo* protein synthesis. This process relies on phosphorylation cascades that target the transcription machinery. In this project, we hypothesized that similar signaling cascades might also target the splicing machinery to induce immediate early splicing (IES). We aimed to delineate this concept and characterize its function in T cell and B cell activation. Furthermore, we investigated whether IES switches influence the translational machinery or whether they operate independently of this process. Through *in silico* bioinformatic analysis and biochemical wet lab experiments, we identified the rapid and transient retention of short introns among several genes within the first 1.5 hours of lymphocyte activation. This concerted splicing switch is independent of *de novo* protein synthesis. Further analysis showed its specific regulation by RAF/MEK/ERK1/2-mediated phosphorylation of the splicing factor - hnRNPC2. This hnRNPC isoform originates from an alternative 5' splice site (A5SS) usage and contains 13 additional amino acids compared to hnRNPC1. Moreover, the T cell specificity of IES is preserved by the involvement of the kinase PKCθ, which is highly expressed in T cells. This is not the case in B cells, suggesting the involvement of another kinase in the hnRNPC2-controlled IES switch. IES affects many components of the translation apparatus, including transcripts encoding ribosomal proteins and translation factors, such as eukaryotic initiation factor eIF5A. Furthermore, we observed an hnRNPC2-dependent reduction in *de novo* translation during the hours immediately following T cell activation. We suggested that this reduction is mediated by the IES switch, as inducing the IES protein variant in eIF5A alone is sufficient to reduce translation globally. Altogether, we present a new paradigm for fast and transient alternative splicing regulation and suggest a fundamental role of IES in coordinating different layers of gene expression upon T cell activation.

ZUSAMMENFASSUNG

Lymphozyten benötigen nach ihrer Aktivierung einen bestimmten Zeitraum (24–48 Stunden), um ihre Effektorfunktionen vollständig zu entwickeln. Daher haben sich die meisten Studien darauf konzentriert, Spleißschalter nach diesem Zeitraum zu charakterisieren. Kurz nach der Aktivierung von Lymphozyten (0 bis 4 Stunden) treten jedoch rasche Genexpressionsänderungen auf, die zur Produktion und Sekretion von Zytokinen sowie zur Initiierung der Zellproliferation und -differenzierung führen. Die Expression von Immediate Early Genes (IEG) wird bei der T-Zell-Aktivierung vorübergehend induziert, wobei die Regulation unabhängig von der de novo-Proteinsynthese erfolgt. Dieser Prozess beruht auf Phosphorylierungskaskaden, die auf den Transkriptionsapparat abzielen. In diesem Projekt haben wir die Hypothese aufgestellt, dass ähnliche Signalkaskaden auch den Spleißapparat anvisieren könnten, um ein Immediate Early Splicing (IES) zu induzieren. Wir hatten uns zum Ziel gesetzt, dieses Konzept zu definieren und seine Funktion bei der Aktivierung von T- und B-Zellen zu charakterisieren. Darüber hinaus untersuchten wir, ob IES-Schalter die Translationsmaschinerie beeinflussen oder unabhängig von diesem Prozess arbeiten. Durch in silico bioinformatische Analysen und biochemische Experimente im Nasslabor identifizierten wir die rasche und vorübergehende Retention von kurzen Introns in mehreren Genen innerhalb der ersten 1,5 Stunden nach Lymphozytenaktivierung. Dieser konzertierte Spleißschalter ist unabhängig von der de novo-Proteinsynthese. Weitere Analysen zeigten, dass er spezifisch durch die Phosphorylierung des Spleißfaktors hnRNPC2 durch RAF/MEK/ERK1/2 reguliert wird. Dieses hnRNPC-Isoform entsteht durch die Nutzung einer alternativen 5‘-Spleißstelle (A5SS) und enthält im Vergleich zu hnRNPC1 13 zusätzliche Aminosäuren. Darüber hinaus wird die T-Zell-Spezifität von IES durch die Beteiligung der Kinase PKCθ aufrechterhalten, die in T-Zellen hoch exprimiert wird. Dies ist bei B-Zellen nicht der Fall, was auf die Beteiligung einer anderen Kinase im hnRNPC2-gesteuerten IES-Schalter bei B-Zellen hindeutet. IES beeinflusst viele Komponenten des Translationsapparats, einschließlich Transkripten, die ribosomale Proteine und Translationsfaktoren wie den eukaryotischen Initiationsfaktor eIF5A kodieren. Darüber hinaus beobachteten wir eine hnRNPC2-abhängige Reduktion der de novo-Translation in den Stunden unmittelbar nach der T-Zell-Aktivierung. Wir vermuten, dass diese Reduktion durch den IES-Schalter vermittelt wird, da die Induktion der IES-Proteinform von eIF5A allein ausreicht, um die Translation global zu reduzieren. Insgesamt stellen wir ein neues Paradigma für die schnelle und vorübergehende

Regulation des alternativen Spleißens vor und schlagen eine grundlegende Rolle von IES bei der Koordination verschiedener Ebenen der Genexpression während der T-Zell-Aktivierung vor.

Contents

1. Introduction

1.1. From DNA to proteins: central dogma of molecular biology

Since the discovery of the deoxyribonucleic acid (DNA) structure in 1953 as the central unit of genetic information, our understanding of cell biology has progressed tremendously. We now know the complete genome sequences for thousands of different organisms, revealing fascinating insights into their biochemistry [1]. Throughout more than 70 years, scientists have refined modern technologies to unlock secrets of cellular functionalities and structures. This development is crucial to investigate targeted treatments and therapies.

The genetic information of cells is stored in the form of double-stranded DNA molecules - long, unbranched, paired polymer chains consisting of nucleotide monomers. These nucleotides consist of a deoxyribose sugar, a phosphate group, and one of four nucleotide bases (adenine - A, thymine - T, cytosine - C, and guanine - G). DNA harbors its information to guide the synthesis of another class of polymers: ribonucleic acid (RNA). This process starts with a templated synthesis of RNA called transcription, in which segments of DNA sequences serve as templates for building molecules of RNA. The RNA molecules that ultimately direct the synthesis of proteins are called messenger RNA (mRNA). Their composition is remarkably similar to DNA, with ribose sugar instead of deoxyribose and uracil - U instead of thymine. Later, many of these RNA molecules are exported to the cytoplasm, where they direct the synthesis of proteins through a process called translation (Fig. 1). Therefore, mRNA acts as an intermediate between DNA and protein. The flow of genetic information thus follows the order: DNA→ mRNA→ protein. This fundamental principle is called the central dogma of molecular biology [2,3]. It is worth mentioning that RNA can indeed produce DNA through reverse transcription. In this process, RNA is used as a template to generate complementary DNA (cDNA), catalyzed by an enzyme known as reverse transcriptase. The newly synthesized DNA can then integrate into the genome and replicate alongside it. This mechanism is primarily observed in viruses (e.g., human immunodeficiency virus – HIV) and in retrotransposons, which are elements that can „copy “ and „paste“ to new locations within the genome[4].

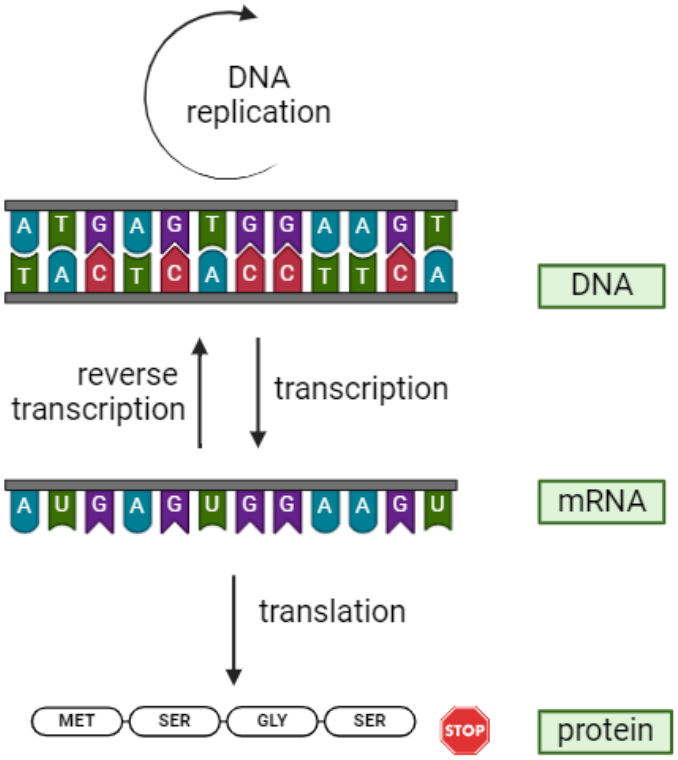

Figure 1. Central dogma of molecular biology in eukaryotic cells. The scheme illustrates the flow of genetic information from DNA to mRNA (transcription) and from mRNA to protein (translation). RNA can also be converted back to DNA is reverse transcription – adapted from [3–5]. Created using BioRender.com

1.2. Processing of pre-mRNA

Transcription is the first step to produce a mature mRNA molecule. During its elongation phase, the nascent RNA undergoes three types of processing events: a modified guanine nucleotide (7-methylguanosine (m7G)) is added to its 5' end (capping), intron sequences are removed from the RNA molecules (splicing), and a poly-A tail is incorporated into the 3' end of the RNA (cleavage and polyadenylation) (Fig. 2). Each of these processes is facilitated by proteins that bind to the long C-terminal tail of RNA polymerase II. Both 5' capping and 3' polyadenylation are required to enhance mRNA stability and ensure efficient translation. Only properly processed mRNAs are transported through nuclear pore complexes (NPC) into the cytoplasm, where they are translated into proteins[6].

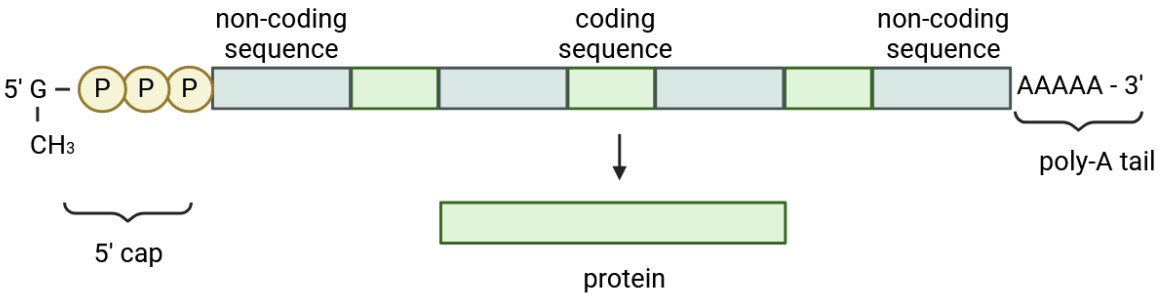

Figure 2. A schematic illustration of pre-mRNA processing. Left: Adding (7-methylguanosine (m7G)) to 5', center: removal of non-coding sequences (dark green blocks) and joining of coding sequences (bright green blocks) by RNA splicing, right: polyadenylation (poly-A tail) in 3' end. Created using BioRender.com

1.3. Pre-mRNA splicing

The protein-coding sequences (exons) of eukaryotic genes are usually divided by noncoding sequences (introns). This discovery from 1977 was unexpected for scientists, who, until that time, were familiar only with bacterial genes, which contain a continuous stretch of coding DNA that is directly transcribed to mRNA[7,8]. In the process known as splicing, introns are precisely removed, and exons are joined together to produce a mature mRNA molecule. In humans, the average exon length is approximately 150 base pairs[9], while introns consist of around 5200 base pairs[10].

1.3.1. Nucleotide sequences signals for splicing

The splicing machinery recognizes four sequences of the pre-mRNA: the 5' splice site (5'SS) and the 3' splice site (3'SS), which define the intron-exon boundaries, the polypyrimidine tract (PPT), and the branch point (BP) within the intron sequences. Each region has a consensus nucleotide sequence that guides the splicing machinery on where splicing takes place. Typically, the 5'SS consists of conserved GU dinucleotides at the start of introns, while the 3'SS includes a conserved AG dinucleotide preceding the start of the exon. The PPT is located about 5-40 base pairs upstream of the 3' end of the intron to be spliced and contains 15-20 pyrimidine nucleotides, usually a stretch of uracil nucleotides. The branch point is 20-50 nucleotides upstream of the 3' splice site within the intron. It usually contains a conserved adenine (A) nucleotide (Fig. 3)[11].

1.3.2. Transesterification reaction of splicing

Each splicing event removes one intron through two sequential phosphoryl-transfer reactions of transesterifications. First, the 2'-hydroxyl (2'-OH) group of the adenine (A) at the BP binds to a phosphate group of the 5'SS through a 2'-5' phosphodiester bond, generating an intron lariat-3' exon and a free 5' exon. Subsequently, the 3'-hydroxyl (3'-OH) group of the upstream exon is released. It binds to the phosphate group at the 3'SS, ligating the 5' exon and the 3' exon. The intron, now in a lariat structure, is then excised from the mRNA and degraded by cellular enzymes (Fig. 3)[12 13].

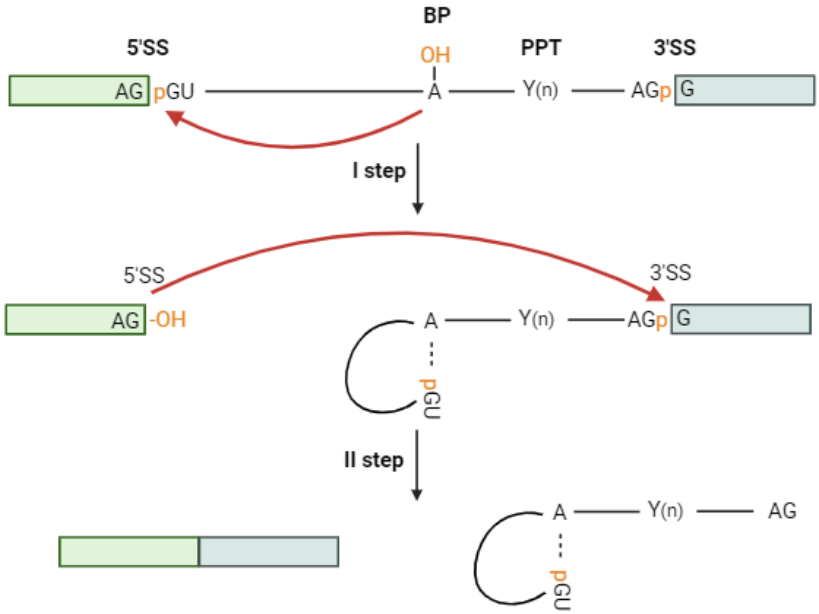

Figure 3: The schematic representation of two transesterification reactions of RNA splicing. Exons and introns are depicted as boxes and lines, respectively. The splicing sites 5'SS and 3'SS, and the branch point (BP) adenine and polypyrimidine tract are also shown. Adapted from [13]. Created using BioRender.com

1.3.3. RNA splicing is performed by the spliceosome

Key steps in RNA splicing are performed by a unique combination of RNA molecules and proteins, forming a spliceosome, unlike other cellular mechanisms that are mainly regulated by proteins alone. These RNA molecules - U1, U2, U4, U5, and U6, known as snRNAs (small nuclear RNAs), are complexed with a set of auxiliary proteins to form small nuclear ribonucleoproteins (snRNP). These snRNPs constitute the core of the spliceosome. Several snRNAs bind to the consensus RNA sequences through base-pairing. U1 snRNA binds to the 5'SS, while U2 snRNA binds to the branch point. Furthermore, U5 snRNA binds to the 3'SS and helps align the 5' and 3' exons at the splice junction, ensuring accurate ligation after the intron

is removed. U4 snRNA and U6 snRNA interact with each other to form a duplex, playing regulatory function during splicing[14,15].

Each splicing cycle performs stepwise processes: assembly and activation of the spliceosome, an accurate ATP-dependent splicing reaction, and disassembly of the spliceosome[16]. During the splicing cycle, different complexes may be highlighted in a following order (Fig. 4):

Early E complex:

First, the U1 snRNP recognizes the GU sequence at the 5'SS. Additionally, splicing factor SF1 binds to the branch point, and U2AF (U2 auxiliary factor) binds to the polypyrimidine tract (U2AF65) and 3'SS (U2AF35) [15,17]. This process is ATP-independent.

A Complex (Pre-Spliceosome):

In the next step, U2 snRNP replaces SF1, and U2AF forms base pairs with the polypyrimidine tract and 3'SS. These interactions are required to direct the position of U2 snRNP to the branch point. This process is ATP-dependent.

B complex (pre-catalytic complex):

Subsequently, the U4/U6 and U5 snRNPs are assembled as a triple-snRNP complex onto the pre-mRNA. U4 and U6 snRNPs are linked together by base-pair interactions. U2AF is no longer required and is typically released from the spliceosome.

B complex* (activated form):

Further extensive conformational rearrangements of the U4/U6 duplex unwind the linkage, and U6 replaces U1 snRNP at the 5'SS. U1 and U4 are released. This marks the first transesterification step of splicing.

C complex (catalytic step I spliceosome):

At this stage, the 5'SS and branch point are bound together by the interaction of U6 snRNP and U2 snRNP, forming a lariat structure of the intron.

C complex* (step II catalytically activated spliceosome):

This complex represents a further rearrangement of the C complex, after additional conformational changes necessary for the second step of the transesterification reaction. The 5' and 3' exons are ligated together, resulting in the spliced mRNA and the release of the intron lariat.

Spliced product:

The snRNPs are recycled for another round of splicing. Immediately after splicing, exon junction complexes are deposited at the intron-exon boundaries, marking the mRNA as a correctly processed sequence "ready" to be exported to the cytoplasm and translated.

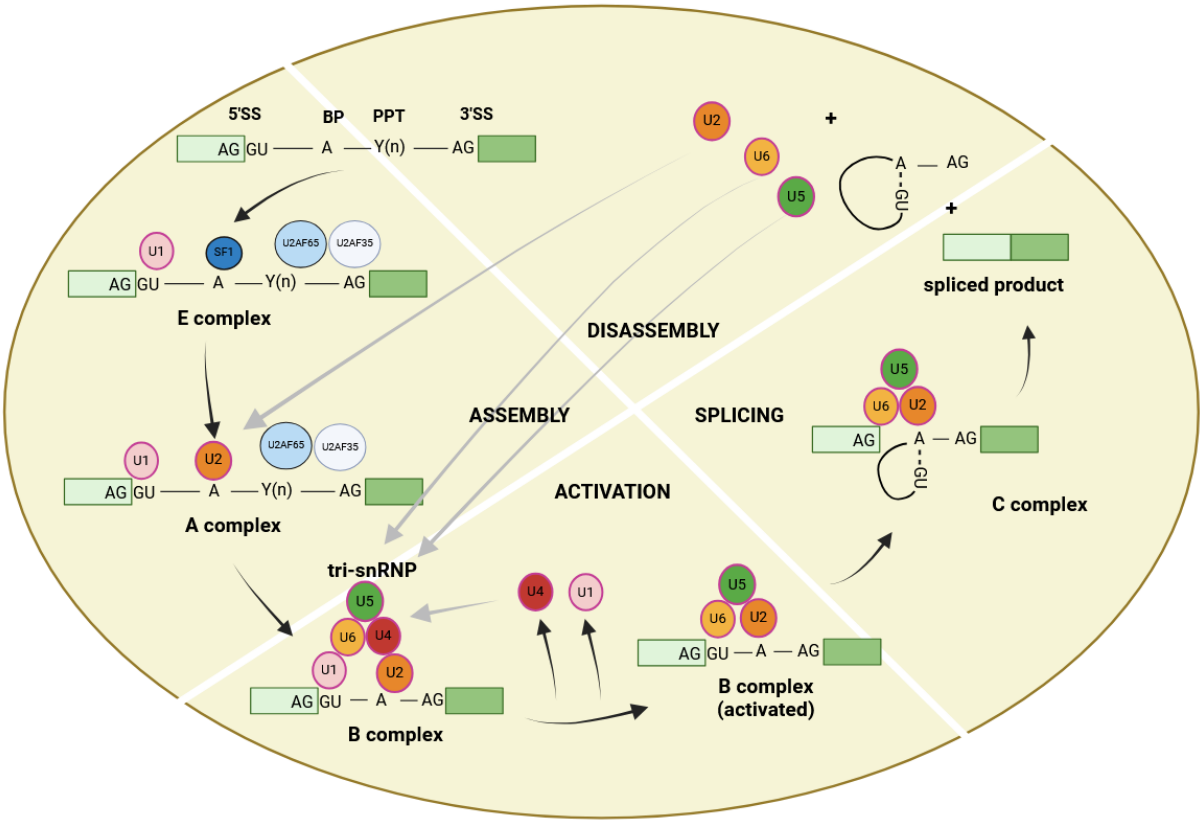

Figure 4: The mechanism of pre-mRNA splicing. RNA splicing is catalyzed by snRNPs (shown as colored circles) and other proteins (most of which are not shown), which together constitute the spliceosome. The spliceosome recognizes the splicing signals on a pre-mRNA molecule, joins the adjacent exons together and removes the intron in a form of lariat and provides the enzymatic activity for two transesterification reactions required. Adapted from[15,17]. To simplify the scheme, C* complex (step II catalytically activated spliceosome) was not shown. Created using BioRender.com.

1.4. Alternative splicing

The process in which an RNA transcript is spliced in different portions and thereby may create variable polypeptide chains from the same gene is called alternative splicing[18]. It plays a crucial role in increasing the genome's coding capacity and contributes to establishing cell type and tissue-specific functionality. In addition, alternative splicing has long been known to dynamically adapt the transcriptome to changing conditions, including altered body temperature[1920], circadian time[21] or immune cell activation and differentiation[22]. Furthermore, several studies have revealed the association of AS with various diseases, including cancer, neurodegenerative disorders, and cardiovascular diseases[23].

1.4.1. Types of AS

Alternative splicing (AS) refers to the various ways in which pre-mRNA can be spliced to produce different mRNA isoforms. Approximately 95 % of all human genes undergo AS[24]. There are at least five major types of AS[25], with exon skipping being the predominant one in humans. It results in the complete omission of one or more exons. Although relatively rare in humans, distinct functional proteins may also be produced by mutually exclusive exons, where two or more splicing events are no longer independent. They are included or excised in a coordinated manner[26]. The spliceosome may also use different 5'SS or 3'SS resulting in shorter and longer exons, respectively. Intron retention refers to inefficient splicing; the intron (or introns) remains unspliced in the mRNA. Factors increasing the likelihood of IR include weak splice sites, short intron length, or the regulated activity of splicing factors[27] . Several intron-containing mRNA can insert premature termination stop codons (PTCs) into the mature transcript, likely leading to degradation by nonsense-mediated decay (NMD), but others may generate new protein isoforms[28] (Fig. 5).

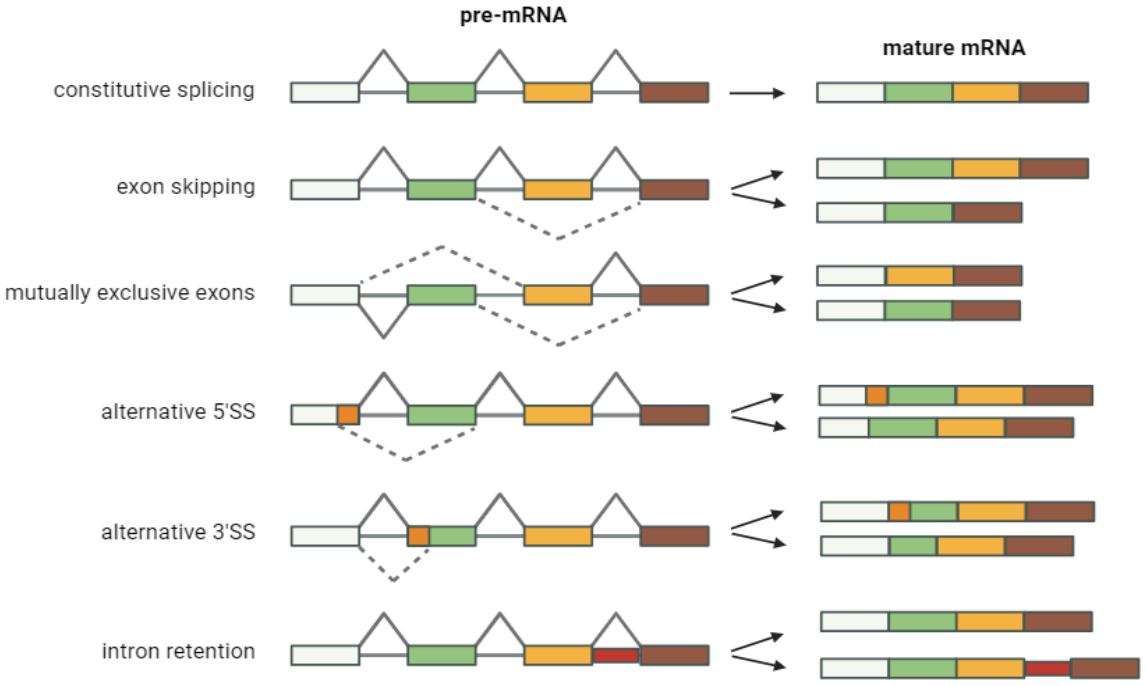

Figure 5: Patterns of alternative RNA splicing. Boxes represent exons, grey lines represent introns. Adapted from[23]. Created using BioRender.com

1.4.2. Regulation of alternative splicing

The use of splice sites is determined by their direct interaction with intrinsic sequences and splicing factors that recognize and bind to specific target cis-acting sequences located in exons or introns. These elements include exonic splicing enhancers and silencers (ESEs and ESSs, respectively) and intronic splicing enhancers and silencers (ISEs and ISSs, respectively)[18]. The most studied splicing regulatory factors are serine/arginine-rich (SR) proteins, which often bind to splicing enhancers and promote exon inclusion[29]. In contrast, the binding of members of the heterogeneous nuclear ribonucleoprotein (hnRNP) family to splicing silencers can promote exon skipping[30](Fig. 6). It is worth noting that hnRNP proteins often regulate the AS in specific context. For example, hnRNPL has been shown to activate or repress alternative splicing depending on its binding position[31]. Furthermore, several hnRNP proteins interact with SR proteins to fine-tune AS outcomes, acting as activators of splicing rather than their repressors[32].

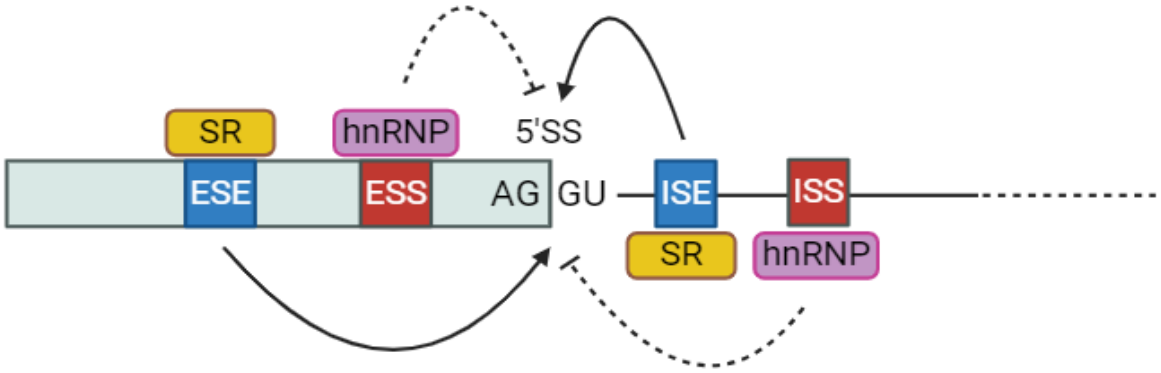

Figure 6. A scheme representing cis-and trans-acting factors involved in the regulation of AS. SR proteins and hnRNPs (colored circles) bind cis-regulatory elements to promote or inhibit splicing, respectively. Intronic splicing silencers (ISS) and exonic splicing silencers (ESS) inhibit splicing and are depicted by dashed lines. In contrast, intronic splicing enhancers (ISE) and exonic splicing enhancers (ESE) promote splicing and are shown in continuous lines. Exon is marked by a green box and the intron is represented by a black line. Created using BioRender.com.

1.4.3. The family of hnRNP proteins

The hnRNP family consists of at least 33 RNA-binding proteins playing significant roles in almost every stage of mRNA metabolism, including controlling pre-mRNA maturation, stabilization, transport, and translation[33]. First, together with several transcription factors, they bind to promoter sequences to direct DNA transcription. They are the first to bind to nascent RNA to prevent degradation and stabilize it. Furthermore, as mentioned earlier, they are known as inhibitors of splicing. They bind to ESS or ISS to prevent splicing, thereby increasing the accuracy of splicing and avoiding the inclusion of non-functional exons[18,34–36]. However, hnRNPs can also be recruited to splicing enhancers through the interaction with splicing activator complexes, promoting accurate splice site selection[37]. Huelga, et al. performed a genome-wide analysis comparing thousands of hnRNP-dependent splicing events and identified that over half of all AS events are regulated by different hnRNP proteins[36]. Furthermore, several hnRNPs pack nascent mRNAs into nuclear pore complexes (NPS) facilitating their transport to the cytoplasm for translation[35]. Most hnRNPs are located in the nucleus during the steady state[34]. However, they may translocate to the cytoplasm upon post-translational modification (PTM) or when recruiting other hnRNPs. In recent years, hnRNPs have gained increasing interest due to findings of altered gene expression in different types of cancer[38]. Additionally, they have been associated with neurodegenerative diseases including spinal muscular atrophy (SMA)[39], amyotrophic lateral sclerosis (ALS)[40] and Alzheimer's disease (AD) [41].

1.4.3.1. hnRNPC

hnRNPC is a ubiquitously expressed RNA-binding protein involved in the stability, processing, and regulation of pre-mRNA splicing. It exists in two isoforms, hnRNPC1 and hnRNPC2, which are produced through A5SS usage. hnRNPC1 is the more abundant form and is composed of 293 residues. hnRNPC2 contains an additional 13 amino acids (107-119 residues), making it 306 residues in length[42] (Fig. 7). Both hnRNPC isoforms contain an RNA-recognition motif (RRM) located at the N-terminal end (residues 1-106) and a C-terminal carboxy-terminal domain (CTD, residues 208-306; C2 numbering). RNA-binding determinants were also observed in the basic leucine zipper-like motif (bZLM, residues 140-214[43], Fig. 7). The hnRNPC RRM binds to at least five consecutive uridines, with longer uridine stretches increasing the affinity of binding[44, 45]. Due to the presence of only one RRM, the hnRNPC

monomer must oligomerize to form strong and specific interactions with RNA targets. This oligomerization is driven by a 28-residue helical region (residues 180-207), referred to as hnRNPC zipper-like (CLZ) oligomerization domain. This specific region promotes the hnRNPC oligomerization by forming a coiled coil heterotetrametric structure (mainly as a $(C1)_3(C2)$ oligomer)[43]. Furthermore, the 155–161 aa sequence contains a nuclear localization signal (NLS), which is usually a short peptide sequence responsible for the precise directing the protein from the cytoplasm to the nucleus[46].

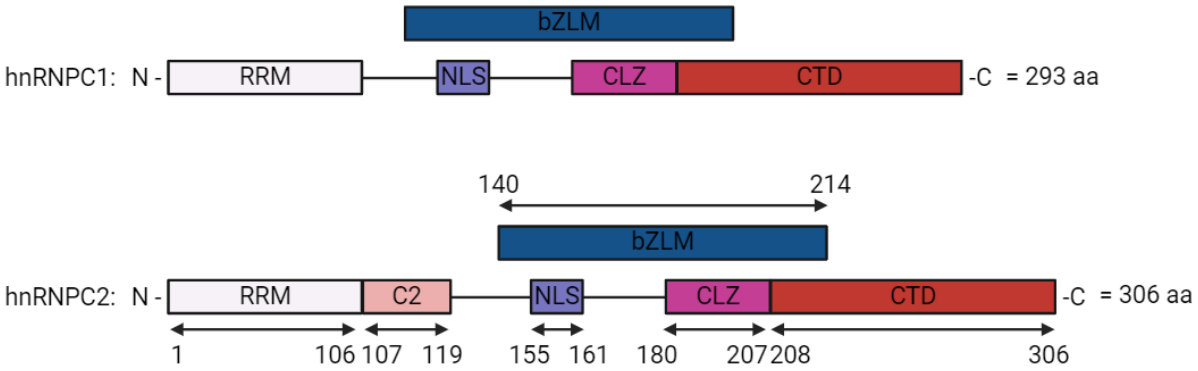

Figure 7: Scheme representing two hnRNPC isoforms. (RRM) - RNA-recognition motif; (C2) - additional 13 amino acid sequence in the C2 variant; (NLS) – nuclear localization signal; (bZLM) – basic leucine zipper-like motif, (CLZ) – zipper-like oligomerization domain; (CTD) - carboxy-terminal domain. A number of amino acids in each hnRNPC isoform are depicted on the right. Numbers represent aa position. Adapted from[45]. Created using BioRender.com.

hnRNPC wraps elongating nascent RNA longer than 200-300 nucleotides around the hnRNPC tetramer, allowing it to tightly occupy RNA region centering on the uridine stretch. In this way, hnRNPC sorts transcripts based on whether the RNA length exceeds this threshold[47]. This protein, together with major hnRNPA2/B1 and hnRNPA1, builds 40S nuclear ribonucleoprotein particles (hnRNP particles). Each hnRNP particle contains three copies of hnRNPC tetramers. Similarly, hnRNPA2/B1 also assembles with a 3:1 ratio to form hnRNP particle[48]. Experiments with purified hnRNPC tetramers and *in vitro*-transcribed RNAs revealed that one, two and three tetramers bind about 230, 460 and 700 nts of RNA, forming ellipsoidal, bi-lobed and triangular complexes, respectively[48]. Packing of mRNA transcripts by hnRNP particles into complexes is required to transport them to the cytoplasm for translation[49]. Additionally, they protect transcripts from premature degradation by exonucleases. In a steady state, hnRNPC does not shuttle between the nucleus and cytoplasm due to the presence of a nuclear retention sequence (NRS). Therefore, mRNA binds to hnRNPC

only in the nucleus; mRNA is transported to the cytoplasm only after it loses its binding to hnRNPC[50].

Furthermore, it has been shown that hnRNPC masks the splicing of cryptic exons (mostly Alu elements) that can potentially produce aberrant transcripts. Cryptic exons contain splice sites that exhibit similar sequences to true splice sites. Under normal conditions, these splice sites are overlooked by the splicing machinery in favor of stronger, canonical splice sites. Short, repetitive transposable elements - Alu exons become cryptic exons when their inclusion in mature mRNA results from splicing errors, which are often associated with several diseases, including hyperphenylalaninemia, congenital cataracts, and facial dysmorphism neuropathy[51,52]. Quantitative individual-nucleotide resolution crosslinking-immunoprecipitation (iCLIP) data revealed that hnRNPC competes with splicing factor U2AF65 for binding to the polypyrimidine tract upstream of the 3'SS. In the absence of hnRNPC, cryptic splice sites in Alu exons are recognized by U2AF65, leading to aberrant exon inclusion. When hnRNPC is present, it binds to the poly-U stretches upstream of Alu exons and prevents recognition of U2AF65 at cryptic 3' splice sites, leading to the exclusion of cryptic exons from the transcriptome, and thereby ensuring accurate splicing[53].

In addition to packaging newly formed transcripts and controlling cryptic exons splicing, hnRNPC plays a role in internal ribosome entry site (IRES)-related translation by facilitating the assembly of the translational machinery. The IRES element, located primarily in the 5'UTR of the mRNA, allows translation initiation by recruiting the small ribosomal subunits to its RNA close to the initiator AUG, independent of the 5' cap. This strategy is mediated mainly during stress conditions, when genes involved in 5' capping are downregulated[54]. Several studies have shown that hnRNPC stimulates the IRES-mediated translation of proto-oncogenes *c-myc* [55], and *c-sis*[56], translational regulators Unr proteins[57] and X-chromosome-linked inhibitor of apoptosis, XIAP [58].

Furthermore, hnRNPC turned out to be identified as a „reader" of m6A modification. This reversible reaction relies on the methylation of N6-methyladenosine at the sixth position of adenine in mRNA[59]. This modification affects the stability of mRNA transcripts, the recognition and selection of splice sites, translation efficiency, mRNA export and localization within the cell. m6a modifications are post-transcriptionally installed, erased and recognized

by m6A methyltransferases („writers “), demethylases („erasers“) and m6A-specific binding proteins („readers“), such as hnRNPC[60]. hnRNPC has been also studied for its crucial associations with cancer including hepatocellular carcinoma (HCC) [61], glioblastoma[62], breast cancer[63] and head and neck squamous cell carcinoma[64]. Abnormal splicing patterns and changes in RNA stability due to altered hnRNPC activity were associated with tumorigenesis by producing oncogenic proteins or disrupting the expression of tumor suppressors. Its activity has also been critical in the context of neurodegenerative diseases [65].

1.5. Co-transcriptional splicing

The assembly of splicing components on pre-mRNA is, in most cases, **co-transcriptional**; thus, splicing occurs simultaneously with transcription by RNA polymerase II (RNA Pol II), which remains engaged with the chromatin template (Fig. 8). This process has been studied in different organisms and plays a role in coordinating both constitutive and alternative splicing[66]. While the nascent, newly transcribed RNA is still being synthesized, the splicing machinery begins to assemble, removes introns, and joins exons, even if transcription is not yet completed. These two processes are spatially and temporally coupled. Immediately after the RNA polymerase II transcribes from a DNA template, the spliceosome recognizes 5’SS and starts splicing. Therefore, the main player in this process is RNA polymerase II, containing a large, unstructured C-terminal domain (CTD) composed of numerous heptad repeats (YSPTSPS). Co-transcriptional splicing is facilitated by the recruitment of splicing factors to the RNA Pol II CTD. For instance, it has been shown that the SR protein SRSF3 promotes exon skipping of the fibronectin gene, dependent on its localization to the CTD of RNA Pol II [67]. David et al., revealed that phosphorylated CTD binds with the splicing protein U2AF65 to promote its association with pre-mRNA [68]. Other factors influencing the efficiency of RNA processing include the speed of RNA pol II, the availability of splicing factors, changes in chromatin structure and conformation, and histone post-translational modifications. In recent years, more and more studies have highlighted the role of histone modifications in regulating the rate of transcription, which may affect the activity of splicing machinery. These histone rearrangements provide dynamic and reversible mechanisms to turn the RNA synthesis on or off, depending on different times and intra or extracellular stimuli [69]. Nascent RNA is not fully processed yet; some mechanisms including splicing or 3’ polyadenylation have not yet occurred. This RNA is chromatin-associated when it interacts with DNA. Therefore, chromatin-

associated RNA represents a broader range of RNA, including co-transcriptionally processed nascent RNA and any other RNA interacting with DNA, such as long non-coding RNA (lncRNA) or small interfering RNA (siRNA). It is worth noting, splicing can also be post-transcriptional, where the splicing kinetics of individual introns is slower than the transcription machinery[70]. This process can be mediated either close to the gene in a chromatin environment or at distinct sites throughout the nucleoplasm[71].

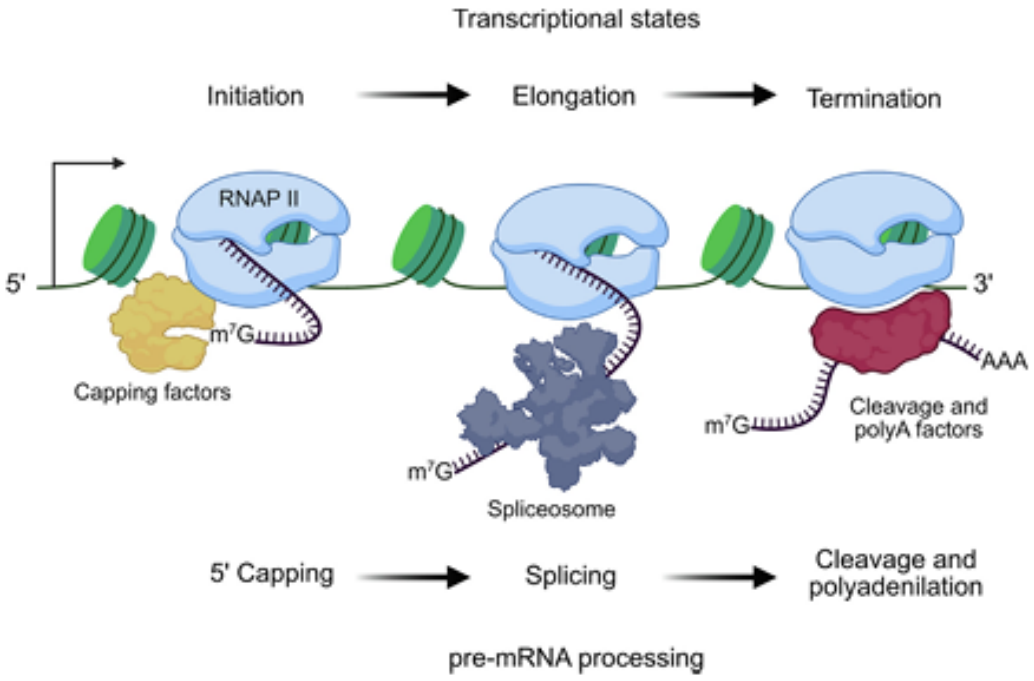

Figure 8: Coupling between pre-mRNA splicing and transcription. While the flow of the transcription moves forward, the RNA Pol II recruits components of the splicing machinery. All these factors are recruited through C-terminal CTD of RNA Pol II. The co-transcriptional splicing occurs within the chromatin. Adapted from[63,64]. Created using BioRender. com.

1.6. The process of lymphocyte activation

Lymphocyte activation induces vast changes in gene expression that lead to functional alterations such as proliferation, migration and the production and secretion of effector molecules. The well-defined changes in functionality and the availability of cell culture models have made lymphocyte activation a frequently used model system for studying how external signals are transmitted to the nucleus to alter gene expression and impact on diverse aspects of cellular functionality. In this chapter, we defined the role of alternative splicing patterns during lymphocyte stimulation, reflecting their functional consequences in activated cells.

1.6.1. Immune response

The ability to specifically recognize and respond to antigens is controlled by B cells producing antibodies and T cell receptors detecting the antigen. T cells are divided based on their function into cytotoxic T cells (Tc) destroying infected and cancerous cells and helper T cells (Th) controlling the immune response. These two subsets of T cells are distinguishable by the expression of mutually exclusive cell surface molecules of CD8 and CD4, respectively [72–74]. To precisely control the function of the adaptive immune system, close cooperation between T and B cells is required. This interaction between an antigen and its receptor alone is not sufficient for B cells to produce antibodies; helper T cells and secreted cytokines are also required to stimulate the B cell response (Fig. 9).

There are two types of immune response: humoral and cellular. Both responses require the function of B and T cells, but only one may function more intensely than the other one. Antibodies produced by B cells are key players in the humoral response. They are predominantly present in the blood, lymph, tissue fluids and mucosal surfaces. One B cell can release even several thousand antibodies in a second[22 75]. In the cellular response, T cells react with the antigenic peptides bound to major histocompatibility complex (MHC) molecules expressed on the surface of antigen-presenting cells (APCs). This interaction leads to the cytokine secretion that engages APCs to actively process an immune response (Fig. 9). The main types of APCs are dendritic cells, macrophages, monocytes, and B cells.

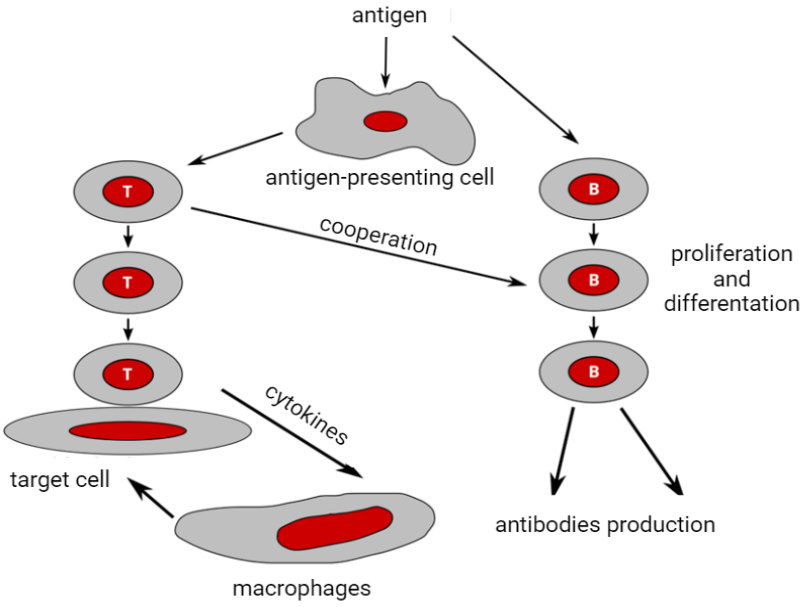

Figure 9: The development of immune cellular (with the T cell usage) and humoral (with the B cell usage) immune response. Adapted from[68]. Created using BioRender. Com

Most lymphocytes exhibit low metabolic, transcriptional, and translational activities in a quiescent G_0 phase of the cell cycle[76]. In this state, they remain dormant, "waiting" to participate in an immune response. Upon activation, lymphocytes pass into the G_1 phase and begin proliferating. This transition is accompanied by an increase in cell size, an expansion of the cell nucleus, changes in its chromatin structure, and the appearance of nucleoli [77]. According to Lea et al., $G_0 \rightarrow G_1$ transition occurs 3 to 5 hours after the activation of human CD4 or CD8 T cells[78].

T cell activation can only be initiated through direct contact with APCs. For activation to occur, a T cell must receive two signals: the first comes from the recognition of the antigen by the T cell receptor (TCR), and the second from co-stimulatory molecules. The most crucial co-stimulatory interaction is between CD28 located on the T cell membrane and CD80/CD86 located on the surface of APCs (Fig. 10). CD28 is present on 30-50% of human Tc cells and 95-100% on human Th cells. The signal with its ligand CD80/CD86 increases IL-2 cytokine release and T cell proliferation[79]. Additionally, the development of fully functional effector cells requires signals from cytokines. Without these signals, the survival time of lymphocytes is shortened, and their ability to differentiate or form memory cells is compromised.

1.6.2. Immunological synapse

The lymphocyte activation occurs in the peripheral lymphoid organs. Most antigens that enter the body reach these organs on the surface of APCs. The lymphocyte activation process begins with the formation of an immunological synapse (IS) between a T cell and an APC. Within the synapse, antigen-binding TCRs are concentrated and stabilized by adhesion proteins. The IS remains stable for many hours[80].

Lymphocyte activation leads to the formation of TCR microclusters (TCR-MC). These are intracellular protein conglomerates that consist of a TCR receptor with signaling molecule - CD3 complex, proteins controlling T cell response, including ZAP-70 tyrosine kinase, and adaptor protein LAT, and proteins responsible for cytoskeletal reorganization [81]. Over time, TCR-MCs move toward the center of the IS. New TCR-MCs continue to form at the periphery of the intercellular protein interface. The mature form of the IS is completed within a few minutes of contact between the lymphocyte and the APC. It contains well-organized multimolecular aggregates of molecules involved in adhesion and signaling, known as supramolecular activation clusters- SMACs. The central SMAC (cSMAC) is the area of

endocytosis and degradation of TCR complexes. It is also the space into which cytokines are secreted after lymphocyte activation. The cSMAC is composed of TCRs and TCR-associated proteins (CD3, CD4), costimulatory molecules and their ligands (CD28/CD80) and cytoplasmic transmitters - protein kinase C θ (PKCθ)[82] and IKK kinase[83]. Surrounding the cSMAC is the peripheral SMAC- pSMAC, which is formed by a ring of adhesion molecules (integrin LFA-1 binding to intercellular adhesion molecule -1 ICAM-1), cytoskeletal linker talin and transferring receptors, which facilitate stabilization of lymphocyte-APC interactions. Beyond the pSMAC is the distal SMAC (dSMAC) region containing CD43 molecules and several phosphatases. The dSMACs are enriched in TCR-MC that are driven the cSMAC driven by F-actin[84].

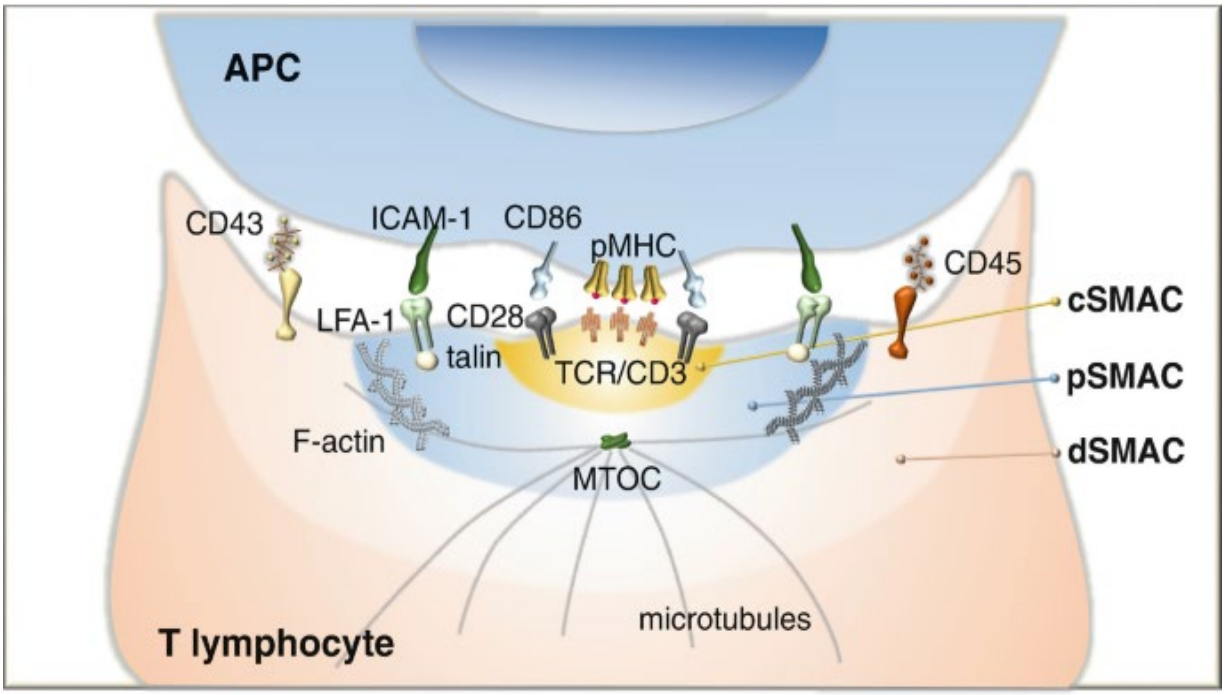

Figure 10: The structure of immunological synapse (adapted from [84]).

1.6.3. Intercellular pathways to activate lymphocytes

Two main intercellular pathways are involved in T cell activation. The first one is initiated by the metabolism of phosphatidylinositol (PI) in the cell membrane and is associated with activating of calcium-dependent kinases and phosphatases[85]. The second pathway involves the signaling cascades of mitogen-activated protein kinases (MAPK) including extracellular-signal-regulated kinases (ERK 1/2), or stress-activated protein kinases (SAPK)[86].

Following antigen recognition by the TCR, phospholipases in the cell membrane are activated by phosphorylation via protein tyrosine kinases (PTKs). This results in the catabolism of phospholipids of a cell membrane which leads to the generation of second mediators:

inositol triphosphate (IP_3) and diacylglycerol (DAG) (Fig. 11). The role of IP_3 is to release calcium ions from intracellular stores (for instance, endoplasmic reticulum - ER). It triggers the activation of calcineurin and then transcription factor NFAT (nuclear factor of activated T cells). These molecules are phosphorylated in resting T cells and are localized in the cytoplasm. After activation by calcineurin (dephosphorylation), they move into the nucleus, where they form a complex with the transcription factor AP-1, upregulating, for example, IL-2 or IL-4 responsible for T cell activation[87].

The second main transducer in T-cell activation is membrane-bound DAG, which directly activates serine-threonine kinases called protein kinase C. This family of ten kinases is divided into three subfamilies based on their activation mechanisms. PKCα, PKCβ1, PKCβ2, and PKCγ belong to classical PKC that are regulated by both DAG and Ca^{2+}. Novel PKC isoforms (including PKCδ, PKCε, PKCη, and PKCθ) are DAG-dependent, but do not require Ca^{2+}. Atypical PKC isoforms (PKCζ and PKCι) are independent of both DAG and Ca^{2+} for activation[88]. All the PKC kinases contain a specific DAG-binding motif. Several PKC isoforms are implicated in T cell functions. For instance, after TCR stimulation, PKCθ is predominantly expressed in T cells, where it activates the IKK complex. This activation leads to the phosphorylation and degradation of IκB, an inhibitor of NF-κB. The degradation of IκB allows NF-κB to translocate to the nucleus and promote the transcription of genes involved in T cell activation, proliferation, and survival. This PKCθ–IKKβ–NF-κβ pathway is involved mainly in T cell survival, homeostasis and activation[89]. Additionally, DAG can activate the MAPK signaling pathway through PKC kinases. They can also cooperate with calcineurin during the activation of IP_3-NFAT pathway to regulate the expression of target genes (Fig. 11).

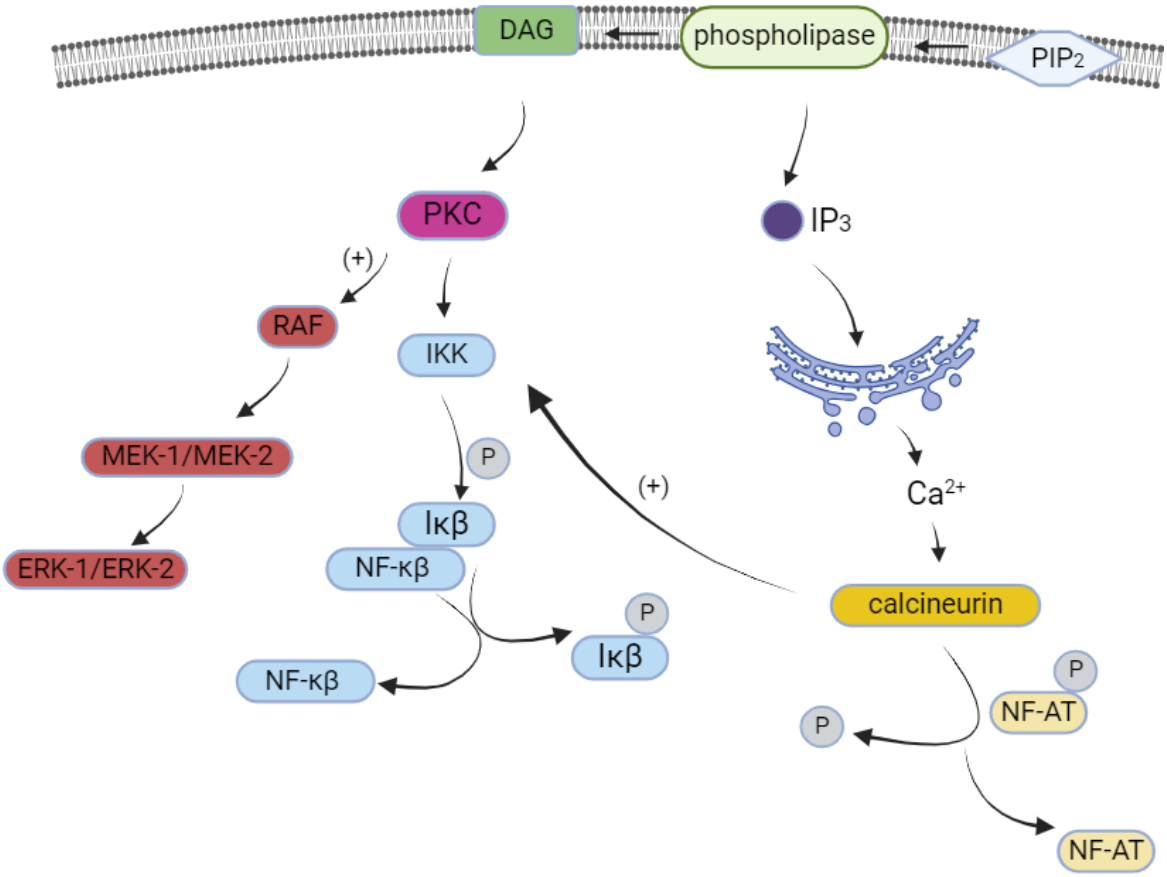

Figure 11: The involvement of protein kinases in TCR receptor signal transduction. Adapted and modified from[79,90]. Created using BioRender.com

The intracellular signaling from B cell receptors (BCRs) is mainly dependent on T cell activation. It involves Th cell activity that support antigen recognition and cytokine secretion, which is necessary for efficient B cell proliferation and differentiation. The activation mechanisms between these lymphocytes are very similar, with phospholipids activating DAG and IP_3. However, these pathways differ in the presence of appropriate kinases. For example, PKCθ is not expressed in B cells, suggesting that another subtype of PKC (predominantly PKCβ) is involved in IκB phosphorylation and activation of NF-κB [91].

Immortalized Jurkat T cells or Raji/Ramos B cells stimulated with PMA (phorbol 12-myristate 13-acetate) are commonly used as research models to study mechanisms of cellular activation. Structurally, PMA closely resembles DAG and acts as its synthetic analog. It contains a ring of the diterpene alcohol phorbol with a myristate ester at C12 and an acetate ester at C13. Due to these structural features, PMA mimics DAG, thereby activating PKC proteins, and triggering a cascade of intracellular signaling pathways. PMA activation results in various

cellular processes such as gene expression, cell proliferation, and differentiation, making it a valuable tool for understanding T and B cell functions and signaling[92].

1.6.4. The role of alternative splicing in lymphocyte activation

During the recognition of an antigen by TCRs, numerous physical and biochemical changes are required, including cytoskeleton rearrangements and increased expression and secretion of cytokines whose action must be fast, precise, and efficient. These changes occur at the level of transcription and regulation of pre-mRNA splicing.

Many immune-related genes, which include cell surface receptors (CD28, CD44, CTLA-4, IL7R), kinases, and phosphatases such as CD45 or Fyn, or transcription factors (LEF1, FOXP3) undergo AS during an immune response[93,94]. For instance, the CD44 gene encodes a cell surface glycoprotein involved in cell-cell interactions, cell adhesion and migration. This gene contains 10 "variable" exons that can be included to mature mRNA into different combinations. AS of this gene results in multiple isoforms, including standard form (CD44s) and variable forms (CD44v). All these CD44 variants affect the strength of the association with other proteins, affecting the migration speed to sites of inflammation. However, naïve T cells express the standard CD44, while activated T cells express multiple CD44v isoforms[95]. Furthermore, resting lymphocytes express the full-length isoform of the transmembrane protein tyrosine phosphatase - CD45. In contrast, activated T cells express the shorter isoforms that arise from the regulated AS of exons 4, 5, and 6 in the CD45 pre-mRNA. Different short CD45 isoforms are expressed at various stages of lymphocyte activation. T cells expressing the short CD45 isoforms exhibit decreased phosphatase activity, which indeed acts as a negative feedback mechanism, dampening TCR signaling to prevent prolonged activation[96]. Another mechanism of inhibiting prolonged T cell signaling is mediated by AS of CTLA-4. This gene competes with CD28 for binding to its ligand CD80/CD86. In resting T cells, CTLA-4 is expressed at a low level and in a soluble form. CTLA-4 expression is strongly induced in T cell activation through the inclusion of a transmembrane-encoding exon, which prevents hyperstimulation[97]. Therefore, studies of both CD45 and CTLA-4 show the role of AS in attenuating the expression of genes after degradation of the foreign molecules thereby controlling T cell homeostasis. Table 1 reveals several other examples of AS changes during T cell activation that contribute to the complexity of immune response. We chose those genes that due to AS they encode different protein isoforms with already known immune-related function.

Table 1. The summary of the various AS changes involved in lymphocyte activation.

Gene	Protein name	Type of AS	Function	Reference
Cell surface receptors				
CD44	surface glycoprotein	exon inclusion	altered association with other proteins involved in T cell activation	95
CD45	transmembrane protein tyrosine phosphatase	exon inclusion	change in phosphatase activity	96
CD6	surface glycoprotein	exon skipping	disrupted transport of CD6 to immunological synapse	98
CTLA-4	cytotoxic T-lymphocyte antigen 4	exon skipping	formation of membrane- bound CTLA-4 upon T cell activation	97
Fas	surface death receptor	exon skipping	soluble form that blocks FAS ligand-induced apoptosis	89
HMMR	hyaluronan-mediated motility receptor	exon skipping	aberrant cell proliferation and apoptosis	99
Fyn	protein tyrosine kinase	mutually exclusive exons	increased Ca^{2+} flux and IL-2 production	100
Cytokine-related genes				
IL-2	interleukin -2	exon skipping	impaired T cell signaling	101
IL-4Rα	interleukin - 4	Mutually exclusive exons	soluble isoform impairing T cell signaling	102
IL-6	interleukin-6	exon skipping	dominant-negative inhibitor of IL-6 signaling blocking the differentiation of T cells to CD4+T cells.	103
IL7R	interleukin 7	exon inclusion	soluble isoform increasing a risk of multiple sclerosis	104
Transcriptional regulators				
FOXP3	forkhead box protein P3	exon skipping	increased levels of CD25 expression in CD4+ T cells, altered interactions with other transcriptional co-regulators, affecting immune regulation	105
GATA3	transcription factor: GATA-binding protein 3	exon skipping	increased expression in T helper cells upon T cell activation, regulation of cell fates upon T cell activation	106
LEF1	lymphocyte enhancer factor 1	exon skipping	uncoupling of the multiple activities of this transcription factor: LEF1, regulation of TCR signaling in thymic development	107

1.7. Immediate early genes – fast responders among genes

A distinct group of diverse genes that respond rapidly to regulatory signals are known as immediate-early genes (IEGs). Although their baseline expression is low, they can be transiently and quickly activated in response to a broad range of internal or external cellular stimuli. This activation typically occurs within the first 30 minutes following stimulation[108]. The stimuli influencing the IEGs response can be categorized into environmental factors (e.g., changes in light/dark phases, exposure to stressors like intruder animals, learning sessions

during acquisition tasks, viruses), pharmacological factors (growth factors like platelet-derived growth factor (PDGF), epidermal growth factor (EGF), mitogens, and phorbol ester), and physical factors (such as glucose, hypoxia, UV exposure, irradiation)[109]. Therefore, IEGs play a role in adapting cells to adverse conditions, primarily by regulating apoptosis, inflammation and DNA repair pathways. They serve as rapid responders, allowing cells to quickly adapt to environmental changes by activating secondary gene programs that influence cell fate and function.

The IEG expression is independent of *de novo* protein synthesis, as it does not require the production of new transcription factors[110]. Instead, it relies on post-translational modifications of existing proteins (including transcription factors), such as phosphorylation cascades[108]. As a result, cells can transcribe mRNA for IEGs even in the presence of protein synthesis inhibitors, since the necessary proteins for their expression are already present within the cell[110]. A notable feature of IEGs is their relatively short average length (approximately 19kb) and significantly fewer exons[108]. They also possess many regulatory regions with binding sites for transcription factors. The rapid expression of IEGs is associated with histone acetylation, which enhances promoter accessibility to RNA pol II and other transcriptional machinery components, thereby promoting transcription. The products of IEGs function may act as transcriptional repressors; once synthesized, they bind to the promoter regions of their own genes, inhibiting further transcription. This leads to the swift downregulation of mRNA and increased degradation of the translated products by the proteasome, highlighting the IEGs instability[111]. This mechanism of preventing IEG overexpression ensures their precise and transient control. In addition to their role in autoregulatory functions, IEGs can act as transcription factors, such as *c-fos*, *EGR-1*, *c-myc*, and *c-jun*, which control the expression of downstream genes involved in the early regulation of cell growth, development or activation. They regulate cell cycle progression and are involved in the transition from the quiescent state (G0 phase) to the growth phases of the cell cycle (G1 phase).

The first discovery of IEGs occurred in 1984 when the proto-oncogene *c-fos* was shown to be rapidly and synchronically induced by growth factor stimulation. Its expression peaks 30-60 minutes after stimulation and returns to basal expression after 90 minutes[110,112]. The

resulting FOS protein plays roles in many cellular processes including proliferation, differentiation, survival and cellular death[113,114].

There are many signaling pathways leading to the activation of IEGs. The most common signaling pathway is through ERK1/2 kinase that controls chromatin structures at IEG promotors and directly phosphorylates and activates transcription factors, which together induce IEG transcription. The phosphorylation is preferentially catalyzed among substrates containing Pro-XXX-Ser/Thr- Pro sequence[115]. This pathway is involved in transient expression of IEGs due to the induction of phosphatases that act in negative feedback loop[116]. Other known pathways involved in IEGs expression are through RhoA-actin, p38 MAPK and PI_3K. These pathways lead to the phosphorylation of regulatory proteins that directly affect the activity of IEGs expression.

The rapid increase in IEG expression leads to long-term cellular effects. The induction of IEGs plays a critical role in acute inflammation, neuronal activity, cell proliferation and differentiation[117] and regulation of circadian clock[118]. In the context of neurobiological functions, IEGs are associated with modifications of synaptic activities and have been linked to the development of schizophrenia, panic disorder, and post-traumatic stress disorder[119].

1.7.1. Temporal patterns of expression of genes involved in T cell activation

Since the complete development of an effector cell takes at least 24-48 hours, most studies have focused in AS after this period[120–122]. The first day following activation is primarily aimed at coordinating gene expression processes; many genes are up- or downregulated during that time based on the dynamic behavior of the signaling network[123]. Immediately after activation, many genes associated with the maintaining the resting state are downregulated[124,125] followed by metabolic reprogramming to provide energy for growth. Furthermore, during this period, T-cells respond to IL-2 signaling and initiate effector functions, such as cytokine production. These mechanisms are required to obtain a full T cell effector function after 24 hours. However, changes in splicing patterns among at early stages of lymphocyte activation remain under investigation.

Recent studies have demonstrated the rapid induction of IEGs (such as *c-fos*) upon T cell activation, followed by increasing transcriptomic changes, that peak after one day or later. For instance, Rade et al. analyzed the temporal expression patterns of different components

involved in T cell activation. They found that most transcriptomic changes reach their peak levels after 16-24 hours of activation[123]. However, analyzing transcript levels alone is not sufficient to predict protein levels, especially during the dynamic translational changes that occur upon T cell activation. Post-translational modifications, such as phosphorylation add further complexity to this challenge. To better understand the dynamics of proteome and phosphoproteome during T cell activation, Tan et al. performed proteomic and phosphoproteomic analyses. They revealed that global *de novo* protein synthesis is reduced in the early phases of T cell activation. Instead, proteomic changes are driven by the rapid induction of phosphorylation events in pre-existing proteins, reconfiguring protein-protein interaction networks and their functionality. The reduction in *de novo* protein synthesis during this early phase post activation, when the naïve transcriptome is still predominant, likely serves to facilitate the turnover of the proteome from a naïve to an activated state[126]. However, a significant increase in *de novo* synthesized proteins is observed only in the later phase of T cell activation (8-16 hours post activation), driven by the extensive reprogramming of the entire proteome and phosphoproteome. This induction is primarily observed due to the upregulation of molecular machineries involved in ribosomal biogenesis and protein translation. Tan et al., also showed the enrichment of protein degradation through the proteasome quickly after T cell activation. This tight coordination between transcriptional changes, translation, and protein degradation is crucial to maintain the proper T cell homeostasis and ensuring an adequate amino acid supply during their long-term activation[126].

2. Goals of the study

The expression of IEGs during lymphocyte activation has been already known for three decades. However, how this expression is linked to changes in splicing patterns and the functional consequences of these associations have yet to be thoroughly studied. This project focused on investigating the concept of immediate early splicing (IES) through a combination of *in silico* bioinformatic analysis and subsequent biochemical wet lab experiments. The primary goals of the project were to:

1. Identify the mechanism of IES upon lymphocyte activation
2. Identify the main regulators of IES upon lymphocyte activation.
3. Identify the signaling pathways that lead to IES.
4. Conduct experimental manipulations to delineate the details of IES mediated during lymphocyte activation.
5. Determine the specificity of IES to lymphocytes.
6. Check whether IES is processed in other cell lines or by different stimuli
7. Identify the functional consequences of IES in cells.

3. Materials and methods

3.1 Buffers

Media, buffers and solutions were prepared with deionized water (Millipore) and, if required, autoclaved (121 °C, 20 min, 3 bar). All buffers were filter-sterilized (0.22 µm). The pH was adjusted using 5 M KOH, 5 M NaOH, 3 M KCl, or 32% HCl.

10x PCR Buffer

- 200 mM Tris pH 8.3
- 500 mM KCl
- 5 mM $MgCl_2$
- 0.1% Gelatine

Extraction buffer

- 1% Gelatine
- 10x PCR Buffer
- 10% Tween
- 10% NP-40

50x TAE buffer

- 2 M Tris Base
- 5.7% Glacial acetic acid
- 400 mM EDTA pH 8.0

10x Taq Buffer

- 0.5 M KCl
- M Tris pH 8.3
- 15 mM $MgCl_2$
- 0.01% Gelatine

CTX Buffer

- 10 mM HEPES–NaOH, pH 7.9
- 1.5 mM $MgCl_2$
- 10 mM KCl

NX Buffer

- 20 mM HEPES–NaOH, pH 7.9
- 1.5 mM $MgCl_2$

- 420 mM KCl
- 0.2 mM EDTA
- 25% (v/v) Glycerol

5x Hybridization Buffer

- 1.5 M NaCl
- 50 mM Tris pH 7.5
- 10 mM EDTA

1.25x RT mix

- 12.5 mM DTT
- 12.5 mM Tris pH 8.0
- 7.5 mM $MgCl_2$

2x Formamide loading dye

- 80% Formamide
- 1 mM EDTA
- 0.05% (w/v) Bromophenol blue
- 0.05% (w/v) Xylene cyanole

5x TBE Buffer

- 1.8 M Tris Base
- 1.8 M Boric acid
- 400 mM EDTA

2x RIPA

- 20 mM Tris-HCl pH 8.0
- 200 mM NaCl
- 4 mM EDTA
- 2% NP-40
- 10 mg/mL Sodium Deoxycholate

2x SDS Loading Dye

- 0.125 M Tris-HCl, pH 6.8
- 4% SDS
- 10% β-mercaptoethanol

- 20% Glycerol
- 0.2% bromophenol blue

SDS-PAGE running buffer

- 25 mM Tris-HCl, pH 6.8
- 192 mM Glycine
- 1% (w/v) SDS
- 21.2% (w/v) Glycerol
- 0.12% (w/v) bromophenol blue

Western blot-blocking buffer

- 1 X LS - TBST
- 2 % (w/v) BSA

10 X Western blot transfer Buffer

- 500 mM Tris-HCl, pH7.5
- 400 mM Glycine
- 0.1% (w/v) SDS

1x LS TBST

- 50 mM Tris-HCl, pH 7.5
- 150 mM NaCl
- 0.1% Tween-20

1x HS TBST

- 50 mM Tris-HCl, pH7.5
- 400 mM NaCl
- 0.1% Tween-20

1 X PNK buffer

- 70 mM Tris-HCl, pH8.3
- 10 mM MgCl2
- 5 mM DTT, pH 7.6

EMSA binding buffer

- 20 mM Tris-HCl pH 8.0,

- 0.25M NaCl
- 1mM DTT,
- 10% glycerol
- 0.2mM EDTA

3.2. Cell culture

Human Jurkat cells, Raji, Ramos, HEK293 cells, HeLa cells, and murine EL4 cells, RAW 264.7, and N2a cells were preserved in liquid nitrogen, with early passage aliquots periodically thawed. Suspension cells (Jurkat and EL4 T cells and Raji and Ramos B cells) were cultured in RPMI medium, supplemented with 10% (v/v) fetal bovine serum (FBS) and 1% (v/v) penicillin/streptomycin (Invitrogen, USA). Adherent cell lines were cultured in DMEM High Glucose (Biowest, France), augmented with 10% (v/v) fetal bovine serum (FBS) and 1% (v/v) penicillin/streptomycin (Invitrogen, USA) (Table 2). All cell lines were maintained at 37°C with 5% CO_2 conditions. To sustain cell cultures at approximately 70-85% confluency, adherent cells were trypsinized by adding 2 mL of trypsin solution (Gibco, 25200-056), and incubated at 37°C for 5 min. The trypsinization reaction was stopped by adding 10ml of pre-warmed fresh medium. RAW 264.7 cells were detached from the flask bottom using a cell scraper. Suspension cultures were centrifuged for 5 minutes at 100 g for dilution. Subsequently, cells were resuspended in a fresh medium. The cells were tested for *Mycoplasma* sp. contamination monthly using a PCR-based assay.

Table 2. A list of cell lines used in this study

Cell line	Name	Supplier
Jurkat	human T lymphoblast cells	ATCC, USA
HEK293	human embryonic kidney cells	ATCC, USA
HeLa	human cervical cancer cells	ATCC, USA
RAW 264.7	mouse macrophage cell line	ATCC, USA
EL4	mouse T lymphoblast cells	ATCC, USA
N2a	mouse neuroblastoma cell line	Prof. Dr Gary Lewin, MDC, Berlin
Raji	human B lymphocyte cell line	ATCC, USA
Ramos	human B lymphocyte cell line	ATCC, USA

3.2.1. Cryopreservation

After trypsinization, the cells were collected into the falcon tubes and centrifuged for 5 minutes at 100g. Subsequently, the supernatant was carefully aspirated, and the cell pellet was resuspended in 10ml of freezing medium containing 10% DMSO solution (1ml) and 50%

FBS (5ml). Cryo tubes (Sarstedt AG, Germany) were placed in a freezing box at -80°C overnight and stored later in liquid nitrogen.

3.3. Stimulation and inhibition experiments

Cells were stimulated with 20ng/ml of phorbol myristate acetate (PMA, Sigma- Aldrich, USA) or dimethyl sulfoxide (DMSO) as solvent control for different time points depending on the experiment design. As the alternative for PMA condition, Jurkat cells were activated with coated anti-CD3 antibody (1ug/ml, clone OKT3, BioLegend). N2a cells underwent depolarization by 60mM of KCl, and RAW264.7 cells were stimulated with 0.1 µg/mL of lipopolysaccharide (LPS, Invitrogen, Thermo Fisher Scientific, USA) (Table 3). FastAP Thermosensitive Alkaline Phosphatase (1 U/µL, Thermo Fisher Scientific™) was used to allow dephosphorylation of hnRNPC2 isoform; lysates were incubated for 1h at 37°C.

Table 3. A list of stimulators

Name	Abbreviation	Supplier
Phorbol myristate acetate	PMA	Sigma-Aldrich, USA
-	coated anti-CD3 Ab	BioLegend, USA
Potassium chloride	KCl	Carl Roth. Germany
Lipopolysaccharide Solution 500× eBio-science™, #00-4976	LPS	Invitrogen, Thermo Fisher Scientific, USA

For NMD/translation inhibition, cycloheximide (Sigma-Aldrich, USA) was used at a final concentration of 40 ng/mL, with DMSO as the solvent control. The following small molecule inhibitors were utilized: PD0325901 (MEK1/2), MK2206 (AKT1/2/3), VX-745 (p38), Ruxolitinib (JAK1/2), JNK inhibitor VIII (JNK1/2/3). For the PKCθ inhibition experiment, Jurkat T cells were exposed to the PKCθ inhibitor for 30 minutes before collection (Selleck, Houston, TX, USA), which was dissolved in DMSO at 5 mM and diluted to the working concentration (5 µM).

3.4. RNA sequencing

3.4.1. RNA sequencing from PMA-stimulated Jurkat T cells for 0, 30 and 150 minutes.

This analysis was performed by Dr. Marco Preußner (Prof. Florian Heyd's group).

For RNA-seq, Jurkat cells were seeded on T175 flasks and grown for 48 h at 37°C. Cells were then stimulated with PMA for 0 minutes (as a control), 30 minutes and 150 minutes. Chromatin-associated RNA was extracted as described below. Sequencing was performed on

an Illumina HiSeq 2500 system with V4 sequencing chemistry, generating around 40 million 125 bp paired-end reads per sample. Sequencing data are made available under GSE271051 (reviewer access token: mzmpqeqgflkjvch). The raw sequenced reads were aligned to the human hg38 reference genome with STAR (v2.7.9a) default parameters, resulting in ~65% unique alignment rate. AS analysis was done with rMATS turbo (v4.1.1), including variable-read-length criteria. We focused on alternative splicing events of exon skipping (SE), intron retention (IR), alternative 5'SS (A5SS) and alternative 3'SS (A3SS). Events were considered significant between two conditions if the mean absolute difference in percentage spliced in (PSI) was larger than +/- 0.15, if the false discovery rate (FDR) was smaller than 0.01 and if a splicing event has at least 100 combined junction reads across the tested samples. For PCA plot and heatmap PSI values of significant IR events comparing 0- and 30-minutes PMA treatment were used. In the heatmap, events are sorted by the fold change of mean PSI values 30 minutes divided by 0 minutes. STAR was run in GenCounts mode to allow gene level quantifications. Gene counts provided by STAR were tested for strandness and extracted using RSeQC (v4.0.0). The resulting count matrix was used as input for DESeq2 (version 1.28.1). Significantly differential genes were identified by filtering on Benjamini-Hochberg adjusted p-value (Padj) ≤ 0.001 and absolute log2FC ≥ 1 (or ≤ -1). Gene ontology (GO) term enrichment was performed using ShinyGO (0.80) for GO biological processes, comparing genes with retained introns after 30 minutes with all genes containing IR events quantified in Jurkat cells.

3.4.2. RNA sequencing from HEK293 and HeLa cells transfected with ΔhnRNPC2 knockout cell lines and WT CTRL

This analysis was performed by Dr. Bruna Los and Dr. Marco Preußner (Prof. Florian Heyd's group).

For CRISPR/Cas9 edited HeLa and HEK293 cells (see below) lacking hnRNPC2 isoform, triplicate DNase I-digested RNA samples of CTRL or ΔhnRNPC2 knockout were used for library preparation. Libraries were prepared as above. The raw sequenced reads were aligned to the human hg38 reference genome with STAR (v2.7.9a) default parameters, resulting in or ~95% (HeLa or HEK293) unique alignment rate. AS analysis was done as above with rMATS turbo (v4.1.1). Libraries were prepared using the mRNA enrichment method at BGI Genomics and sequenced using Eukaryotic Strand-specific Transcriptome Resequencing PE150 technique. STAR was run in GenCounts mode to allow gene level quantifications. Gene counts provided

by STAR were tested for strandness and extracted using RSeQC (v4.0.0). The resulting count matrix was used as input for DESeq2 (version 1.28.1). Significantly differential genes were identified by filtering on Benjamini-Hochberg adjusted p-value (Padj) ≤ 0.001 and absolute log2FC ≥ 1 (or ≤ -1). Sashimi plots were generated using the IGV browser.

3.4.3. RNA sequencing from HEK293 and HeLa cells transfected with hnRNPC2-inducing MO and CTRL MO

This analysis was performed by Luiza Zuvanov and Dr. Marco Preußner (Prof. Florian Heyd's lab).

For morpholino treated HeLa and HEK293 cells (see below), triplicate DNase I-digested RNA samples of CTRL or hnRNPC2 inducing morpholino samples were used for library preparation. Libraries were prepared as above. The raw sequenced reads were aligned to the human hg38 reference genome as above. AS analysis was done with rMATS turbo (v4.1.1). Libraries were prepared using the mRNA enrichment method at BGI Genomics and sequenced using Eukaryotic Strand-specific Transcriptome Resequencing PE150 technique. STAR was run in GenCounts mode to allow gene level quantifications. Gene counts provided by STAR were tested for strandness and extracted using RSeQC (v4.0.0). The resulting count matrix was used as input for DESeq2 (version 1.28.1). Significantly differential genes were identified by filtering on Benjamini-Hochberg adjusted p-value (Padj) ≤ 0.001 and absolute log2FC ≥ 1 (or ≤ -1).

3.5. Transfection

3.5.1. Transfection to adherent cells

HEK293 and HeLa cells were transfected using either ROTIFect (Carl Roth, Germany) or Lipofectamine 2000 (Thermo Fisher Scientific, USA), respectively, following the protocols provided by the manufacturers. Briefly, 2 µg of plasmid DNA of interest or 20 µM siRNA were mixed in 100 µL of Opti-MEM (Opti-MEM® I (1X) + GlutaMAX™-I - Reduced Serum Medium - Thermo Fisher Scientific, USA). In parallel, 2 µL of ROTIFect (or Lipofectamine 2000 for HeLa cells) was mixed in 100 µL of Opti-MEM and left at room temperature (RT) for 5 min. The plasmid or siRNA mix and the ROTIFect (or Lipofectamine 2000 for HeLa cells) mix were combined and incubated at RT for 20-30 min. The resulting transfection mixture was then added gently to each well. Morpholino oligos were transfected according to the manufacturer's protocol using Endo-Porter. After a 48-hour transfection period, cells were

rinsed once with ice-cold 1x PBS and then harvested for RNA or protein extraction. If required, cells were stimulated with different reagents at various time points directly before harvesting.

3.5.2 Transfection to suspension cells by electroporation

Transfections of Jurkat T cells were carried out using a Gene Pulser electroporation system (Bio-Rad) for morpholino experiments and a Nucleofector II (Amaxa Biosystems) for siRNA transfections. Electroporation procedures were executed according to the manufacturer's instructions.

3.5.3. Anti-sense morpholinos

Morpholino oligos (MO) were delivered to HEK293 and HeLa cells using the EndoPorter transfection reagent. Briefly, 3 µL of MOs were gently mixed with 6 µL of Endo-Porter and then added to wells containing the tested cell lines. Following a 48-hour incubation period, cells were harvested for RNA or protein extraction.

Before electroporation, Jurkat T cells were washed twice with 10 mL of Opti-MEM® I (1X) + GlutaMAX™-I – Reduced Serum Medium, transferred to 0.4cm gap cuvettes, and mixed with 20 nmol of morpholinos (stock: 300 nmol, standard control: 100 nmol). Samples were electroporated using the Gene Pulser electroporation system (Bio-Rad) under the following conditions: 250 mV, 960 µF, and time constant. Electroporated cells were transferred into 6-well plates containing 5 mL of fresh media and incubated at 37°C for 48 hours unless otherwise indicated. Anti-sense morpholinos and the Endo-Porter transfection reagent were purchased from Gene Tools (Table 4).

Table 4. Anti-sense morpholinos used in this study

Anti-sense morpholino	**Sequence (5' → 3')**
hnRNPC2	GGTGTTCTGTTACTGACCCGTACAT
eIF5A_IR	AGGGAGGCACCATACCAGGATCTCT
standard control	CCTCTTACCTCAGTTACAATTTATA

3.5.4 Small interfering RNA

For the siRNA transfection, either siRNAs (20 µM/mL) against PKCθ or a pool of four individual siRNAs against hnRNPC, hnRNPK, and U2AF35 were electroporated into Jurkat cells using the Nucleofector, II (Amaxa Biosystems) (Table 5). Jurkat cells were split one day before transfection to achieve 70-85% confluency. Cells were washed twice with 10 mL of Opti-MEM®

I (1X) + GlutaMAX™-I – Reduced Serum Medium, transferred to 0.1 cm gap cuvettes, and mixed with 20 nM of siRNA. Electroporation was performed using the cell-type specific program (G-10). Cuvettes were rinsed with fresh RPMI medium, and cells were transferred into a 12-well plate. At 48 hours post-transfection, cells were stimulated with PMA at different time points, and splicing modulation analysis was conducted. The transfection of siRNA into HEK293 and HeLa cells is described in Section 3.5.1.

Table 5. Sequence of the siRNAs against genes of interest

Name	**Target sequence (5' → 3')**
hnRNPC	CUUAAAUAGGAGAGGCUCA
	GUAAGUAACCCGUGACUAG
	UUUCAUAGCAUGCGGCACU
	CCUAGGCGCUUGUCUAAGA
hnRNPK	UAAACGCCCUGCAGAAGAU
	GGUCGUGGCUCAUAUGGUG
	UGACAGAGUUGUUCUUAUU
	GCAAGAAUAUUAAGGCUCU
U2AF35	CGCCGUCGCAAGAAGCAUA
	UGACCAAACCAGUUCAUAA
	UAGAAAGUGUUGUAGUUGA
	CAAGUUUCGCCGUGAGGAA
PKCθ	AAUUGACAUGCCACACAGA
	UUAGAAUUCCCAACCAUACA
siAllstar (control)	UUCUCCGAACGUGUCACGU

3.6. Generation of CRISPR/Cas9-edited HEK293 and HeLa cells

For CRISPR/Cas9-mediated deletion of the alternative hnRNPC2 in HEK293 and HeLa cells, sgRNA candidates were designed *in silico* using the Benchling tool [127]. Two pairs of oligonucleotides with the highest-ranked candidate sgRNA, targeting the alternative 5' splice sites in exon 4 (without affecting the upstream hnRNPC1) and one targeting the downstream intron (Fig. 21F), were synthesized and subcloned into either the pSpCas9(BB)-2A-GFP (pX458) plasmid (Addgene, USA) or pX459 (kindly provided by Stefan Mundlos). The sgRNA sequences are listed in Table 6. Briefly, the ligation of the two pairs of sgRNA sequences (either #1+#3 or #2+#3) was performed in the S1000 Thermal Cycler (Bio-Rad, USA) under the following conditions: 37°C for 30 min, 95°C for 5 min, followed by a ramp down to 25°C at 5°C/min. The pX458 and pX459 plasmids were digested with BpiI for 1 hour at 37°C and purified using the NucleoSpin® Gel and PCR Clean-up Kit (Macherey-Nagel, Germany) according to the manufacturer's protocol. BpiI-digested plasmids were combined with annealed oligo duplexes

by ligation (1 hour at rt, ~21°C). The ligated products were transformed into chemically competent Top10 *Escherichia coli* (*E. coli*). Following the incubation of grown bacterial cells, plasmids were isolated using the NucleoBond® Xtra Midi Kit (Macherey-Nagel, Germany) as described in the manufacturer's protocol. The sequence was verified by Sanger sequencing (Microsynth Seqlab, Germany).

Table 6. Sequences of guide RNAs

sgRNA:	**Sequence (5' → 3')**
sgRNA#1	TTCTCCGTCCCCTCTACTC
sgRNA#2	CTCTACTCAGGTCCGGAAC
sgRNA#3	CTGCATTGTGTCCATCAGT

sgRNA #3 and either #1 or #2 subcloned to pX459 plasmid were co-transfected to HEK293 cells using ROTIFect or HeLa cells using Lipofectamine 2000 according to the manufacturer's instructions (as shown in Section 3.5.1). 48h after transfection, cells were selected with 1 µg/ml puromycin (InvivoGen, USA) and clonal cell lines were isolated by dilution. To confirm the A5SS knockout on the DNA level, genomic DNA was extracted, and PCR was performed. Subsequently, potential independent positive clones were confirmed on the RNA and protein level, by performing radioactive, splice-sensitive PCR (Section 3.9) and Western-blot (Section 3.12.3).

3.6.1 Flow cytometry

sgRNA #3 and either #1 or #2 subcloned to pSpCas9(BB)-2A-GFP pX458 plasmid were co-transfected into HEK293 cells using ROTIFect or into HeLa cells using Lipofectamine 2000 according to the manufacturer's instructions (as detailed in Section 3.5.1). After 48h of transfection, cells were sorted based on GFP signal into 96 well plates using a BD FACS Melody™ Cell Sorter (BD Biosciences, USA). The sorted single cells were maintained in DMEM medium supplemented with 10% (v/v) FBS, and 1% (v/v) penicillin/streptomycin. To confirm the A5SS knockout on the DNA level, genomic DNA was extracted, and a PCR was performed. As shown above, potential independent positive clones were confirmed on the RNA and protein level, by performing radioactive, splice-sensitive PCR (Section 3.9) and Western-blot (Section 3.12.3).

3.6.2 DNA extraction

Prior the DNA extraction, 1ul of proteinase K (20 mg/mL; Serva, Germany) was added to the extraction buffer. Cells were resuspended in a fresh medium and transferred to 1.5ml Eppendorf tubes, followed by centrifugation for 4 min at 7000 RPM, 4°C. The cell pellet was resuspended in 300 µL of extraction buffer containing proteinase K and incubated at 56°C for 4h or overnight. After that time, samples were incubated at 95°C for 15 min to inactivate the proteinase K. Samples were then centrifuged at 13000RPM, 4°C and the supernatant was washed with 300ul of isopropanol. After the next centrifugation process and washing the pellet with 70% of ice-cold ethanol, the pellet was dried, and the DNA was used as a template for PCR. The DNA concentration was measured using a nanodrop spectrophotometer according to the manufacturer's instructions. The procedure to perform genotyping PCR is shown in Table 7. The PCR conditions for DNA genotyping are shown in Table 8. Primers used for DNA genotyping are listed in Table 9.

Table 7. Composition of a standard DNA genotyping PCR

Component	Stock concentration	Final concentration
Taq buffer	10x	1x
dNTPs	10 mM	200 µM
$MgCl_2$	50 mM	5 mM
Genomic DNA	Variable	<1000 ng
Forward primer	10 µM	100 nM
Reverse primer	10 µM	100 nM
Taq polimerase	5 U/µL	1.25 U/µL
H_2O	-	-

Table 8. Program of a standard DNA genotyping PCR

Step	Temperature [°C]	Time [min]	Cycles
Initial denaturation	95	5:00	1
Denaturation	95	0:30	35
Annealing	primer specific (usually 60)	0:30	
Extension	72	0:45	
Extension	72	7:00	1
Hold	4	∞	1

Table 9. A list of PCR primer sequences

Name	Target sequence (5' → 3')	Goal
hnRNPC2_F	ACTTTGTAGTTTGTTTTACCCGG	RT-qPCR
hnRNPC2_R	GGGTGTGGGGAGGTTTAAGT	RT-qPCR
mHPRT_qF	CAACGGGGGACATAAAAGTTATTGGTGGA	RT-qPCR
mHPRT_qR	TGCAACCTTAACCATTTTGGGGCTGT	RT-qPCR
hHPRT_qF	CCTGGCGTCGTGATTAGTGA	RT-qPCR
hHPRT_qR	TCTCGAGCAAGACGTTCAGT	RT-qPCR
mPKCθ_F	CAGGGACCTGAAGCTTGATAAT	RT-qPCR
mPKCθ_R	GCATCTCCTAGCATGTTCTCTT	RT-qPCR
hPKCθ_F	GAGGACAAGTGGAAAGTGAGAG	RT-qPCR
hPKCθ_R	CTTTCCATCCACCCATTCTCA	RT-qPCR
NheI_PKCθ_F	AATTGCTAGCATGTCACCGTTTCTTCGGTC	Cloning
XhoI_PKCθ_R	AATTTCTCGAGTCAGGAGCAAATGAGAGTCT	Cloning
c-FOS_F	CAA GCG GAG ACA GAC CAA CT	RT-qPCR
c-FOS_R	GTG AGC TGC CAG GAT GAA CT	RT-qPCR
hTraf4_F	CACCTCTGAGTGCCCCAAG	Splicing PCR
hTraf4_R	AGCCGGAGTCTTTGAATGGG	Splicing PCR
mTraf4_F	AGGTCCAGGTGTTAGGCTTGG	Splicing PCR
mTraf4_R	CCACTGAAGTCACAGCCACAG	Splicing PCR
RPL7A_F	TTAACACCGTCACCACCTTG	Splicing PCR
RPL7A_R	CAGTCTTGCCTTTCCCTTGA	Splicing PCR
hRPL10_F	GTAAGAACAAGCCGTACCCA	Splicing PCR
hRPL10_R	AGGACAGCTGCTCATATTCATCT	Splicing PCR
mRPL10_F	GGTATTGTAAGAACAAGCCATACC	Splicing PCR
mRPL10_R	CCACAAAGTGGGAATTCATCAAC	Splicing PCR
RPL13_F	GTTCGGTACCACACGAAGGT	Splicing PCR
RPL13_R	GTTGGCCTGCAGGGACTC	Splicing PCR
hEIF5A_F	CAGGACAGCGGGGAGGTA	Splicing PCR
hEIF5A_R	ATGGCCTTGATTGCAACAGC	Splicing PCR
mEIF5A_F	TACCTATCCCTGCTCCAGGAC	Splicing PCR
mEIF5A_R	GCCTTGATTGCAACAGCTGC	Splicing PCR
UBXN1_F	GCAATTGCTCAGTGGCTTC	Splicing PCR
UBXN1_R	GGACATTTCTTGGCCACAAT	Splicing PCR
USP11_F	CCTGGTCAGCTGGTATGGTC	Splicing PCR
USP11_R	ATTGTGCCGGACAAGCAG	Splicing PCR
HindIII_hnRNPC_F	ATATAAGCTTATGGCCAGCAACGTTACCA	Cloning
BamHI_hnRNPC_R	ATATGGATCCTTAAGAGTCATCCTCGCCATTGGC	Cloning
hnRNPC_S/Y-A_F	GCCGGGGCAGTAACAGAACACCCTGC	Cloning
hnRNPC_S/Y-A_R	AGCGTCCAAGTCAAAAGCGGCGGGGA	Cloning
BamHI_hnRNPC_FLAG_R	ATATGGATCCAGAGTCATCCTCGCCATTGG	Cloning
C2FL_S115D_FP	GAAGAGGACAGCAGAGGATCGGGAGAGGGGTGCTCAG	Cloning
C2FL_S115D_RP	CTGAGCACCCCTCTCCCGATCCTCTGCTGTCCTCTTC	Cloning
hnRNPC _F	TAGCAGGAGAGGATGGCAGA	RNA genotyping
hnRNPC _R	TCCCGTTGAAAGTCATAGTCCA	RNA genotyping

3.6.2. Electrophoresis

DNA products after PCR were loaded on agarose gels by electrophoresis. Agarose gels contained 1x TAE Buffer and 2% agarose (or 1% for molecular cloning or RNA electrophoresis). Gels were stained with ethidium bromide (0.5 mg/mL) for visualization of the DNA fragments. The PCR products were mixed with 10x orange gel loading dye and separated by electrophoresis at 150 V for 40 min. The Quick-Load® 1kb Plus DNA Ladder (New England Biolabs Inc., USA) was used to evaluate the size of the DNA fragments. The bands were visualized with UV light using the UVsolo touch system (Analytik Jena, Germany).

3.7. RNA extraction

3.7.1. Total RNA extraction

Before extracting RNA, all required buffers and reagents were prepared in advance. The bench and the hood were cleaned by RNase AWAY™ Surface Decontaminant (Molecular BioProducts, USA). The whole experiment was carried out in ice blocks. Cultured cells were rinsed once with ice-cold PBS. Then 1ml of RNA Tri-flüssig (BIO&CELL) was directly added to each well and transferred to a 1.5ml RNAse-free tube. Subsequently, 200ul of Trichloromethane/Chloroform (Carl Roth, Germany) was added and mixed thoroughly by vortexing (1:5 ratio according to the manufacturer's instructions). Suspension cells were harvested similarly, but the RNA Tri-flüssig was added to an already transferred 1.5ml RNAse-free tube. The mixture was incubated for 10 min, followed by a centrifugation step at 13000 RPM and 4°C for 10 min. The aqueous layer was transferred to new 1.5ml tubes containing 600ul of isopropanol. Cells were vortexed and centrifuged at 13000 RPM for 30 min at 4°C. The pellet was then precipitated with 1ml 70% ethanol absolute, dried at rt, and resuspended in RNA-se free H_2O.

In the following step, DNase-I digestion was performed to remove DNA contamination. 2ul of DNase I (Biosearch Tech, UK) and 2ul of 10x DNase buffer were added to RNA tubes, followed by 20 min of incubation at 37°C. After that time, 200ul of ROTI®Aqua-P/C/I (Carl Roth, Germany) was added to these samples. Further, this mixture was vortexed and centrifuged for 15 min at 13000 RPM and 4°C. The aqueous layer was then transferred to new RNA-se free tubes containing 600ul of 100% ethanol absolute, 1ul of glycogen and 20ul of 3M sodium acetate. Samples were vortexed thoroughly and then centrifuged at 13000 RPM for 4°C. The

pellet was then washed with 1ml 70% ethanol absolute, dried at RT and resuspended in RNA-se free H_2O to have at least 500ng/ul or the lowest concentration among all tested RNA samples. The RNA concentration was determined using a Nanodrop spectrophotometer (at wavelengths of 260 nm and 280 nm) according to the manufacturer's instructions.

3.7.2. Chromatin-associated and cytoplasmic RNA extraction

Before extraction, all required buffers were prepared one day earlier. RNA-se inhibitor (Thermo Fisher Scientific, USA) was added to each buffer directly before starting the procedure. Cells were resuspended in 100ul of cold CTX buffer and incubated for 5 min on ice to extract chromatin-associated RNA. After that time, an additional 100ul of cold CTX buffer was added containing 0.2% (v/v) NP-40, gently pipetted up and down 3-5 times and again incubated for 5 more min. Cytosolic and nuclear fractions were separated by a centrifugation step at 6500 RPM for 3 min at 4°C. The supernatant (cytosolic fraction) was discarded or transferred to another 1.5ml RNA-free epi tube and 400ul of RNA Tri-flüssig was added to continue RNA extraction as shown in Section 3.7.1. The nuclear pellet was resuspended in 40ul of NX buffer. The additional step of centrifugation (3 min, 4°C, 13000 RPM) allowed the separation of nuclei into nucleoplasm and chromatin. The supernatant with the nucleoplasm was removed and the chromatin pellet was resuspended by RNA Tri-flüssig, which was followed as shown in Section 3.7.1.

3.7.3. RNA electrophoresis

To check the quality of RNA extracted, 2ul of RNA was mixed with 10x orange gel loading dye (2ul) and separated by electrophoresis as shown above. Before loading samples to the gel, champers, combs, pipettes etc. were sprayed with RNase AWAY™ Surface Decontaminant. 1% agarose gels were made with fresh RNA-se free H_2O. The gel was run at 150 V for 12-15 min. The bands were visualized with UV light using the UVsolo touch system (Analytik Jena, Germany).

3.8. Reverse transcription polymerase chain reaction

The goal of this experiment was to generate single-stranded cDNA from isolated RNA. At first, 5x hybridization buffer and gene-specific reverse primer mix (1ng/ul) were mixed in a 1:1 ratio. Further, 2ul of isolated RNA (≤500ng/ul) was mixed with a mixture of reverse primers and 5x hybridization buffer. PCR samples were run in PCR program I (Table 10).

Table 10: PCR program I

Cycles	Temperature [°C]	Time [sec]
1	90 … 70	20
	69 … 51	30
	50 … 44	40
	43	∞

While the PCR program I was running, 1.25x RT buffer containing dNTPs was pre-heated to 43°C in the heating block (Bioer Technology Co, China). When the PCR program I was finished, MMuLV reverse transcriptase (Enzymatics Inc., USA) was added to the RT buffer, quickly vortexed and the mixture was added to all PCR samples. Further, they were run in PCR program II (Table 11).

Table 11: PCR program II

Cycles	Temperature [°C]	Time [min]
1	43	30
	94	5
	4	∞

3.9. Radioactive, splicing sensitive RT-PCR

The radioactive, splicing-sensitive RT-PCR was performed to analyze alternative splicing changes. The components of the PCR mix are listed in Table 12. Single-stranded cDNAs were used as a template. Forward gene-specific primers were labeled radioactively using 1ul T4 PNK (10 U/Ml, Thermo Fisher Scientific, USA) enzyme, 10 µL of PNK buffer and γ-^{32}P-dATP (10 µCI/µl, 6000 Ci/mmol, Hartmann Analytic, Germany). The marker (pBR322-Mspl Digest (New England Biolabs Inc., USA) was also radioactively labeled. To protect samples from evaporation, they were covered with mineral oil. The PCR program is shown in Table 13.

Table 12: Composition of the radioactive, splicing-sensitive PCR

Component	Final concentration
10x Taq buffer	1x
Forward primer	2.5ng
Reverse primer	5ng
[^{32}P]-labeled forward primer	2.5ng
Taq Polymerase (5U/µL)	2.5U
Template	variable

Table 13: The PCR program for radioactive, splicing-sensitive PCR

Step	Temperature [°C]	Time [min]	Cycles
Initial denaturation	95	5:00	1
Denaturation	95	0:30	30
Annealing	primer specific (usually 60)	0:30	
Extending	72	0:45	
Extending	72	7:00	1
Hold	4	∞	1

PCR products were then mixed with 2x formamide loading dye, incubated for 5 minutes at 95°C and loaded on the previously prepared denaturing polyacrylamide (PAGE) gels in the presence of 7 M urea. The same volume of 7 M Urea/0.5x TBE and 10% Acrylamide/7 M Urea/0.5x TBE were mixed, followed by the addition of 10% APS (ammonium persulfate, 1:100) and TEMED (1:100) (Table 14). This mixture was poured between glass plates covered with tape. The gel was dried for 15-30 min. Radioactively labeled markers were also loaded to evaluate sizes of bands. The electrophoresis was performed at 28-32 mA for 30-40 min. After the run, gels were washed by fixation buffer and transferred to Whatman paper, vacuum-dried for up to 2h at 50°C and put in a cassette for overnight exposure. Strongly radioactive bands were measured earlier than 24h of exposure. The cassette was then imaged with the GE Healthcare Typhoon 7000 FLA imager and the result was quantified using the GE ImageQuant TL 8.1 software.

Table 14: PAGE gel composition

Stock concentration	Final concentration
7M Urea/0.5x TBE	50%
10% acrylamide/7M urea/0.5x TBE	50%
10% APS	0.1%
TEMED	0.01%

3.10. RT-QPCR

RT-qPCR was performed to analyze the expression of target genes in different conditions. Gene-specific primers are shown in Table 9. For this experiment, housekeeping genes were used as follows (hHPRT for human cell lines and mHPRT for mouse cell lines). The RT-qPCR was performed in 96-well plates using Absolute QPCR SYBR Green Mix (Thermo Fisher, USA) in the Stratagene Mx3000P instrument (Bioer Technology Co, China). For one experiment, a maximum of 4 different genes were tested, including the housekeeping gene.

250 nM of gene-specific reverse and forward primer, 1x qPCR S'Green BlueMix (Biozym, Germany), and diluted cDNA were mixed in a total volume of 20 µL. The reactions were performed in duplicates and at least three biological replicates. Mean CT values from target genes were normalized to the expression of the housekeeping gene. The ΔCT was calculated using the CT of the housekeeping gene and the gene of interest. Error bars represent standard deviation, and p values were calculated using Student's unpaired t-test. Significance is indicated by asterisks (*p < 0.05; **p < 0.01; ***p < 0.001; ****p < 0.0001).

3.11. Molecular cloning

Cloning of PKCϑ

The PKCθ overexpression construct inserted into pBS plasmid was ordered and delivered from addgene (Plasmid #8426). Cloning was performed using NheI and XhoI restriction sites introduced through PCR primers. PCR products were digested, ligated directly into a pCMV-N3-FLAG expression vector to yield an N-terminally FLAG-tagged protein, and transformed into competent Top 10 *E. coli* cells. Midi prep was performed afterward according to the manufacturer's instructions using the NucleoBond Xtra Midi kit. Constructs were then identified by Western Blot and verified by sequencing to confirm correct insertion.

Cloning of EIF5A_WT and EIF5A_IR

EIF5A_WT and IR codon optimized-inserts were cloned into pTWIST CMV expression vectors containing FLAG-tag at the N-terminal end. These constructs were ordered as synthetic DNA oligonucleotides purchased from Twist Bioscience ready-to-use for transfection experiments and verified by sequencing.

Cloning of hnRNPC2_WT and hnRNPC2_S→A/Y

To design a non-phosphorylated hnRNPC2 frameshift mutant, all potential phosphorylation sites in the hnRNPC2-specific amino acids and surrounding residues in hnRNPC1 were substituted with alanine or tyrosine. hnRNPC2 substitution mutants were generated by PCR with a WT hnRNPC2 expression plasmid as a template. hnRNPC2 mutant open reading frame was amplified and cloned into pCMV-N3-FLAG expression vector using plasmid-complementary primers (Table 9) to yield an N-terminally FLAG-tagged protein. Subsequently, DNA fragments and vectors were digested by restriction enzymes (HindIII and BamHI), ligated and then transformed into competent Top 10 *E. coli* cells. Midi prep was

performed afterward according to the manufacturer's instructions using the NucleoBond Xtra Midi kit. Constructs were then verified by sequencing to confirm correct insertion. Cloning of two hnRNPC2 variants (WT and S→A/Y) was performed by Dr. Debojit Bose.

3.11.1. PCR amplification

To introduce the restriction sites into the constructs mentioned above the DNA fragments were amplified by PCR in a maximum volume of 50 µL (Table 15). In Table 16, we showed the conditions for standard PCR.

Table 15. Composition of standard PCR

Component	Final concentration
Phusion® HF Buffer (5 X)	1x
Forward primer	200nM
Reverse primer	200nM
dNTP mix	200uM
DNA Polymerase (100U/µL)	0.02 U/µL
Template (plasmid)	1 ng/µL

Table 16. The conditions for standard PCR

Step	Temperature [°C]	Time [min]	Cycles
Initial denaturation	98	3:00	1
Denaturation	98	0:30	30
Annealing	primer specific (usually 60)	0:30	
Extending	72	1:30	
Extending	72	7:00	1
Hold	4	∞	1

3.11.2. DNA digestion

The digestion of PCR products and plasmids was performed using restriction enzymes and FastDigest Buffer (10x). The total reaction volume was 20ul. Samples were digested at 37°C for 1h. Subsequently, the digested plasmids were resolved on a preparative 1 % agarose gel and the band of interest was cut, while digested PCR products were purified directly. Both products were purified by using the NucleoSpin® Gel and PCR Clean-up kit.

3.11.3. Ligation of digested insert and plasmid

The ligation of the insert and plasmid was performed in 10ul reaction volume at RT either for 1h or at 16°C for overnight incubation. The ligation product was immediately transformed into competent *E. coli* cells.

3.12. Protein isolation

All steps of total protein extraction were performed on ice. Cells were harvested and washed once with 1x ice-cold PBS. The pellet was washed with 1X RIPA buffer containing protease and phosphatase inhibitors (PMSF -1:100, Aprotinin-1:200, Leupeptin-1:200, and Vanadate-1:500, Carl Roth, Germany). 50ul of RIPA buffer was added to each sample. Samples were vortexed for 10 min on ice and then centrifuged at maximal speed (13000 RPM) for 15 min at 4°C. The obtained lysates were transferred to a fresh epi-tube and stored on ice.

3.12.1. Protein quantification

The Roti-Nanoquant Bradford assay was used to measure the protein concentration extracted. The assay uses Coomassie Brilliant Blue G250 (5X stock, Carl Roth, Germany) for colorimetric detection. A BSA (bovine serum albumin, Thermo Fisher Scientific, USA) calibration curve was made every time of protein quantification. Absorbance for 450nm and 590nm was measured from each cuvette using a Nanophotometer (Serva, P-330). The ratio between OD450/OD590 was calculated and the samples were adjusted with 1xRIPA buffer to maintain the same protein concentration. Protein samples were supplemented with 2X SDS loading dye (1:1 ratio) and denatured at 95°C for 5 min.

3.12.2. Denaturing SDS polyacrylamide gel-electrophoresis (SDS-PAGE)

Polyacrylamide gels were prepared (Table 17) before performing the SDS-PAGE electrophoresis. The separating gel included 12-15% polyacrylamide (depending on the size of proteins of interest; stock: 30%, 37.5:1) and the stacking gel contained 4% polyacrylamide. The same amount of protein was loaded on wells, alongside the PageRuler Plus Pre-stained protein ladder (Thermo Fisher Scientific, 26620). The electrophoresis was performed in 1X SDS running buffer for approximately 2h at 80-140V. Proteins in a gel were transferred to a nitrocellulose membrane (Amersham Protran nitrocellulose 0.45 µm), to perform Western Blot.

Table 17. Composition of polyacrylamide gels

Component	Stock concentration	Separation buffer	Stacking buffer
Acrylamide	30%	12%/15%	4%
Tris-HCl, pH 6.8	1M	-	125mM
Tris-HCl, pH 8.8	1M	375mM	-
SDS	10 % (w/v)	0.1%	0.1%
APS	20 % (w/v)	0.14%	0.1%
TEMED	100%	0.07%	0.1%

3.12.3. Western Blot

After SDS-PAGE electrophoresis, gels were transferred into nitrocellulose membranes using the BioRad Mini Trans-Blot wet/tank blotting system. For assembling the transfer sandwich, six pieces of Whatman paper and the membrane were soaked in pre-cooled 1X transfer buffer containing 20% methanol. The sandwich assembly was as follows: sponge, three Whatman papers, SDS-PAGE gel, nitrocellulose membrane, three Whatman paper, and sponge. The electrotransfer was conducted at 110V for 1h with the BioRad Mini Trans-Blot Electrophoretic Transfer cell system. Ice blocks were used to prevent overheating of the transfer buffer. Subsequently, the membrane was blocked in 2% BSA in 1X LS-TBST for one hour. Then primary antibodies were added to the membranes and incubated at 4°C overnight. Primary antibodies are listed in Table 18. The immunoblotting was followed by 3 washing steps, each lasting around 6 min with 1 X HS-TBST. Afterward, the membrane was incubated with the secondary antibody (horseradish peroxidase-conjugated anti-mouse or anti-rabbit) for 1h at RT. After three washing steps with 1 X HS-TBST, proteins were detected by enhanced chemiluminescence using Pierce™ ECL Western Blotting Substrate (Thermo Fisher Scientific, USA) according to manufacturer's instruction. Membranes were imaged using a GE Al600 RGB GEL Imaging System and the results were quantified using the GE ImageQuant TL 8.1 software.

Table 18. Antibodies used in the study

Antibody	Dilution	Supplier
hnRNP C1/C2	1:1000	Santa Cruz Biotechnology, sc-32308
p-ERK	1:1000	Santa Cruz Biotechnology, sc-7383
ERK 1/2	1:1000	Santa Cruz Biotechnology, sc-514302
DYKDDDDK Tag	1:2000	Cell Signaling Technology
GAPDH	1:1000	Santa Cruz Biotechnology, sc-32233
hnRNPL	1:1000	Santa Cruz Biotechnology, sc-32317
Puromycin	1:5000	Sigma-Aldrich, 12D10

3.12.3.1. Western blot SUnSET (WB-SUnSET)

For measuring protein synthesis *in vitro* by WB-SUnSET assay, HEK293 and Jurkat cells were treated with 10ug/ml puromycin (P8833, Sigma-Aldrich) for 10 min before harvesting. To confirm that WB-SUnSET was suitable to detect changes in protein synthesis, cells were treated with cycloheximide (Sigma-Aldrich, USA) at a final concentration (2ug/ml) for 1h before the puromycin treatment. The lysates were then normalized for equal amounts of protein using the Bradford method and Western blot was performed as shown above. The membranes were then incubated with anti-puromycin antibody (Table 18), followed by secondary antibody linked to horseradish peroxidase (anti-mouse IgG HRP, 1:5000, Cell Signaling Technology) and detected as shown above. The results were quantified using the GE ImageQuant TL 8.1 software.

3.12.3.2. ^{35}S-Met Incorporation Assay

Jurkat cells were seeded in 12-well plates and cultured overnight prior to transfection with a pool of 4 siRNA against hnRNPC and control as described in Table 5. At 1-day post transfection, cells were washed twice with methionine-free DMEM supplemented with 10% FBS and stimulated with PMA for different times (from 0 min to 24 hours). During PMA stimulation, 1 ul of ^{35}S-Met (>1,000 Ci (37.0TBq)/mmol; Hartmann Analytic) was added to each well for 30 minutes before harvesting. Labeled cells were washed twice with PBS, and protein lysates were prepared as shown above. Equal amounts of protein were separated on 15% SDS-PAGE (Table 17). The gel was then stained with Coomassie Brilliant Blue G250, dried, and autoradiographed. Radioactivity in whole lysates was determined using a scintillator counter. This experiment was performed by Dr. Debojit Bose.

3.13. hnRNPC2 protein purification

This part was performed by Gopika Sasikumar (Prof. Markus Wahl lab).

The hnRNPC2 full-length construct was designed codon-optimized with an N-terminal Twin-Strep-tag® and SUMO tag for recombinant production from GeneArt custom gene synthesis service (ThermoFisher Scientific) and cloned into pETM-11 vector using primers shown in Table 9. hnRNPC2 WT and S115D mutant were expressed in *E. coli* BL21 RIL cells in terrific broth media. Following normal growth, cells were induced at an OD600 nm of 0.8-1.0 with 0.4mM IPTG followed by protein expression for 16h at 18 °C. Cells were collected by

centrifugation, lysed by sonication in the presence of DNase, lysozyme, and EDTA-free complete protease inhibitor (Roche Applied Science), then re-suspended in binding buffer consisting of 50 mM Tris (pH 8.0), 500 mM NaCl, and 2 mM β-mercaptoethanol (BME). The cleared lysate was passed over a StrepTrap™ 5mL column (GE Healthcare). Elution with 50 mM Tris (pH 8.0), 500 mM NaCl, 2.5mM desthiobiotin, and 2mM BME was followed by tag (TwinStrep-SUMO) removal with PreScission protease (1:20) overnight. The eluate was concentrated using Amicon Ultra (10kDa), Millipore centrifugal filter unit and passed over Superdex 200 16/60 size-exclusion column (GE Healthcare) in a buffer containing 50mM Tris-HCl pH 8.0, 200mM NaCl, and 2mM DTT. The peak fractions were pooled, concentrated, and aliquots were flash-frozen, and stored at -70°C. The amount of proteins loading was stained by Coomassie blue.

3.13.1. EMSA

RNA electrophoretic mobility shift assays were carried out in an EMSA binding buffer (components of the buffer are shown in Section 3.1). The RNA probes containing parts of regulated introns, including the splice site AG (30 nucleotides), were ordered from Eurofins Genomics (Table 19).

Table 19: Sequences of RNA oligonucleotides

Name	Sequence (5'→ 3')
RPL10	ACCCCCUGCACACUUACCCAAUCCUUUUAG
eIF5A	AUCUCUUGGCUAUCCCUCUUGCUUCUCCAG
TRAF4	ACUCCUGCCUCUCUACUUCUGUGGCCCCAG

Furthermore, the 45 nucleotides stretch of poly-U was used as a positive control (ThermoFisher Scientific). The radioactivity of introns of interest was achieved by 5'end ^{32}P-labeling with PNK (T4 PNK (10 U/µL, Thermo Fisher Scientific, USA). 1 X PNK buffer was mixed with RNA (10pmol), and then 1ul of T4 PNK (10 U/Ml) enzyme was added. Samples were kept on ice. Subsequently, 1ul of γ-^{32}P-dATP (10 µCl/µl, 6000 Ci/mmol) was added, mixed, and incubated in a heat block at 37°C for 1.5h. Meanwhile, Illustra MicroSpin G-25 columns (GE Healthcare) were prepared, following the manufacturer's instructions. After incubation, samples were diluted up to 50ul and carefully loaded onto the column. Then, samples were spun down for 2 min at 735g. The column was discarded from epi-tubes, radiation was measured and labeled RNA was stored at -20C. Two versions of hnRNPC2 full-lengths: WT and

S115D mutant were diluted to 20uM to have the same amount of protein used for EMSA (hnRNPC2_WT: stock conc. 268uM, hnRNPC2_S—>D: stock conc. 595uM). Subsequently, increasing concentrations of proteins were added to probes containing ^{32}P-labeled RNA in binding buffer (up to 20ul) and incubated at 37°C for 20 min. Furthermore, 1ul of RNA-se inhibitor and 1ul of heparin (5000U) were added to each PCR sample to inhibit non-specific binding and improve the specificity of RNA:protein interactions, respectively. Subsequently, 5ul of 6x EMSA loading dye was added to each PCR sample and mixed by gentle up-and-down pipetting. The samples were then separated into a pre-prepared 5% polyacrylamide gel and exposed to autoradiography. Table 20 provides the composition of the polyacrylamide gels. The gel containing loaded RNA: protein complexes was run at 150V (8-12mA) for 2-3h at 4°C (Biometra, Standard Power Pack, P-25). After that time, the gel was transferred to Whatman paper, and put into a cassette for overnight exposure at -80°C. The screen was then imaged using the GE Healthcare Typhoon 7000 FLA imager, and the result was quantified using the GE ImageQuant TL 8.1 software. To determine the bindings levels of hnRNPC2 FL and S115D mutant to the introns of interest, binding intensities were quantified relative to free RNA (mean ± SD, n = 3).

Table 20. The composition of polyacrylamide gels for EMSA

Component	Stock concentration	Buffer
Acrylamide	30%	5%
TBE	5X	0.5X
APS	10 % (w/v)	0.16%
TEMED	100%	0.06%

3.14. Statistical analysis

Data represent mean values of at least 3 biological replicates (exact numbers are given in the figure legends), and error bars represent standard deviation. Statistical significance was determined using GraphPad Prism version 8.4.3, calculated by Student's unpaired t-test, and accepted at $p \leq 0.05$. In the figure legends, "ns" indicates $p \geq 0.05$ – non-significant, * indicates $p \leq 0.05$, ** indicates $p \leq 0.01$, *** indicates $p \leq 0.001$ and **** indicates $p \leq 0.0001$.

4. Results

Most of the data and figures in the results part were submitted to: Mateusz Dróżdż, Luiza Zuvanov, Gopika Sasikumar, Debojit Bose, Franziska Bruening, Maria S. Robles, Marco Preußner, Markus Wahl, Florian Heyd. Immediate early splicing mediated by hnRNPC2 phosphorylation controls translation after T cell activation. In revision. *EMBO, 2024.*

4.1. Nascent RNA-seq analysis revealed immediate early splicing upon T cell activation

Analysis of nascent RNA sequencing was performed by Luiza Zuvanov and Dr. Marco Preußner

Studies focused on the altered IEG expression at early stages of T cell activation have already been characterized. The induction of IEGs is known to rely on phosphorylation cascades, mainly involving the RAF/MEK/ERK pathway[108,114128.] We hypothesized that the splicing machinery could be similarly targeted as in the case of transient IEG expression. Therefore, we addressed potentially occurring AS patterns during the first minutes of T cell activation; a timeframe that coincides with the induction of expression of known IEG – *c-fos* (Fig. 12A) [91,113,114,117,119,128]. We stimulated an immortalized line of human T lymphocyte Jurkat cells at 0-, -30-, and -150-minutes using PMA, extracted chromatin-associated RNA and performed RNA sequencing. Only by analyzing this RNA molecule, we could capture immediate early changes in splicing patterns upon stimuli. While performing total RNA-seq, nascent RNA would represent a minor fraction of total RNA in a cell, making it challenging to capture potentially occurring IES switches. Different types of AS were identified by rMATS analysis. We observed changes in splicing patterns by comparing resting Jurkat T cells, with cells stimulated for 30 minutes, and Jurkat T cells stimulated for 30 minutes and 150 minutes. All types of AS were analyzed (Fig. 12B), but intron retention particularly drew our attention (Fig. 12B, C, D). A principal component analysis of significantly changed IR events between 0 and 30 minutes revealed clustering of the biological duplicates, with unstimulated cells showing more similarity to those stimulated for 150 minutes. In contrast, cells stimulated for 30 minutes were distinct from the other conditions (Fig. 12C). A more detailed analysis revealed that the vast majority of these introns are retained after 30 minutes of stimulation but return to basal levels after 150 minutes (Fig. 12D). Only a low percentage of introns showed the opposite pattern – more efficient splicing after 30 minutes of T cell activation (Fig. 12D). Consistently, transcripts containing retained introns after 30 min of PMA stimulation also showed a slight transient induction of gene expression (Fig. 12E). This was also observed

in our target genes – *RPL10, eiF5A* and *TRAF4* (Fig. 12F), which will be analyzed in further experiments. These results suggest that, upon 30 minutes of PMA stimulation, either transcription rate of these genes is increased (more synthesis over decay) or intron-retained transcripts are maintained in the chromatin-associated fraction of the RNA, preventing their export to the cytoplasm.

Many IR events were found within pre-mRNAs encoding components of the translation apparatus, which is also reflected in translation-related GO terms being highly enriched (Fig. 12G). As the vast majority of approximately 6.000 rMATS-quantified introns are unaffected, we rule out a general reduction of splicing efficiency 30 minutes post stimulation and suggest that this splicing switch is specific to certain selected introns. Notably, most of the affected introns were relatively short (<100nts).

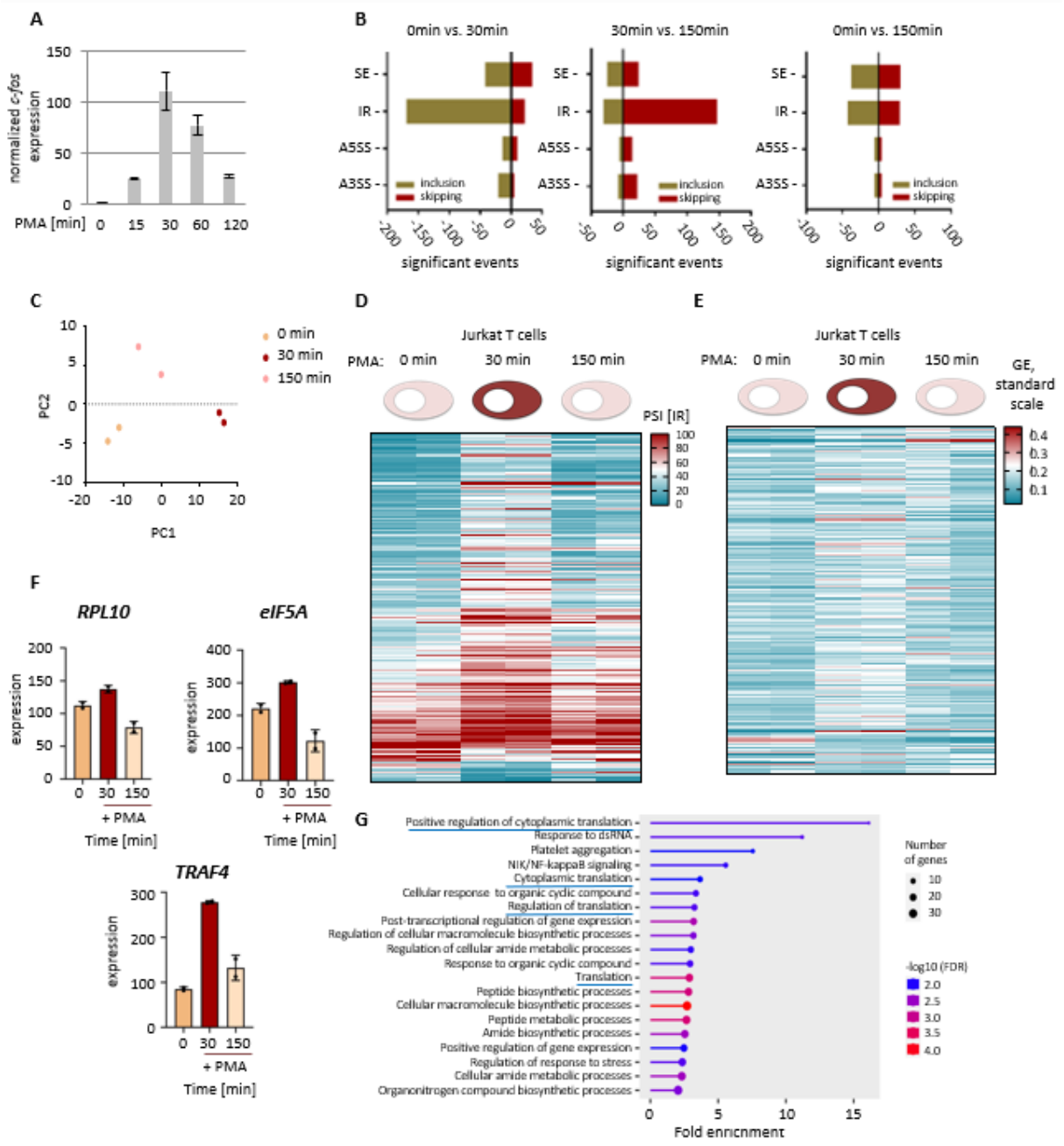

Figure 12: Nascent RNA-seq analysis of Jurkat T cells stimulated with 0 min, -30min, and -150 minutes. A) Jurkat cells were stimulated with PMA at indicated time points. Cells were harvested, and total RNA was extracted. *c-fos* expression was analyzed by RT-qPCR (n = 3, mean ± SD). **B)** rMATS analysis identifying significant changes (see methods) in AS of the following types: skipped exon (SE), retained introns (IR) alternative 5' splice site (A5SS) or 3' splice site (A3SS). Pairwise comparisons for 0 vs 30, 30 vs 150 and 0 vs 150 minutes are shown (from left to right). Increased IR events were observed when non-stimulated cells (0 minutes) were compared with cells PMA-stimulated for 30 minutes. An antagonistic effect was observed when comparing 30 and 150 minutes. **C)** Principal component analysis of the duplicate samples of PMA-stimulated Jurkat T cells analyzed by nascent RNA sequencing, based on significantly changed IR events between 0 and 30 minutes. **D)** Heatmap of IR events as in B and C. PSI (percentage spliced in) values are shown for biological duplicates, sorted by fold change at 30 minutes vs. 0 minutes. **E)** Heatmap of gene expression across all samples representing PMA stimulation at indicated time points. Duplicate samples are shown. Only genes containing significant changes in IR are shown. Genes are sorted by the change in PSI comparing these

conditions, with more IR at 30 minutes at the top. Note a mild increase in gene expression for genes with activation induced intron retention (top) while genes with activation induced intron splicing show rather reduced or unchanged expression (bottom). **F)** Quantifications of expression of target genes based on the nascent RNA-seq analysis (*RPL10, eIF5A*, and *TRAF4*; mean ± SD, n = 2). **G)** The strongest GO term enrichments of genes containing retained introns after 30 min of PMA stimulation. GO terms containing the term „translation", are underlined in blue.

To validate our nascent RNA-seq data findings, changes in splicing patterns during T cell activation were investigated by radioactive, splicing-sensitive RT-PCR. For validation, genes with the highest peak for PSI IR after 30 min of PMA stimulation were selected. All target genes showed a splicing pattern similar to that observed in the nascent RNA-seq data (Fig. 13A), confirming the validity of our analysis pipeline. We observed the same splicing switch when *de novo* protein synthesis was inhibited by the presence of cycloheximide (Fig. 13B). These experiments demonstrate a fast and transient splicing switch that occurs 30 minutes after PMA stimulation of T cells, thereby establishing the concept of immediate early splicing (IES). The validation of the bioinformatic analysis was performed by Dr. Debojit Bose. We chose two target genes, *RPL10* and *eIF5A*, for further experiments as examples representing other validated IEGs. These genes are components of translation machinery and show an approximately two-fold induction of IR 30 minutes after PMA-stimulation (Fig. 13A, B). To prove the activity of this mechanism under physiological conditions, Jurkat T cells were stimulated with two different concentrations of anti-CD3 antibody (1ug and 2ug) and PMA as a positive control. As expected, we observed the induction of IR after 30 min of stimulation with the anti-CD3 antibody, confirming presence of IES in T cells (Fig. 13C for *RPL10* and D for *eIF5A*). Altogether, we revealed the rapid and transient induction of IR events among IEGs upon 30 minutes of PMA stimulation. These IR events were independent of *de novo* protein synthesis, delineating the concept of immediate early splicing.

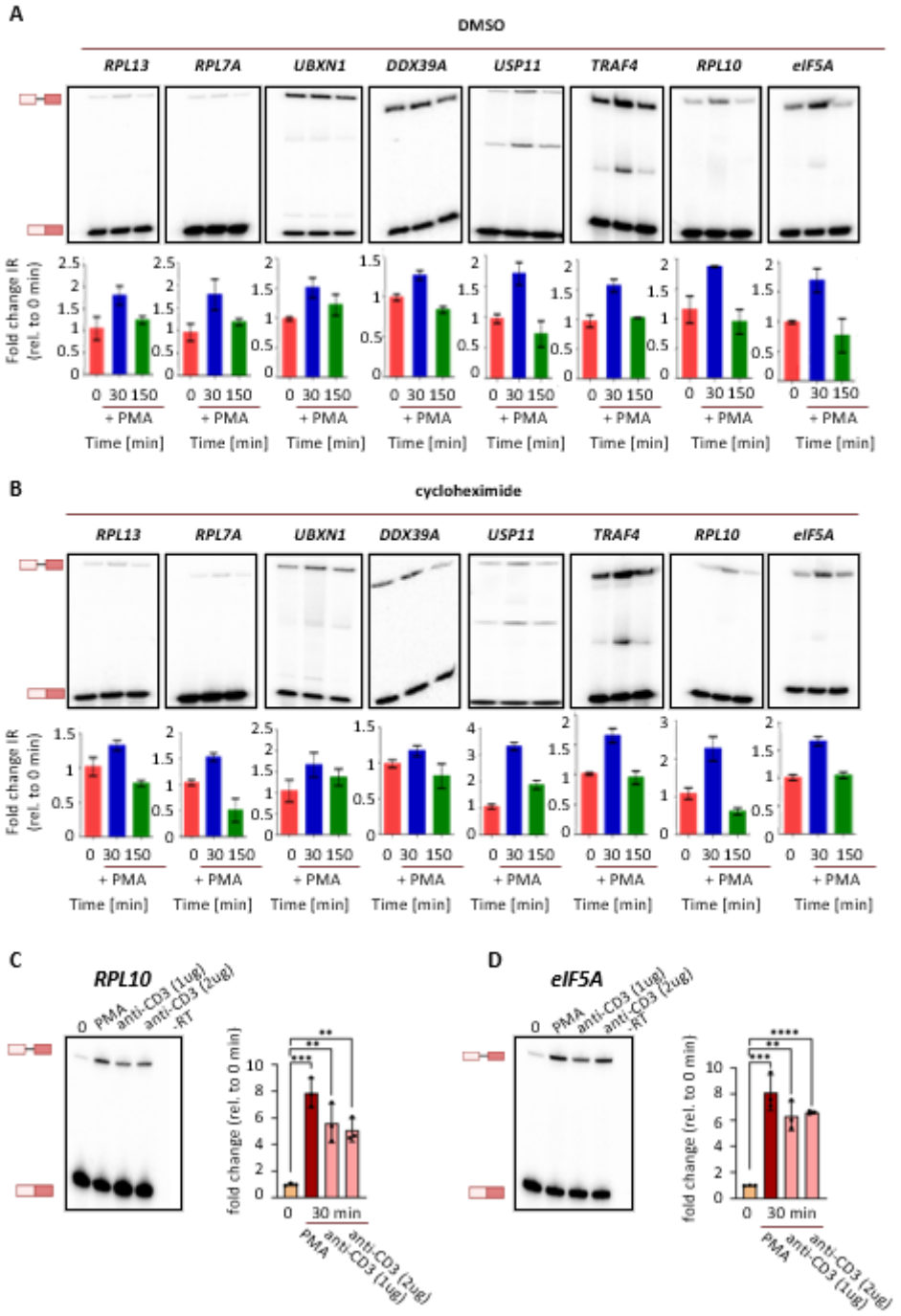

Figure 13. Validation of bioinformatic analysis. A) Jurkat cells were stimulated with PMA for the indicated times (0 min, 30min, 150min). Cells were harvested and chromatin-associated RNA was extracted. Selected IES events were analyzed by radioactive, splicing-sensitive RT-PCR (top) and quantified (bottom, fold change IR normalized to 0 min, mean ± SD, n = 3, performed by Dr. Debojit Bose). **B)** Jurkat cells were stimulated and analyzed as in A but cycloheximide was present during PMA stimulation (performed by Dr. Debojit Bose) **C, D)** Jurkat cells were stimulated for 30 minutes either by PMA or more physiological stimuli - anti-CD3 Ab (with the indicated amounts). Radioactive, splicing-sensitive RT-PCR confirms IES in *RPL10* (C) and *eIF5A* (D), -RT, without reverse transcriptase. Splicing products are indicated on the left side of the gels. Right: corresponding quantifications (fold change, normalized to 0 min; student's unpaired t-test; mean ± SD, n = 3, **p<0.01, ***p<0.001, ****p<0.0001).

4.2. hnRNPC2 phosphorylation is in line with IES

We then aimed to address the upstream mechanism leading to the induction of IR events upon T cell activation. Which spliceosome components or splicing-regulatory proteins regulate the splicing switch? In collaboration with Prof. Maria S. Robles from the Institute of Medical Psychology and Biomedical Center, Ludwig Maximilian University of Munich, Germany, we performed label-free quantitative phosphoproteomics in Jurkat cells stimulated with PMA for 0, 15, 30 and 90 minutes. This experiment revealed many different candidates with a transient change in phosphorylation. One of the most significant changes in phosphorylation over time, which aligned with IES, was observed in hnRNPC. This data showed the highest peak in phosphorylation in one specific serine residue, S115, after 15 min of PMA stimulation, followed by a gradual decrease toward baseline levels over time. Although the phosphorylation level at 90 minutes did not return to the baseline observed at the 0-minutes time point, we speculate longer time points would follow the same trend as observed between 30 and 90 minutes (Fig. 14A). Nevertheless, we focused on identifying the role of hnRNPC in IES in more detail.

As mentioned in the "Introduction" section, hnRNPC has two isoforms: C1 and C2, originating from the usage of an A5SS (Fig. 7). The C1 isoform is more abundant than the C2 isoform, with a macromolecular ratio: 3:1[45], as shown by the analysis of isoform expression at the mRNA level (Fig. 14B). To verify the consistency of our phosphoproteomic analysis, we performed Western-Blot under the same conditions as in Fig. 14A, with additional samples corresponding to 240 minutes of PMA stimulation. We also observed transient phosphorylation of the C2 isoform, with the highest peaks at 15- and 30-minutes after PMA-stimulation, which gradually reverted to the apparent size of the unstimulated samples after 90 and 240 minutes. Notably, the amount/size of C1 isoform was not affected (Fig. 14C). Most studies show that phosphorylation affects only a fraction of a protein population [129]. However, in our case, nearly the entire population of the hnRNPC2 isoform was phosphorylated, which is an uncommon phenomenon (see "discussion" section). Furthermore, to confirm that the upper, slower migrating bands in the WB correspond to the transiently phosphorylated hnRNPC2 isoform, we treated the protein lysate harvested from 15 min and 30 min-PMA-stimulated Jurkat T cells with the phosphatase FastAP. The lysates were incubated with FastAP for 1h at 37°C. This treatment completely prevented the appearance of phosphorylated

hnRNPC2 (Fig. 14D). As the alternative to PMA stimulation, we also used 5ug of an anti-CD3 antibody to stimulate Jurkat T cells for 30 minutes. While using both stimuli, we observed a shift in the size of hnRNPC2 compared to unstimulated samples, confirming the existence of this phosphorylation mechanism in physiological conditions (Fig. 14E). Altogether, these data demonstrate transient hnRNPC2 phosphorylation at a specific phosphorylation site, S115, after 15 and 30 minutes of PMA stimulation in Jurkat T cells, suggesting its potential role in IES.

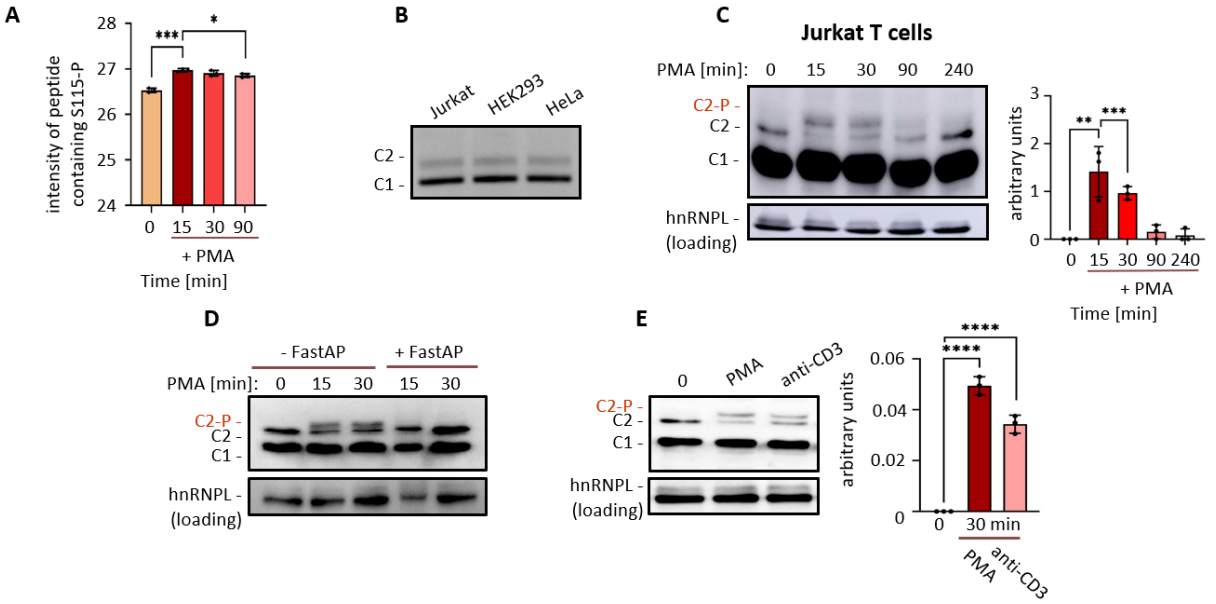

Figure 14: hnRNPC2 phosphorylation aligns with IES. A). Temporal phosphorylation pattern of hnRNPC2 in PMA-stimulated Jurkat T cells, assessed by mass spectrometry (label-free quantification of TiO2-enriched phospho-peptides, log2 intensity mean ± SD, n = 3). **B)** hnRNPC1/C2 isoform expression was detected in Jurkat cells, HEK293, and HeLa cells by standard splicing sensitive RT-PCR. **C)** Reversible phosphorylation of hnRNPC2 was confirmed by Western blot (left) and quantified (right, hnRNPC2-P/hnRNPC1 ratio; student's unpaired t-test; mean ± SD, n = 3, **p<0.01, ***p<0.001). hnRNPL acting as a loading control. **D)** Jurkat cells were stimulated with PMA for the indicated times. FastAP was added to the indicated protein lysate for 1h at 37°C and lysates were analyzed by Western blot. hnRNPL serves as a loading control (n=3). **E)** Jurkat T cells were stimulated for 30 minutes with PMA and 5ug of more physiological stimuli - anti-CD3 Ab. Left: Western blot presents increased phosphorylation of hnRNPC2 in both PMA and anti-CD3 stimulated cells. hnRNPL serves as a loading control. Right: corresponding quantification (mean ± SD, n = 3, ****p<0.0001).

4.3. hnRNPC2 controls IES

To directly link hnRNPC2 with IES, we designed a splice site blocking antisense morpholino (MO) to precisely block the 5' splice site leading to hnRNPC1, thereby increasing the production of hnRNPC2 isoform (Fig. 15A). First, we assessed the efficiency of transfection and the activity of the tested MO and CTRL MO at both the mRNA and protein levels. The MO strongly enhanced the production of the hnRNPC2 isoform (Fig. 15B, C). As shown in the Western Blot, MO-induced hnRNPC2 expression led to increased amount of transiently phosphorylated hnRNPC2 upon PMA stimulation, particularly at 15- and 30-minutes post-stimulation (Fig. 15D). We then examined IES upon 15- and 30-minutes of PMA stimulation in cells electroporated with MO-inducing hnRNPC2 and CTRL MO. We observed a slight increase of basal IR in *RPL10* and *eIF5A* and a significant increase in IR at 15- and 30-minutes post stimulation compared to control MO-transfected cells (Fig 15E, F). These findings demonstrate that temporal hnRNPC2 phosphorylation regulates IES, as MO-induced increased hnRNPC2 expression led to a higher and faster accumulation of IR variants.

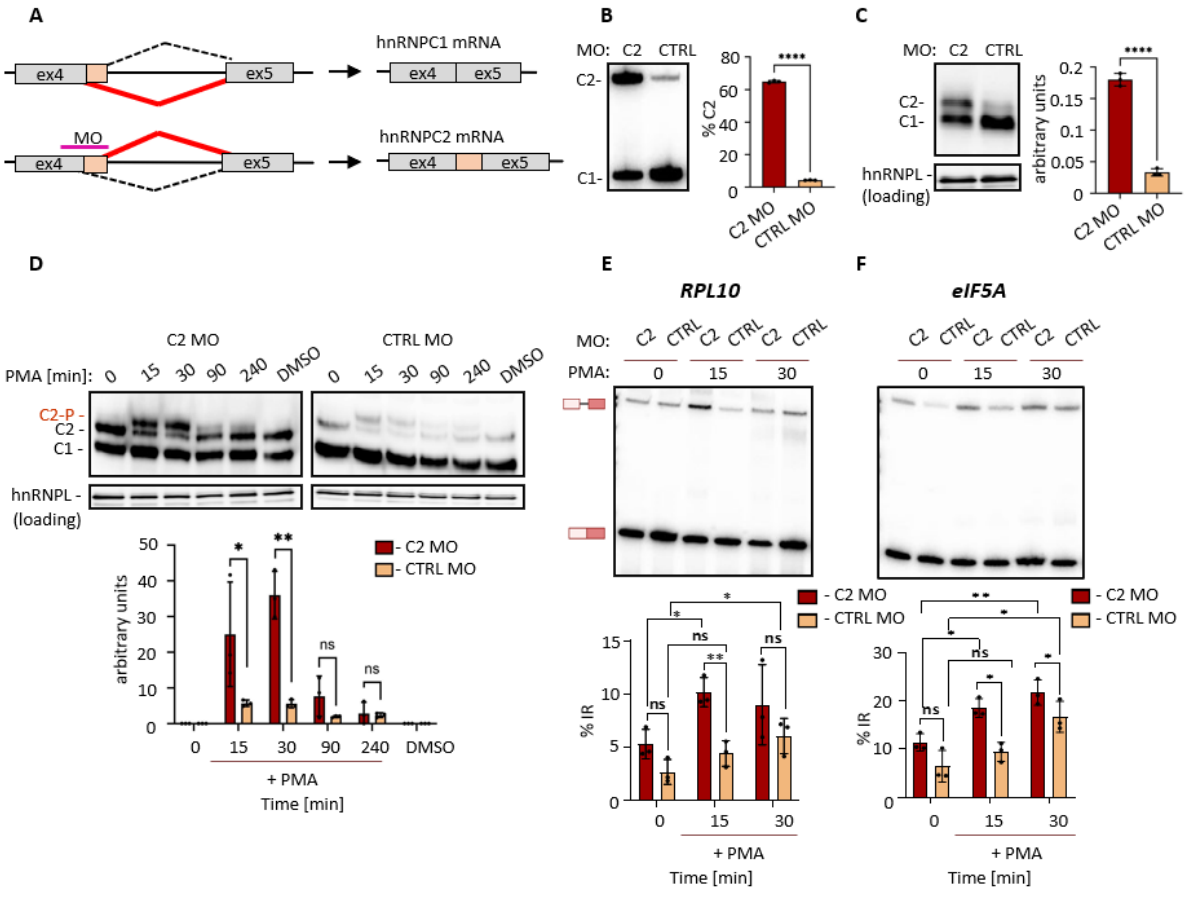

Figure 15: MO-induced hnRNPC2 expression leads to increased temporal phosphorylation of hnRNPC2 and increased IR in *RPL10* and *eIF5A* during T cell activation. A) Schematic view of the morpholino (MO)-induced manipulation of hnRNPC splicing. The MO (pink bar) blocks the proximal 5'-splice site leading to the usage of the distal 5'splice thereby increasing the hnRNPC2 isoform. **B)** Jurkat cells were electroporated with the hnRNPC2-inducing MO (hnRNPC2 MO) or control MO (CTRL MO). Cells were harvested and total RNA was extracted. Left: The efficiency of hnRNPC2 MO was analyzed by radioactive, splicing-sensitive PCR and quantified (right, %C2, student's unpaired t-test, mean ± SD, n = 3, ****p<0.0001). **C)** Jurkat T cells were electroporated as in B and total protein was extracted. Left: The efficiency of hnRNPC2 MO was analyzed by Western blot. hnRNPL acting as a loading control. Right: corresponding quantification; arbitrary units, student's unpaired t-test, mean ± SD, n = 3, ****p<0.0001). **D)** Jurkat cells were electroporated as in C. After 48 hours of indicated MOs transfections, cells were stimulated with PMA for the indicated times or DMSO as a control of treatment. Total protein was extracted. Top: Western blot shows strongly increased amount of hnRNPC2 and phosphorylated C2 protein (C2-P) after stimulation in the hnRNPC2 MO-electroporated cells. hnRNPL serves as a loading control. Bottom: corresponding quantification (hnRNPC2-P/hnRNPC1 ratio; student's unpaired t-test; mean ± SD, n = 3, ns: non-significant, *p<0.05, **p<0.01). **E, F)** Jurkat cells were treated as in C and chromatin-associated RNA was extracted. Top: Radioactive, splicing-sensitive RT-PCR shows increased IR in *RPL10* (E) and *eIF5A* (F) in hnRNPC2 MO-electroporated cells (representative gels, all experiments are representative of three biological replicates). Bottom: corresponding quantifications (% IR; student's unpaired t-test, mean ± SD, n = 3, ns: non-significant, *p<0.05, **p<0.01).

4.4. hnRNPC is required for efficient *RPL10*, *eIF5A* and *TRAF4* splicing

To further investigate the association between hnRNPC and IES, we first downregulated the expression of hnRNPC using siRNA targeting both isoforms, hnRNPC1 and hnRNPC2. After successful knockdown (achieving 30-40% efficiency, as demonstrated by Western blot – Fig. 16A), we performed radioactive, splicing-sensitive PCR to assess its impact on IES in *RPL10*, *eIF5A,* and *TRAF4*. The hnRNPC knockdown completely abolished the IR events, indicating that IES is dependent on hnRNPC (Fig. 16B). In this experiment, total RNA was extracted. Although the fold change of IR among target genes was similar to that observed with chromatin-associated RNA, the absolute IR was lower, as it reflects both nascent RNA and pre-existing, already spliced mRNA. Furthermore, we examined two other trans-acting splicing factors, U2AF35 and hnRNPK, which show temporal phosphorylation upon T cell activation in phosphoproteomic analysis (data not shown). However, their knockdown did not alter the splicing pattern, demonstrating the specificity of IES for the hnRNPC protein (Fig. 16B). Additionally, we observed increased basal intron retention in target genes when hnRNPC was downregulated (experiment conducted by Dr. Debojit Bose). This result suggests that hnRNPC is required for the efficient splicing of introns in the target genes. This conclusion was confirmed using another cell line, HEK293 cells. The hnRNPC knockdown efficiency was tested by RT-qPCR (Fig. 16C). We also observed increased IR in hnRNPC knockdown samples, further

proving the role of hnRNPC in efficient splicing of the analyzed introns (Fig. 16D, E). These findings demonstrate hnRNPC is required for efficient splicing in *RPL10*, *EIF5A* and *TRAF4*.

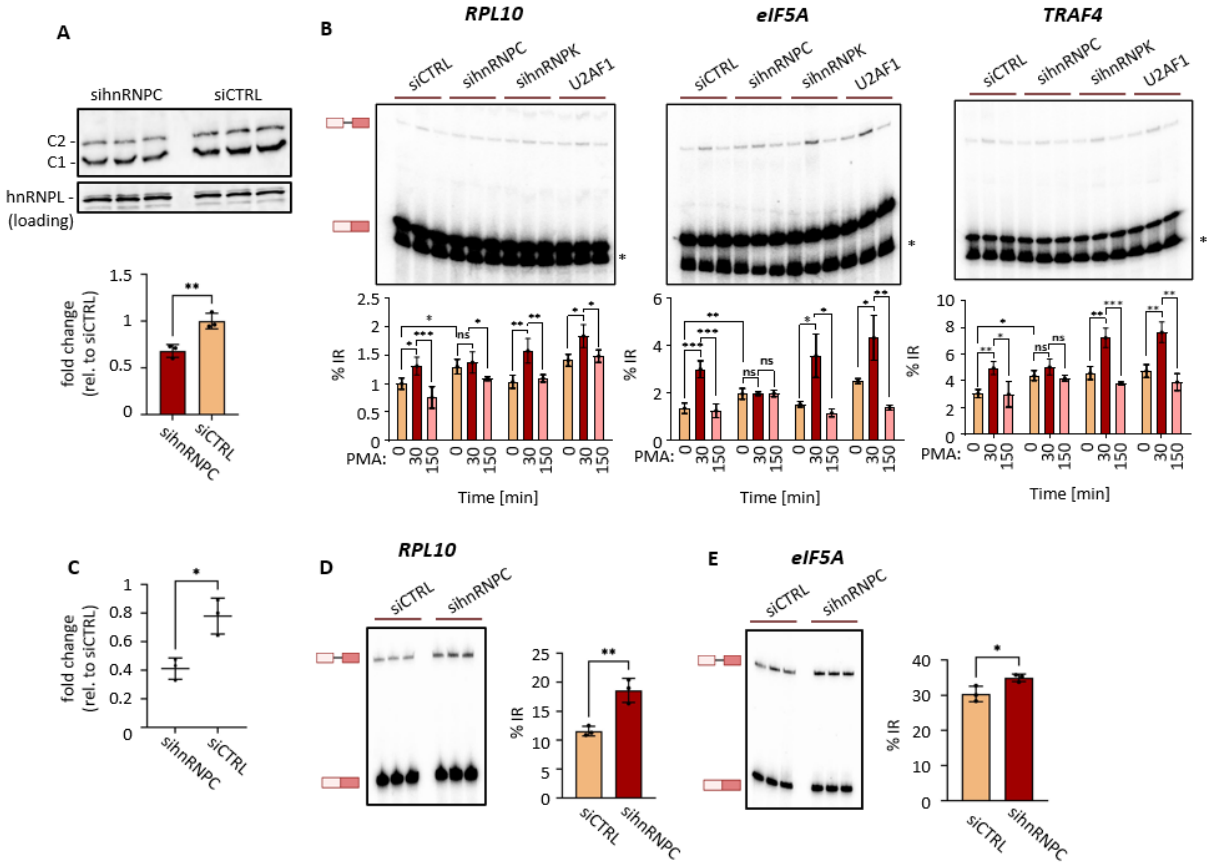

Figure 16: hnRNPC2 is required for efficient splicing of tested IEGs. A) Jurkat T cells were transfected with siRNA against hnRNPC or a control siRNA. Total protein was extracted. The efficiency of hnRNPC knockdown was analyzed by Western blot (top, the gel shows triplicate samples) and quantified (bottom), mean ± SD, n = 3, *p<0.05, **p<0.01. hnRNPL serves as a loading control. **B)** IES depends on hnRNPC. Jurkat T cells were transfected with siRNA targeting hnRNPC, hnRNPK or U2AF35 and after 48 hours of transfection, PMA-stimulated for the indicated times. IR in *RPL10* (left), *eIF5A* (center) and *TRAF4* (right) were analyzed by radioactive, splicing-sensitive RT-PCR in total RNA. * - degradation product. Bottom: corresponding quantifications, % IR; student's unpaired t-test; mean ± SD, n = 3, ns: non-significant, *p<0.05, **p<0.01, ***p<0.001, ****p<0.001). **C)** HEK293 cells were transfected with siRNA against hnRNPC and a control siRNA. After 48h, cells were harvested, and total RNA was extracted. The efficiency of hnRNPC knockdown was determined by RT-qPCR. mRNA expression is relative to hHPRT (mean ± SD, n = 3, *-p<0.05). **D, E)** hnRNPC promotes splicing of *RPL10* (D) and *eIF5A* (E) introns in HEK293 cells. HEK293 cells were transfected with siRNA against hnRNPC and a control siRNA. After 48h, cells were harvested, and chromatin-associated RNA was analyzed by radioactive, splicing-sensitive RT-PCR. Bottom: corresponding quantifications, % IR, student's unpaired t-test; mean ± SD, n = 3, *p<0.05, **p<0.01). Gels show triplicate samples.

4.5. Phosphorylation of hnRNPC2 reduces binding to target introns

To experimentally determine the mechanistic correlations between intron retention and phosphorylated hnRNPC2, we used recombinant, purified wild-type (WT) and phosphomimetic (S115D) hnRNPC2 and tested direct RNA:proteins interactions by electrophoretic mobility shift assay (EMSA). Protein purification was performed by PhD student Gopika Sasikumar, Prof. Markus Wahl's lab. The amount of WT and mutant proteins used for this experiment was verified by Coomassie staining, as shown in Fig. 17A. We designed and ordered 30-nucleotides long intronic sequences of *RPL10, eIF5A* and *TRAF4* that contain the polypyrimidine tract and the 3' splice site, as hnRNPC is known to bind to these intronic regions [44,45]. At first, we radioactively labeled RNA of the *eIF5A* intronic region and performed EMSA with increasing concentrations of two hnRNPC2 protein variants: WT and S115→D (0uM, 1uM, 2uM, 5uM, 10uM, 15uM and 20uM). This experiment revealed binding of WT protein to the *eIF5A* intronic region. In contrast, binding of the phosphomimetic hnRNPC2 mutant was significantly reduced (Fig. 17B). To confirm these results, we adjusted the range of protein concentrations (from 0uM to 10uM) and used additional RNA sequences from *RPL10* and *TRAF4*. This experiment demonstrated a similar binding trend to other intronic fragments of target genes (Fig. 17C, D, E). Furthermore, we used a stretch of 45 nucleotides of poly-U RNA to test the specificity of RNA: protein interactions. In this case, no difference in binding to our control, poly-U RNA between WT and S115D was observed (Fig. 17F).

Our data unveiled a model in which hnRNPC1/2 promotes efficient splicing of target introns through direct interactions. During T cell activation, hnRNPC2 becomes transiently phosphorylated at S115, leading to reduced binding to the target introns, and, in consequence, increased IR events due to inefficient splicing (Fig. 17G). This model is consistent with our MO experiments (Fig. 15), where we manipulated the C1:C2 ratio towards higher hnRNPC2 isoform production. More C2 isoform leads to a higher amount of the phosphorylated form during T cell activation, thereby reducing binding to the intronic regions of interest. This phenomenon disrupts efficient splicing, leading to increased IR events. Thus, our findings underscore the crucial role of hnRNPC2 phosphorylation during T cell activation in differentiating the function of hnRNPC1 and hnRNPC2 isoforms.

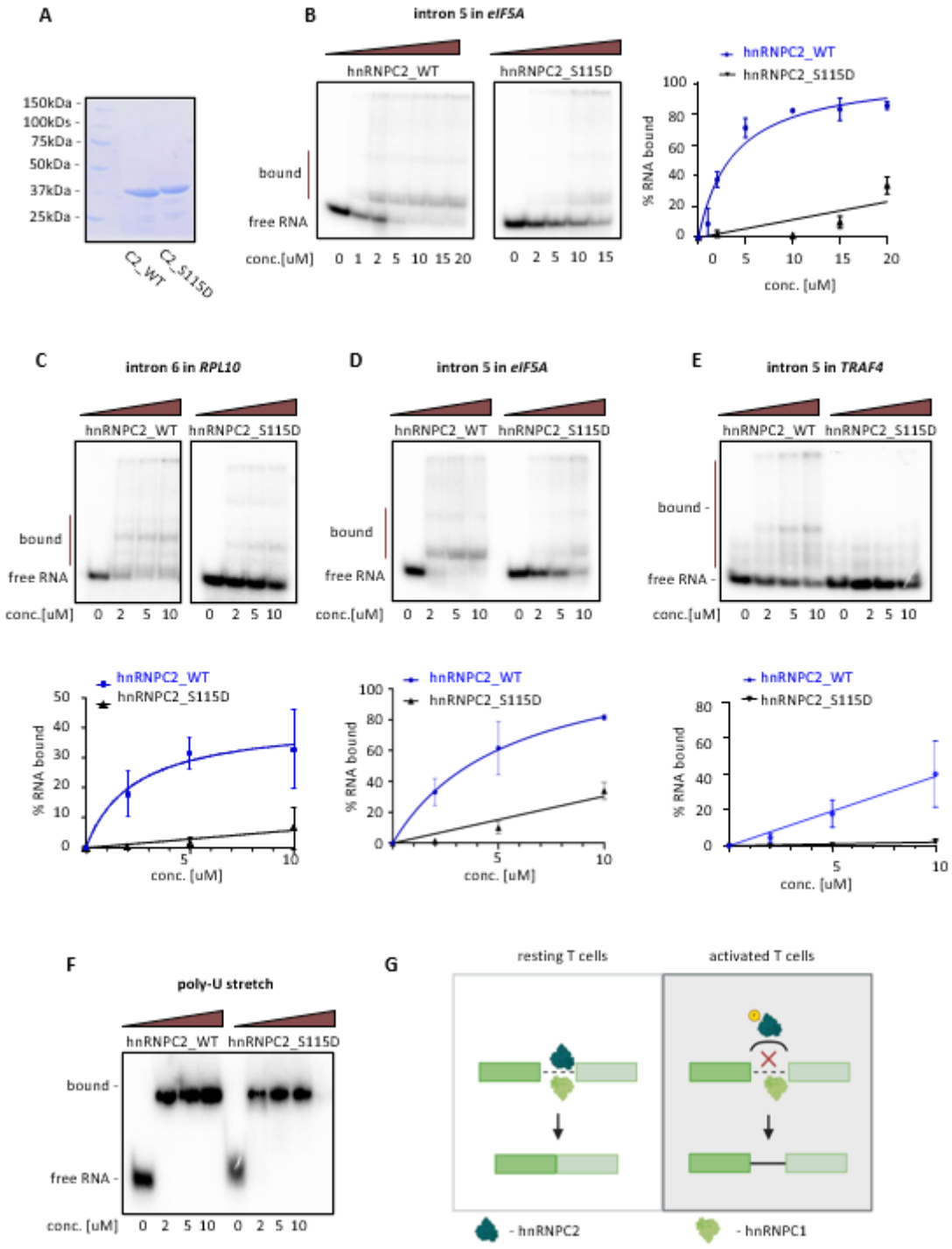

Figure 17. EMSA revealed reduced binding of phosphorylated hnRNPC2 to intronic regions of *RPL10, eIF5A* and *TRAF4*. A) Coomassie-stained SDS-gel showing the amounts of purified hnRNPC2 proteins used for EMSA **B)** Increasing amounts of either hnRNPC2_WT or S115D (0uM, 1uM, 2uM, 5uM, 10uM, 15uM and 20uM) were complexed with 5nmol of radioactively labeled RNA corresponding to a part of the *eIF5A* intron 5 that includes the polypyrimidine tract and the 3' splice site. Left: representative native gel shows a reduction of RNA binding in the S115D phosphomimetic-mutant. Data are representative of at least three independent experiments. Right: corresponding quantifications (mean ± SD, n = 3). **C, D, E)** EMSAs were performed as in B, but with different proteins concentrations (0uM, 2uM, 5uM, and 10uM). Increasing amounts of either hnRNPC2_WT or S115D were complexed with radioactively labeled RNA spanning the polypyrimidine tract and the 3' splice-site of intron 6 in *RPL10* (C) and intron 5 in *eIF5A* (D) and intron 5 in *TRAF4* (E). Top: representative native gels of at least three

independent experiments. Bottom: quantification of EMSAs (mean ± SD, n = 3). **F)** EMSA as in C, D, E using 5nmol of radioactively labeled poly-U (45nt) RNA (representative gel, n=3). **G)** Schematic model based on our findings. Upon T cell activation, hnRNPC2 gets phosphorylated, leading to decreased binding to intronic sequences in *RPL10, eIF5A* and *TRAF4*, and, in consequence, reduced splicing efficiency. Created using BioRender.com.

4.6. RAF/MEK/ERK signaling pathway is involved in hnRNPC2-dependent regulation of IES

This part of the project was performed by Dr. Debojit Bose.

To elucidate the upstream signaling pathway that regulates hnRNPC-dependent IES, Jurkat T cells were PMA-stimulated in the presence of different small molecule kinase inhibitors (such as MEK, AKT, P38, JNK, and JAK inhibitors), at different time points (0min, 30min, 150 min). Total RNA was extracted, and radioactive, splicing-sensitive RT-PCR was performed. In control cells, we again observed the same fold change in IR events as seen during nascent RNA extraction. With the presence of MEK inhibitor, the IR events among target IEGs were completely abolished. The presence of other analyzed kinase inhibitors did not affect the IES (Fig. 18A). Furthermore, the treatment of Jurkat T cells with the MEK inhibitor abrogated the shift in phosphorylated hnRNPC2 observed upon PMA-stimulation, that was shown in Figs. 14C and 15D (Fig. 18B). Thus, our data suggests that the phosphorylation of hnRNPC2 is likely mediated by ERK kinase. Previous studies highlight the high affinity of ERK kinase for proline-rich sequences[115]. Therefore, we checked that the amino acids surrounding temporarily phosphorylated hnRNPC2 in a specific site: S115 (residues 112–PS**P**S**P**LL–118) form such a proline-rich region, further supporting our findings.

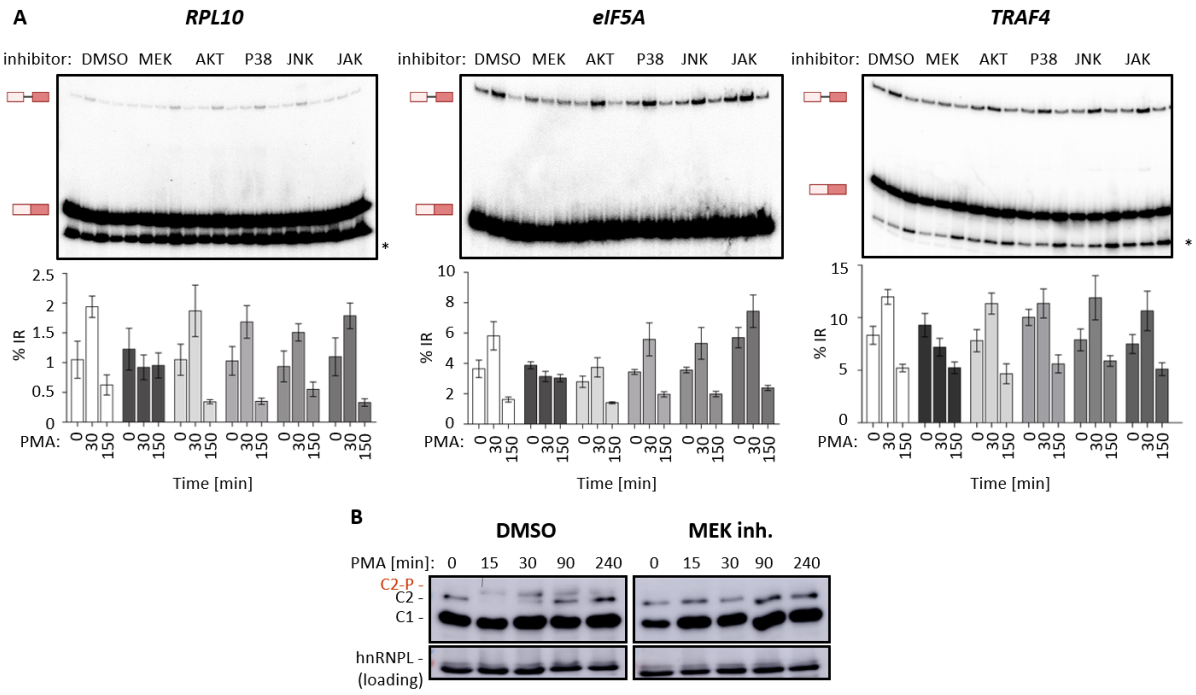

Figure 18: RAF/MEK/ERK signaling pathway mediates hnRNPC2-dependent IES. A) MEK inhibition prevents IES. Jurkat cells were treated for 30 minutes with the indicated small molecule inhibitors, followed by PMA stimulation for the indicated time points. Cells were harvested, and total RNA was extracted. Top: representative graphs from radioactive, splicing-sensitive RT-PCR for *RPL10* (left), *eIF5A* (center), and *TRAF4* (right) (*-degraded product). Bottom: corresponding quantification (% IR; mean ± SD, n = 2). **B)** MEK inhibition prevents transient phosphorylation of hnRNPC2. Cells were treated for 30 minutes with either DMSO (left) or MEK inhibitor (MEK inh.; right) and then stimulated with PMA for the indicated times. Cells were harvested, and total protein was analyzed for hnRNPC2 phosphorylation (data representative of n=3). hnRNPL serves as a loading control.

4.7. IES is T cell specific

The RAF/MEK/ERK signaling cascade is widespread, present in nearly all cell types, such as epithelial, neuronal, muscle, and immune cells, highlighting its diverse roles in various cellular contexts[115,116]. hnRNPC1/2 is also widely expressed[35,44,50,53,57].Thus, we hypothesized that hnRNPC2-dependent IES is a broadly observed mechanism. To experimentally verify our hypothesis, we stimulated the derivative human cell line HEK293 and the human immortalized cell line HeLa cells with PMA at different time intervals and examined IES and temporal hnRNPC2 phosphorylation at the RNA and protein levels, respectively. Unexpectedly, we did not detect a significant induction of IES in *RPL10* (Fig. 19A) and *eIF5A* (Fig. 19B) nor substantial levels of phosphorylated hnRNPC2 upon PMA stimulation (Fig. 19C). However, when conducting this experiment simultaneously with T cells of human and mouse origin (Jurkat and EL4, respectively), we observed a significant induction of IR events among analyzed genes after 30 minutes of PMA stimulation (Figs. 19A, B).

To date, we have found that hnRNPC2-controlled IES is likely specific to T cells. This conclusion is further supported by experiments involving mouse neuronal (N2a) cells. Stimulation of these cells with PMA for 0, 30 and 150 minutes did not alter the splicing efficiency (the percentage of IR remained relatively constant) in *RPL10* (Fig. 19D) and *eIF5A* (Fig. 19E). Similarly, alternative stimuli that induce N2a depolarization, such as KCl, also did not affect splicing in the target genes (Figs. 19D, E).

Since IES appears to be T cell-specific, we tested whether other immune cells are similarly affected. Therefore, we stimulated mouse macrophage RAW264.7 cells with PMA and another stimulation reagent – lipopolysaccharide (LPS). We did not observe IES as seen in Jurkat T cells upon 0, 15, 30 and 150 minutes of stimulation by any of the analyzed stimuli (Figs. 19F, G).

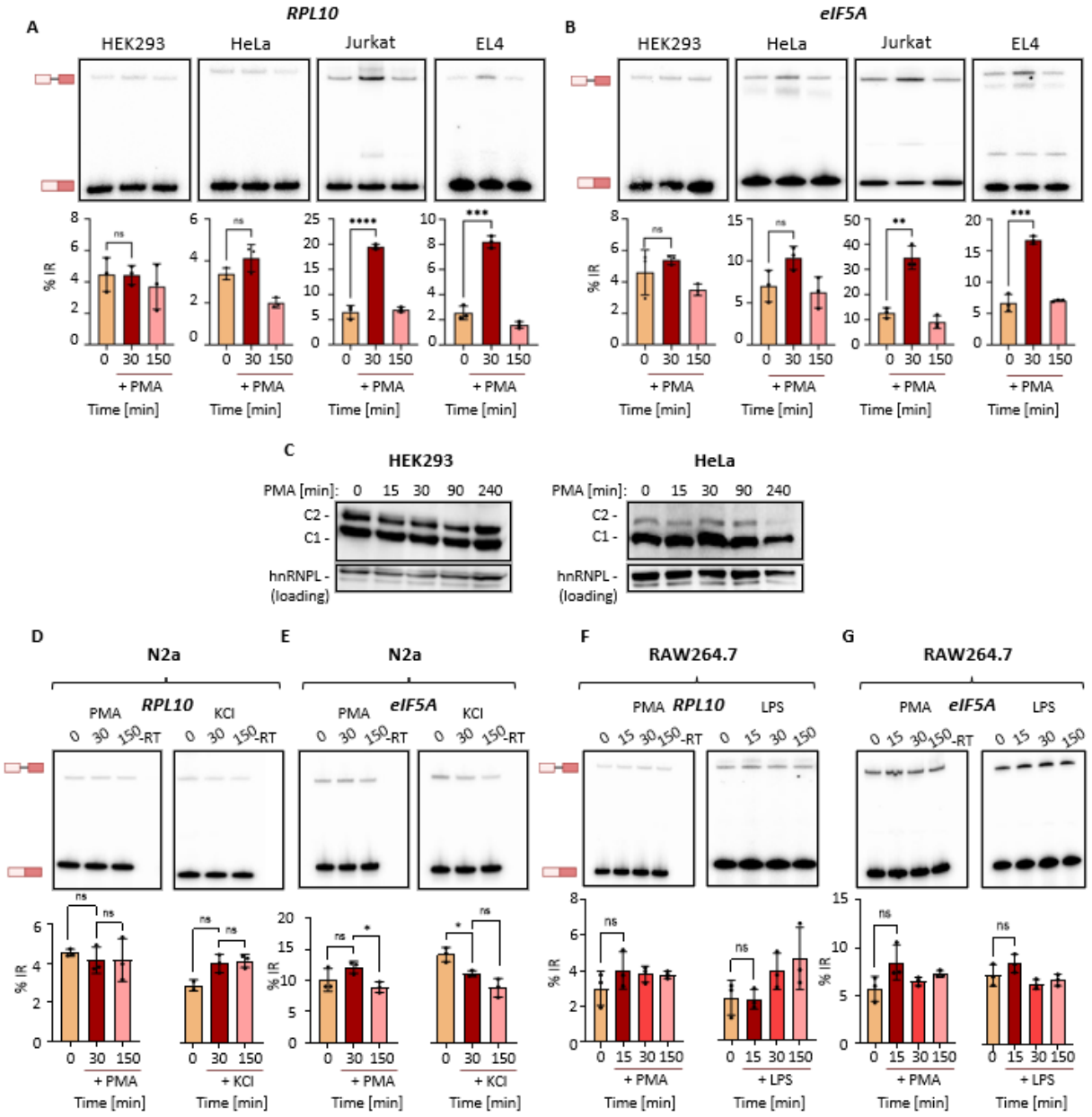

Figure 19: IES is T cell specific. A, B) Absence of IES in non-immune cells. HEK293, HeLa, Jurkat and EL4 cells were stimulated in parallel by PMA for the indicated time points and chromatin-associated RNA was investigated by radioactive, splicing-sensitive RT-PCR for *RPL10* (A) and *eIF5A* (B). Bottom: quantification of gels (% IR; student's unpaired t-test; mean ± SD, n = 3, ns: non-significant, **p<0.01, ***p<0.001, ****p<0.0001). **C)** Absence of reversible hnRNPC phosphorylation in non-immune cells. HEK293 (top) and HeLa (bottom) cells were stimulated with PMA for the indicated time points and protein lysates were investigated for hnRNPC2 phosphorylation. Data representative of n=3. hNRNPL serves as a loading control**. D, E)** N2a cells were stimulated with either 20ng/ml of PMA (left) or 60mM of KCl (right) for indicated times, chromatin-associated RNA was extracted, and radioactive, splicing-sensitive RT-PCR was performed. Representative gels show increased intron retention (IR) in (D) *RPL10*, (E) *eIF5A* only after 30 min of PMA activation (-RT; without reverse transcriptase). Bottom: quantification of gels (% IR; student's unpaired t-test; mean ± SD, n = 3, ns: non-significant, *p<0.05). **F, G)** RAW264.7 cells were stimulated with either 20ng/ml of PMA (left) or 0.1 µg/ml of LPS for the indicated time. Analysis and quantification as in Figs. 19D, E (-RT; without reverse transcriptase).

4.8. IES is T and B cell specific

T cells, like B cells, originate from hematopoietic stem cells in the bone marrow. These two classes of lymphocytes are vital components of the adaptive immune system, and their interaction and cooperation at various levels are crucial for effective immune responses (Fig. 9). To test whether IES is T cell specific or more broadly applicable to lymphocytes, we used different versions of human B cells – Raji and Ramos cells. We extracted chromatin-associated RNA stimulated with PMA at 0, 30 and 150 minutes and performed radioactive, splicing-sensitive RT-PCR. We observed a significant IR induction after 30 min of PMA stimulation in both *RPL10* and *eIF5A* (Figs. 20A, B). Furthermore, by performing WB we confirmed the temporal hnRNPC2 phosphorylation at 15, 30 and 90 minutes of PMA-stimulation in these cells (Fig. 20C, D). Thus, these data indicate the IES specificity extends to both B and T cells.

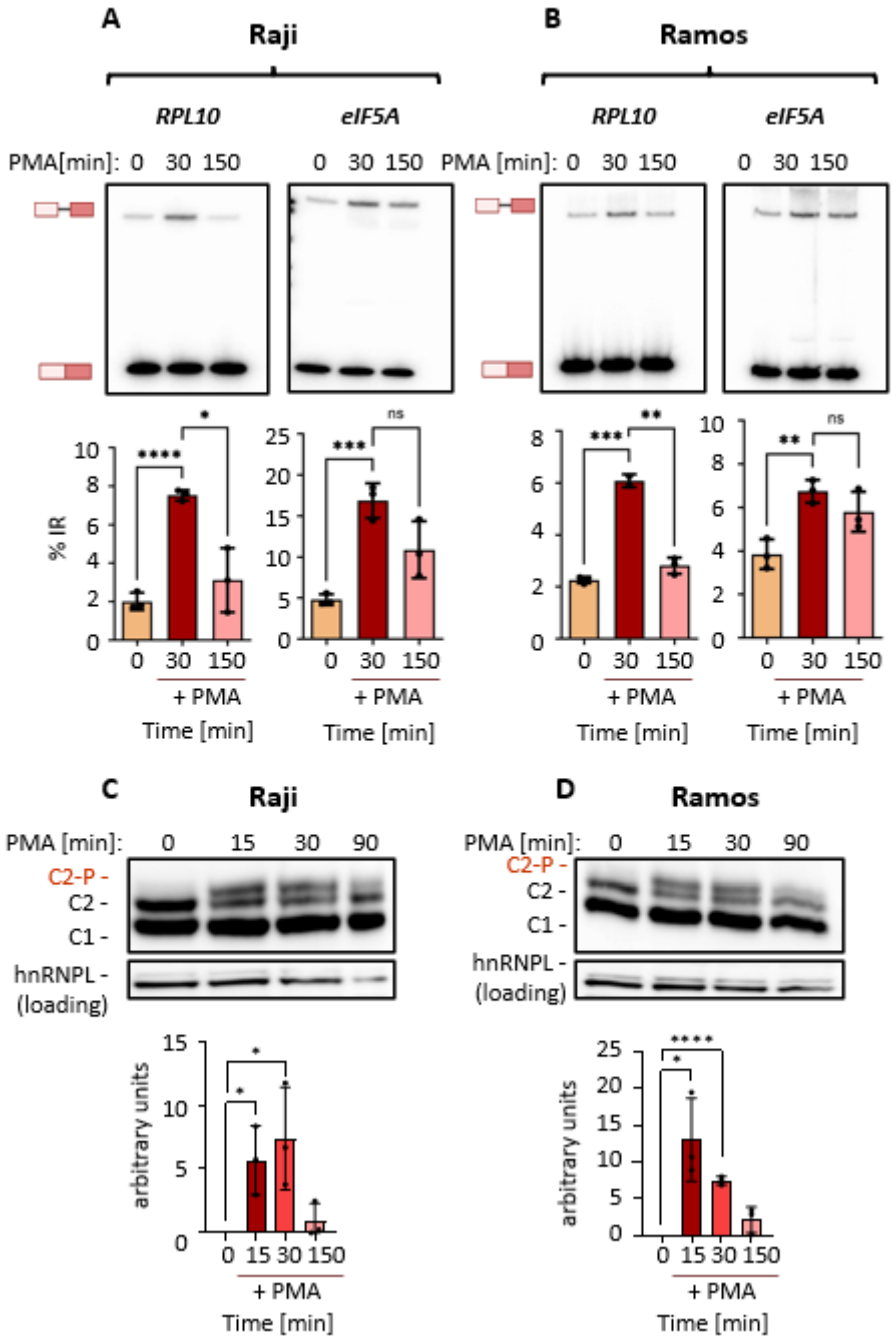

Figure 20: IES is B cell specific. **A, B)** Raji (A) and Ramos (B) B cells were stimulated with PMA in indicated time points. Chromatin-associated RNA was investigated by radioactive, splicing-sensitive RT-PCR for *RPL10* (let) and *eIF5A* (right). Bottom: quantification of gels (% IR; student's unpaired t-test; mean ± SD, n = 3, ns: non-significant, *p<0.05, **p<0.01, ***p<0.001, ****p<0.0001). **C, D)** Reversible hnRNPC2 phosphorylation in C) Raji and D) Ramos cells was analyzed by Western Blot (top) and quantified (bottom, hnRNPC2-P/hnRNPC1 ratio; student's unpaired t-test; mean ± SD, n = 3, ns: non-significant, *p<0.05. ****p<0.0001). hnRNPL acting as a loading control.

4.9. PKCθ is necessary for T and B cell specific hnRNPC2 phosphorylation and IES

To understand the mechanistic reasons behind the T and B cell specificity of hnRNPC2-dependent IES, we considered additional kinases activated by PMA that could be involved in this process. For instance, these kinases might initiate the priming phosphorylation of hnRNPC2, which could then recruit the RAF/MEK/ERK signaling pathway to facilitate temporal phosphorylation at S115 on hnRNPC2 and subsequent IES. Therefore, we hypothesized that the PKC isoform PKCθ might play a role in this mechanism. This kinase is highly expressed in T cells and is pivotal during T cell activation by mediating signals from the T cell receptors (Fig. 11)[73,88]. We experimentally confirmed the high expression of PKCθ in human Jurkat and mouse EL4 cells by RT-qPCR (Fig. 21A, B). Furthermore, we found that PKCθ is almost not detected in HEK293, HeLa and N2a, additionally supporting its role in mediating T cell specificity (Fig. 21A). PKCθ, as a promising candidate for IES regulation, was also examined in tested Raji and Ramos B cells. However, in this case, we did not detect high expression of PKCθ, suggesting the involvement of different, independent mechanisms leading to hnRNPC2-dependent IES in B cells (Fig. 21A).

First, we examined the consequences of pharmacological inhibition of PKCθ. We treated Jurkat T cells with a PKCθ inhibitor for 30 minutes before harvesting and performed radioactive RT-PCR and Western Blot analyses. Before treatment, cells were stimulated with PMA at indicated time points (0, 15, 30, 90 and 240 minutes). PKCθ inhibition completely abolished the splicing switch observed under DMSO control conditions, indicating that PKCθ activity is required for this mechanism (Fig. 21C in *RPL10* and D in *eIF5A*). Consistently, we observed a reduction in reversible hnRNPC2 phosphorylation in PKCθ inhibitor-treated samples after 15 and 30 minutes upon PMA stimulation, demonstrating its direct association with this phosphorylation event (Fig. 21E). Furthermore, Western Blot analysis revealed that PMA-induced ERK1/2 phosphorylation was unaffected by PKCθ inhibitor treatment (Fig. 21F). This indicated that, while PKCθ inhibition reduces hnRNPC2 phosphorylation, it does not impact ERK1/2 activity. The fact that the PKCθ inhibitor did not affect ERK1/2 phosphorylation suggests that the observed reduction in hnRNPC2 phosphorylation is not due to inhibition of ERK1/2 but is instead a direct effect of the PKCθ inhibitor. It is noteworthy that some residual hnRNPC2 phosphorylation was still observed upon PKCθ inhibitor treatment. Therefore, it is

likely PKCθ may cooperate with other components of the signaling pathways involved in regulating hnRNPC2 activity.

To confirm our findings, we designed and ordered siRNA targeting PKCθ. First, we assessed the efficiency of PKCθ knockdown by RT-qPCR. Although the siPKCθ treatment reduced PKCθ expression by only 50% (Fig. 21G), this reduction was sufficient to abolish IES in both *RPL10* (Fig. 21H) and *eIF5A* (Fig. 21I). Consistently, while stimulating Jurkat T cells by 15, 30 and 90 minutes with PMA, we also observed reduced hnRNPC2 phosphorylation in siPKCθ knockdown conditions (Fig. 21J). Thus, these results are consistent with our PKCθ inhibition experiments. Together, these data demonstrate that PKCθ activity is required for PMA-induced hnRNPC2 phosphorylation and IES of *RPL10* and *eIF5A,* and likely other hnRNPC-dependent IES targets.

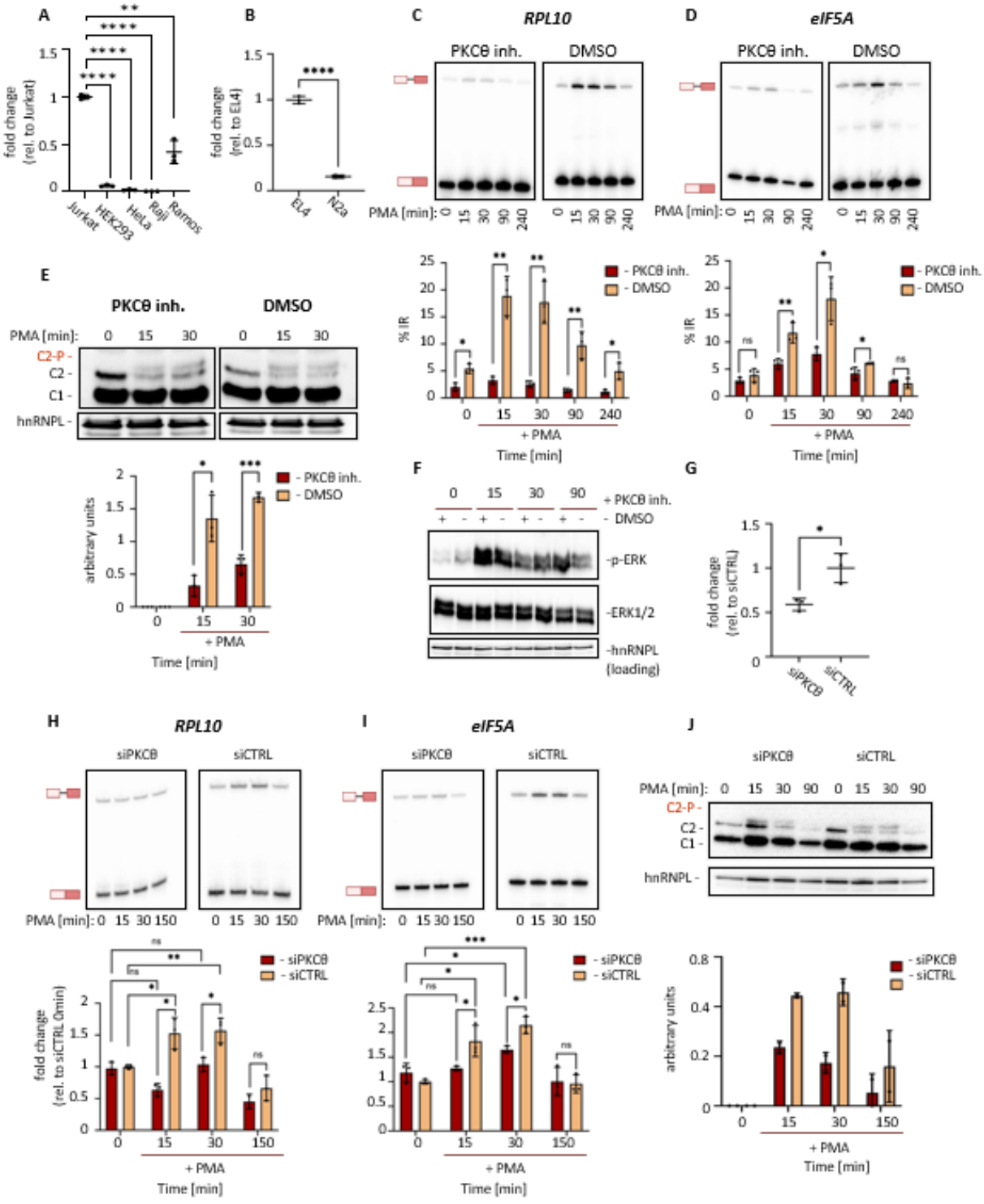

Figure 21. PKCθ is required for T and B cell specific hnRNPC2 phosphorylation and IES A) PKCθ expression in human Jurkat T cells, HEK293, HeLa, Raji and Ramos cells was analyzed by RT-qPCR. mRNA expression is relative to hHPRT. PKCθ is highly expressed in Jurkat cells and not expressed in HEK293, HeLa, Raji cells and barely expressed in Ramos cells. Statistical significance was determined by unpaired t-tests and is indicated by asterisks, mean ± SD, n = 3, **p<0.01, ****p<0.0001). **B)** PKCθ expression in mouse EL4 cells and N2a cells was analyzed and quantified as in 20A. PKCθ is highly expressed in EL4 cells and is barely expressed in N2a. **C, D)** PKCθ inhibition abolishes IES. After Jurkat T cells stimulation by PMA in indicated time points, PKCθ inhibitor (left) or DMSO (right) were added 30 minutes before harvesting. Chromatin-associated RNA was investigated for *RPL10* (C) and *eIF5A* (D) IES by radioactive, splicing-sensitive RT-PCR and quantified (bottom, %IR, mean ± SD, n = 3, ns: non-

significant, *p<0.05; **p<0.01). **E)** PKCθ inhibition reduces hnRNPC2 phosphorylation. After Jurkat T cells stimulation by PMA in indicated time points, PKCθ inhibitor (left) or DMSO (right) were added 30 min before harvesting. Protein lysates were investigated for phosphorylation of hnRNPC2 by Western blot (top) and quantified (bottom) (hnRNPC2-P/hnRNPC1 ratio; mean ± SD, n = 3, *p<0.05, ***p<0.001). **F)** Jurkat cells were PMA-stimulated with PKCθ inhibitor or DMSO as in 21E. A representative blot shows PKCθ did not block ERK1/2 activation after PMA stimulation. hnRNPL serves as a loading control, n = 3. **G)** Knockdown of PKCθ by siRNA was investigated by RT-qPCR. mRNA expression is relative to hHPRT. Statistical significance was determined as in 20A, B. **H, I)** PKCθ knockdown abolishes IES. Jurkat cells were treated with siRNA against PKCθ and siCTRL. 48 hours post transfection cells were stimulated with PMA, chromatin-associated RNA was investigated for *RPL10* (H) and *eIF5A* (I) IES by radioactive, splicing-sensitive RT-PCR. Bottom: Quantification of above data, fold change normalized to siCTRL 0 min sample; mean ± SD, n = 3, ns: non-significant, *p<0.05; **p<0.01, ***p<0.001). **J)** PKCθ knockdown reduces hnRNPC2 phosphorylation. Jurkat cells as in H, I were analyzed by Western blot (top). hnRNPL serves as a loading control; Bottom: Quantification of blots as above (hnRNPC2-P/hnRNPC1 ratio; mean ± SD, n = 2).

4.10. Expression of PKCθ in HEK293 or Hela cells is sufficient to induce IES in an hnRNPC2-dependent manner

To confirm the role of PKCθ in hnRNPC2-dependent IES, we investigated the effect of ectopic PKCθ overexpression on IES in HEK293 cells. Therefore, we subcloned PKCθ into a pFLAG vector and transfected this construct into HEK293 cells. As shown in Fig. 22A, the PKCθ overexpression was successful. We then assessed whether PKCθ overexpression induces IES. Remarkably, PKCθ overexpression was sufficient to induce IES in *RPL10* and *eIF5A*. After 15, 30 and 150 minutes of PMA stimulation, HEK293 cells overexpressing PKCθ recapitulated IES pattern similar to those observed in Jurkat cells (Figs. 22B for *RPL10*, C for *eIF5A*). To validate our findings, we repeated the experiment in another cell line – Hela cells. Again, in this case, we obtained very similar results; IES was increased while overexpressing PKCθ (Figs. 22D for *RPL10*, E for *eIF5A*) upon 15, and 30 minutes of PMA stimulation.

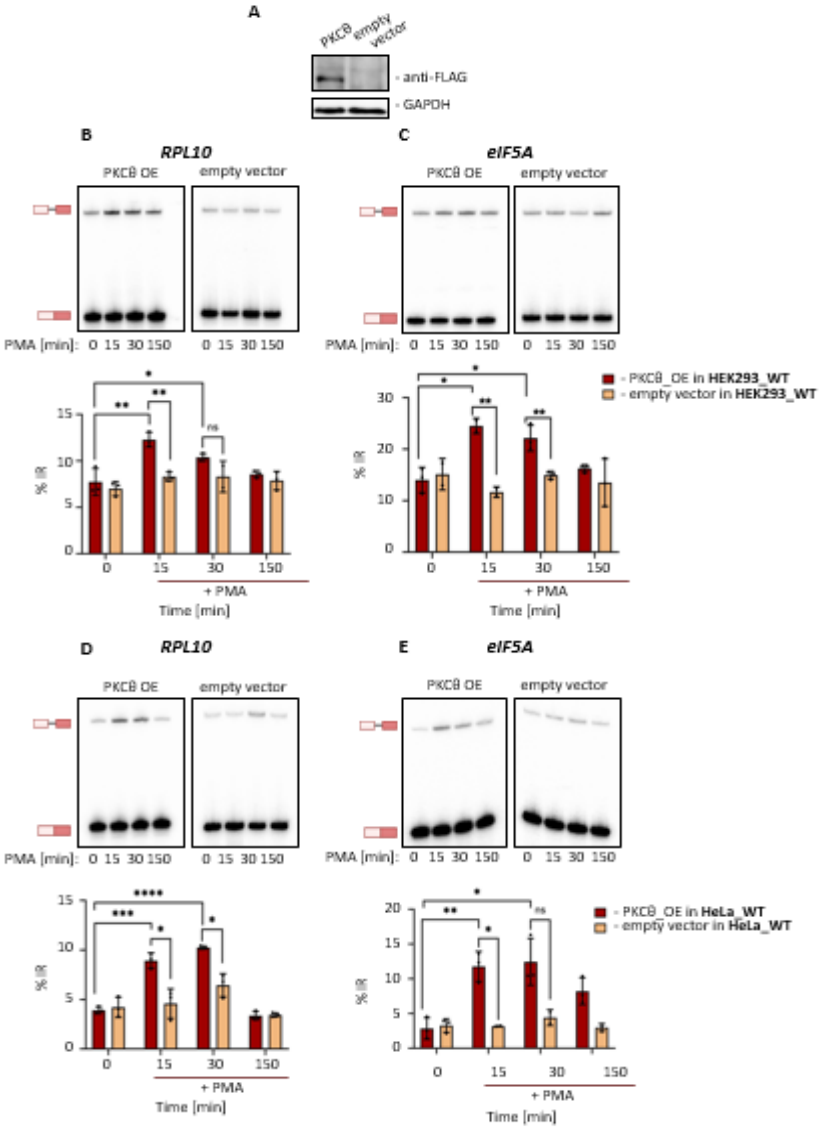

Figure 22. PKCθ overexpression leads to an increase of IES in *RPL10* and *eIF5A* in an hnRNPC2-dependent manner. A) HEK293 cells were transfected with either an overexpression vector for PKCθ and an empty FLAG vector as a control. After 48h, total protein was extracted. Western blot analysis confirmed PKCθ (anti-FLAG) overexpression, with GAPDH serving as a loading control. **B, C)** PKCθ overexpression induces IES in an hnRNPC2-dependent manner. HEK293 cells were transfected with either the empty FLAG vector or the PKCθ overexpression (OE) vector. After 48h, cells were stimulated with PMA for the indicated time points (0, 15, 30 and 150 minutes) and chromatin-associated RNA was investigated by radioactive, splicing-sensitive RT-PCR for IR in *RPL10* (B) and *eIF5A* (C). Autoradiographs were quantified (bottom, % IR; mean ± SD, n = 3, ns: not significant; *p<0.05; **p<0.01). **D, E)** Analysis as in B and C using HeLa cells.

4.11. Introduction of PKCθ into ΔhnRNPC2 knockout cell lines abolishes IES

To demonstrate that the PKCθ overexpression leads to IES through hnRNPC2, we used CRISPR/Cas9 to remove the alternative 5' splice site (Fig. 23A) responsible for generating hnRNPC2, thereby creating HEK293 and HeLa cells that express only the hnRNPC1 isoform. First, we performed DNA genotyping to confirm the absence of the hnRNPC2 in CRISPR/Cas9-edited HEK293 and HeLa cells (Figs. 23B). We tested two pairs of guide RNAs designed using the Benchling tool (see the "Method" section): #1+#3 or #2+#3. We observed several promising, potentially positive clones only with the #2+#3 guide RNAs. (Fig. 23B). Then we tested the expression of ΔhnRNPC2 knockout on both the RNA and protein levels using radioactive, splicing-sensitive RT-PCR and Western Blot, respectively. These experiments confirmed the generation of homozygous, positive ΔhnRNPC2 knockout clones (Fig. 23C, D). Overexpression of PKCθ in these knockout cells showed a complete lack of IES, confirming that hnRNPC2 is required for IES and that PKCθ acts through hnRNPC2 to induce IES upon PMA stimulation in HEK293 (Figs. 23E). Furthermore, we stimulated CRISPR/Cas9-edited HEK293 cells and HeLa cells with PMA at 15, 30, 90 and 240 minutes to assess whether the ΔhnRNPC2 knockout influences the amount of hnRNPC1. As expected, the band corresponding to hnRNPC2 was absent in every well showing different time points of PMA stimulation. Additionally, the amount of hnRNPC1 was not changed over time (Figs. 23F). Therefore, the lack of hnRNPC2 does not reduce the synthesis of hnRNPC1 protein. Altogether, these findings confirm that PKCθ is involved in hnRNPC2-controlled IES in T cells upon their activation.

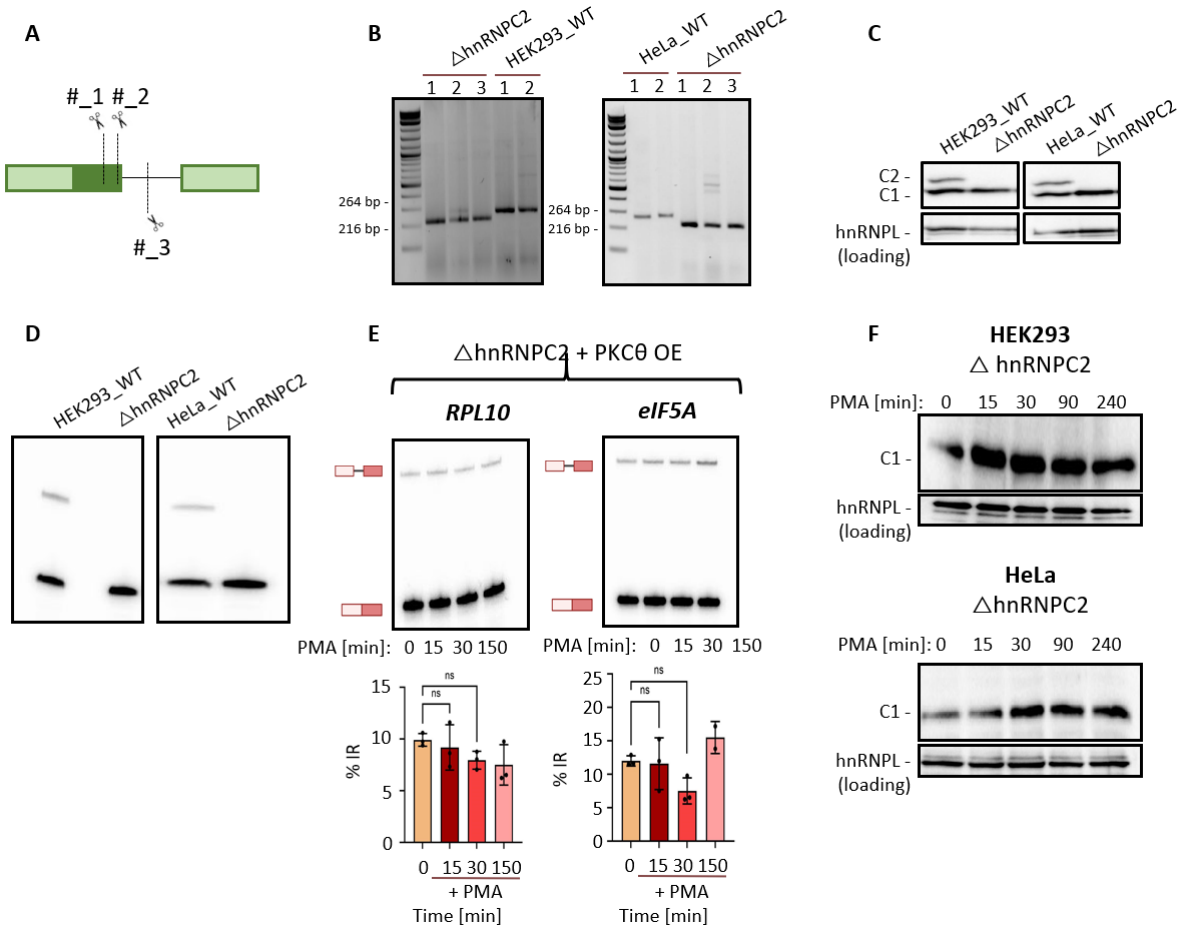

Figure 23. CRISPR/Cas9- edited HEK293 and HeLa cells abolishes IES induction upon PKCθ overexpression. A) Schematic view of the deletion of the hnRNPC2-generating 5' splice site of exon 4 using CRISPR/Cas9. Scissors show the position of the sgRNAs. Created using BioRender.com. **B)** HEK293_WT and CRISPR/Cas9-edited HEK293 with a deletion of hnRNPC2 (ΔhnRNPC2) (left) were harvested and DNA was extracted. Standard RT-PCR shows ΔhnRNPC2 knockout samples (three independent positive clones and two independent controls). The same approach was used in HeLa cells shown on the right. **C)** HEK293_WT and CRISPR/Cas9-edited HEK293 with a deletion of hnRNPC2 (left) were harvested and total protein was extracted. Western Blot confirms the deletion of hnRNPC2 as in B. hnRNPL acts as a loading control. The same approach was used in HeLa cells shown on the right. **D).** One clone of HEK293_WT, HeLa_WT and CRISPR/Cas9-edited HEK293 and HeLa cells with a deletion of hnRNPC2 were harvested and RNA was extracted. Radioactive, splicing-sensitive RT-PCR confirms the ΔhnRNPC2 knockout **E)** HEK293 cells with ΔhnRNPC2 knockout were transfected with an overexpression vector for PKCθ. After 48h, cells were stimulated with PMA for the indicated time points (0, 15, 30 and 150 minutes) and chromatin-associated RNA was investigated by radioactive, splicing-sensitive RT-PCR for IR in *RPL10* (left) and *eIF5A* (right). Autoradiographs were quantified (bottom, % IR; mean ± SD, n = 3, ns: not significant; *p<0.05; **p<0.01). **F)** Absence of hnRNPC2 and no changed activity of hnRNPC1. CRISPR/Cas9-edited HEK293 (left) and HeLa (right) cells were stimulated with PMA for the indicated time points and protein lysates were investigated by Western Blot. Data representative of n=3.

4.12. hnRNPC2 knockout in HEK293 and HeLa cells led to investigate novel changes in gene expression and alternative splicing

To evaluate potential functional differences between hnRNPC1 and hnRNPC2, we performed RNA-seq using generated CRISPR/Cas9 - edited HEK293 and Hela cells lacking the hnRNPC2 isoform and compared these data to WT control HEK293 and HeLa cells. As shown in the Sashimi plots, we confirmed the generation of the hnRNPC2 knockout cell line (Fig. 24A). The usage of A5SS in exon 4 of hnRNPC was observed only in WT conditions. A principal component analysis of the investigated samples from HEK293 revealed two distinct clusters, significantly differentiating between hnRNPC2 knockout and WT cell lines, with some variations in the ΔhnRNPC2 conditions (Fig. 24B). A similar analysis was plotted to HeLa cells, in this dataset, with relatively high variations in WT control conditions (Fig. 24C). Based on the RNA seq data, we identified 3744 differentially expressed genes between ΔhnRNPC2 knockout and WT control conditions in HEK293 cells (54.8%) and 2211 differentially expressed genes in HeLa cells (32.4%) (Fig. 24D). Interestingly, 878 genes were differently expressed in both conditions across the two analyzed cell lines, suggesting specific responses depending on the absence of hnRNPC2 isoform (Fig. 24D). Of these, 338 genes were downregulated in both ΔhnRNPC2 cell lines, 315 genes were upregulated, and the remaining 225 genes showed varying expression patterns, either up- or down-regulated (Fig. 24D). Furthermore, we analyzed different types of alternative splicing events in ΔhnRNPC2 and WT control conditions. The significant types of AS included exon skipping (SE), intron retention (IR) and the usage of alternative 3’ splice site (A3SS). As depicted in the Venn diagram in Fig. 24E, we found 109 splicing changes shared between ΔhnRNPC2 and WT control conditions in both cell lines. Of these 109 splicing changes, 92 were skipped exons, 9 were A3SS, and 8 were retained introns (Fig. 24E). The analysis of RNA-seq was performed by Dr. Bruna Los and Dr. Marco Preußner.

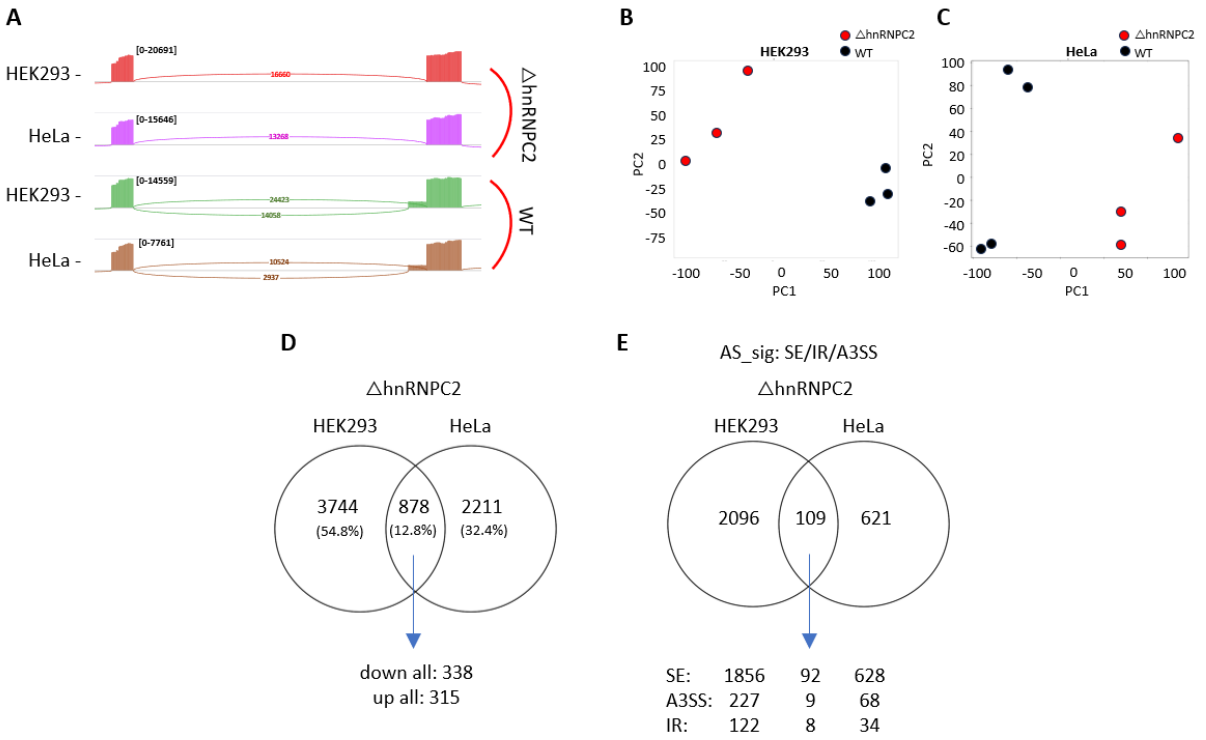

Figure 24: RNA-seq analysis of WT and ΔhnRNPC2 conditions in HEK293 and HeLa cells. A) Sashimi plots of hnRNPC2 knockout in HEK293 and HeLa cells. Sashimi plots were generated using the IGV browser. The alternative 5' splice site was used only in WT conditions. **B, C)** Principal component analysis of the investigated samples of ΔhnRNPC2 and WT control conditions in HEK293 cells (B) and HeLa cells (C). **D)** Venn diagram showing differentially expressed genes between ΔhnRNPC2 and WT control conditions in HEK293 cells and HeLa cells. 878 genes were shared in ΔhnRNPC2 HEK293 and HeLa cells. Genes were considered differentially expressed if Padj ≤ 0.001 and absolute log2FC ≥ 0.8 (or ≤ -0.8) between two conditions. **E)** Venn diagram showing different splicing patterns between ΔhnRNPC2 and WT control conditions in HEK293 cells and HeLa cells. 109 types of AS were shared in ΔhnRNPC2 HEK293 and HeLa cells, including 92 skipped exons (SE), 9 A3SS and 8 retained introns (IR).

To validate our RNA-seq data, we chose genes significantly upregulated and downregulated in ΔhnRNPC2 knockout conditions (genes are depicted in Volcano plots in Fig. 25A, B) in both HEK293 and HeLa cells, ordered primers binding specifically to their mRNAs and performed RT-qPCR. Significantly downregulated genes under ΔhnRNPC2 knockout conditions were *EPDR1, MAGEA2, CSAG* and *TCEAL3.* In contrast, genes *HPGD, MSRA, RPL36L* and *RBM3* acted as upregulated genes in ΔhnRNPC2 knockout cells. Remarkably, all downregulated target genes in two independent ΔhnRNPC2 knockout HEK293 cells showed a similar gene expression pattern to that seen in the RNA-seq data (except *TCEAL3* gene, Fig. 25C). This result was supported using another ΔhnRNPC2 knockout HeLa cells, which shows the same effect as in CRISPR/Cas9-edited HEK293 cell line (Fig. 25D). Similarly, target genes showing upregulation upon ΔhnRNPC2 knockout were also observed in RT-qPCR (except *HPGD*

gene) in HEK293 (Fig. 25E) and HeLa (Fig. 25F) cells, in consistency to data from RNA-seq. Thus, most of these genes show the expected pattern of expression as predicted by RNA seq data.

Furthermore, to validate the identified splicing patterns, we performed radioactive, splicing-sensitive RT-PCR. Since most of the IEGs are expressed in neurons, playing roles in regulation of synaptic activity, neuronal development and learning processes[111,114,119,130], we focused on determining AS changes among genes involved in neuronal development (including *HAUS2, DAP3* and *DPH7*). In all three cases, we observed skipped exons upon ΔhnRNPC2 knockout conditions in HEK293 cells (Fig. 25G).

Nevertheless, it is worth noting that our results using ΔhnRNPC2 knockout HEK293 and HeLa cells should be interpreted with caution due to the relatively high variance across replicates used for RNA-seq analysis, especially in the HeLa_WT samples. The high variability between the WT samples suggests a lack of a reliable reference point for comparing changes in gene expression and AS events resulting from the knockout of hnRNPC2. Furthermore, it is worth considering the possible clonal artifacts that arise from the selection of single cells during generating CRISPR/Cas9-edited cell lines. Such cells may exhibit variations in gene expression due to mutations or genomic rearrangements.

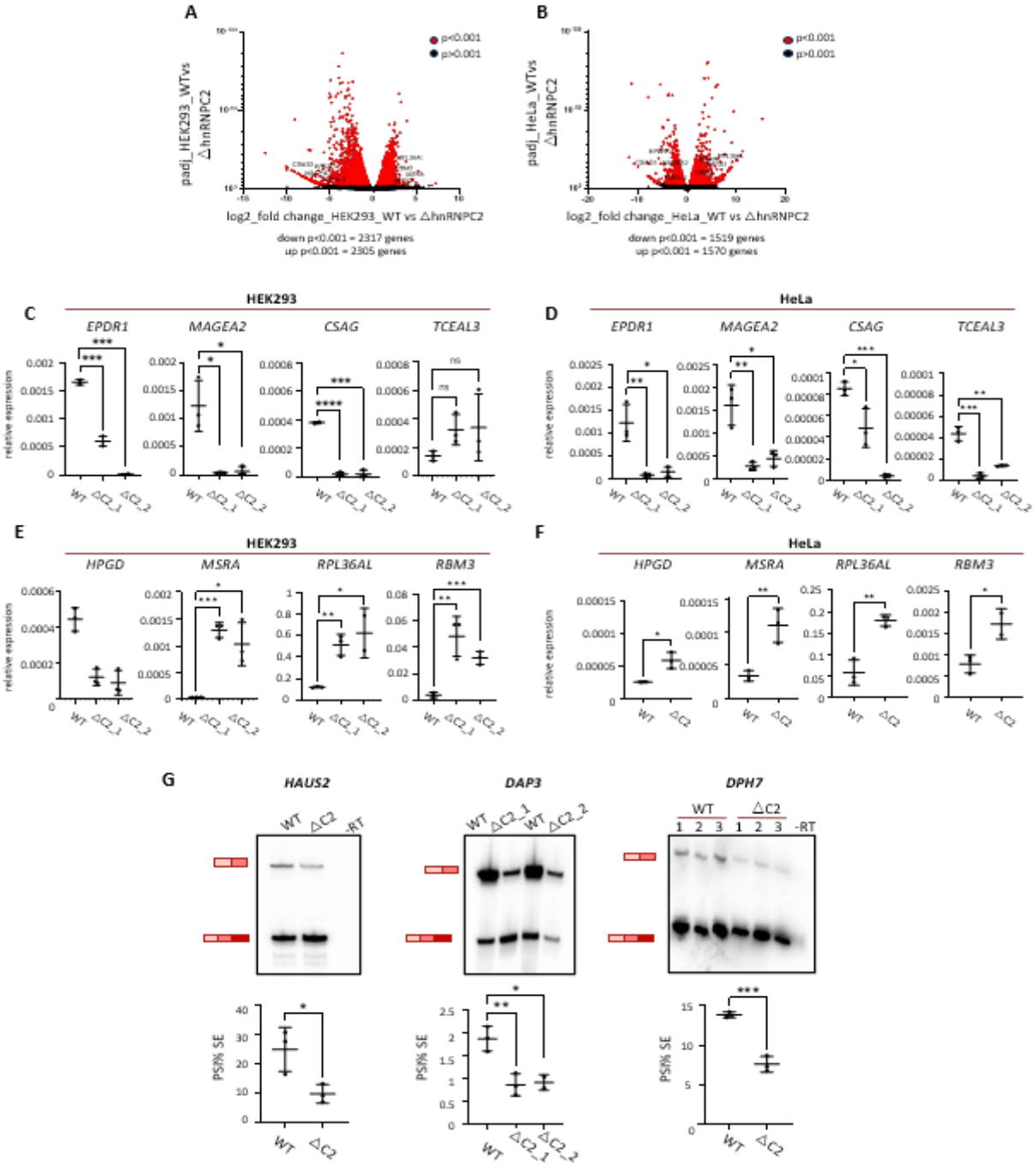

Figure 25: Validation of the RNA-seq of WT and ΔhnRNPC2 conditions in HEK293 and HeLa cells. **A, B)** Volcano plots show the most significant up and down-regulated genes upon hnRNPC2Δ knockout in A) HEK293 and B) HeLa cells. **C, D)** Validation of the selected downregulated genes by RT-qPCR expressed in C) HEK293 cells and D) HeLa cells (mean ± SD, n = 3, unpaired t-tests, ns: not significant; *p<0.05; **p<0.01, ***p < 0.001, ****p < 0.0001). **E, F)** Validation of the selected upregulated genes by RT-qPCR expressed in E) HEK293 cells and F) HeLa cells. (mean ± SD, n = 3, unpaired t-tests, ns: not significant; *p<0.05; **p<0.01, ***p < 0.001, ****p < 0.0001). **G)** Validation of the exon skipping in left: *HAUS2*, center: *DAP3*, and right: *DPH7* upon ΔhnRNPC2 knockout done by radioactive, splicing-sensitive RT-PCR. Top: representative gels confirming exon skipping in response to ΔhnRNPC2 knockout (*DPH7* gene shows triplicate samples), bottom: corresponding quantifications (PSI% SE: percent spliced-in of skipped exons; mean ± SD, n=3, unpaired t-tests, *p<0.05; **p<0.01, ***p < 0.001, ****p < 0.0001).

4.13. MO-induced hnRNPC2 did not show changes on alternative splicing and gene expression between hnRNPC1 and hnRNPC2.

To confirm our RNA sequencing data from CRISPR/Cas9-edited HEK293 and HeLa cells lacking the hnRNPC2 isoform, we conducted another RNA sequencing experiment. This time, we used splice-site blocking morpholinos (MOs) targeting the proximal 5' splice site (5'SS) in exon 4 of hnRNPC, leading to the increase of hnRNPC2 expression. The same hnRNPC2-inducing MO was employed, as previously shown in Fig. 15. The goal of this approach was to replicate our previous findings in the reverse scenario: while we had removed hnRNPC2 in cells using the CRISPR/Cas9 method, here we induced the expression of hnRNPC2 using the splice-site blocking MO. Both the hnRNPC2-inducing MO and CTRL_MO were transfected into HEK293 and HeLa cells. Radioactive, splicing-sensitive RT-PCR revealed that the MO treatment led to an increase in hnRNPC2 production in HEK293 (Fig. 26A) and HeLa cells (Fig. 26B). Based on RNA-seq analysis that was performed by PhD student Luiza Zuvanov and Dr. Marco Preußner (Prof. Florian Heyd's lab), we observed negligible effects on AS or gene expression in both tested cell lines (data not shown).

We investigated the effect of hnRNPC2-indcing MO expression using RT-qPCRs. We selected four down (*EPDR1, MAGEA2, CSAG* and *TCEAL3*) and upregulated (*HPGD, MSRA, RPL36L* and *RBM3*) genes identified upon hnRNPC2 knockout in both CRISPR/Cas9-edited HEK293 and HeLa cells as shown in the Volcano plots (Fig. 25A, B). The hnRNPC2-inducing MO and control MO were used as a rescue approach. We hypothesized that hnRNPC2 MO treatment would lead to the upregulation of genes that were downregulated in hnRNPC2 knockout conditions, and the downregulation of genes that were upregulated in the hnRNPC2 knockout. However, we did not observe significant changes in the expression of ΔhnRNPC2 knockout-downregulated genes upon hnRNPC2 MO treatment in HEK293 (Fig 26C; except *EPDR1* gene) and HeLa cells (Fig. 26D, except *EPDR1* gene). Similarly, there were no significant changes observed among ΔhnRNPC2 knockout-upregulated genes (Fig. 26E for HEK293 and 26F for HeLa cells). This data suggests that the hnRNPC1 and hnRNPC2 isoforms appear to fulfill similar and redundant functions. While hnRNPC2 may indirectly influence the expression or splicing of target genes, further investigation is required to fully understand this mechanism. Based on our study, we conclude that the functional differences between hnRNPC1 and hnRNPC2 become only apparent upon hnRNPC2-specific phosphorylation, which reduces binding to selected RNAs and controls AS. Further research into the specific

pathways and targets affected by hnRNPC2 phosphorylation could provide deeper insights into its role in RNA regulation.

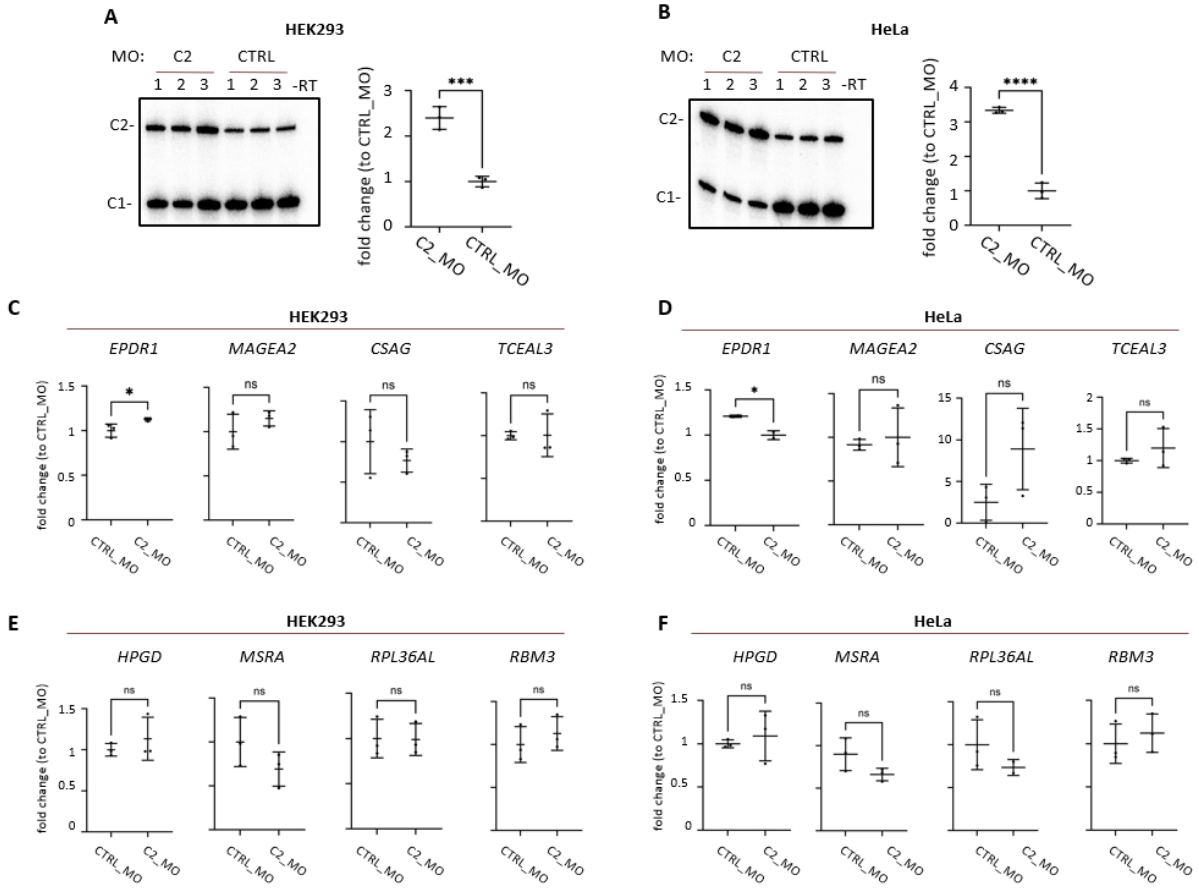

Figure 26: Rescue experiments with hnRNPC2-induced MO revealed no direct functional differences between hnRNPC1 and hnRNPC2. A, B) HEK293 (A) and HeLa (B) cells were transfected with hnRNPC2-inducing MO (hnRNPC2 MO) or control MO (CTRL MO). Cells were harvested and total RNA was extracted. Left: The efficiency of hnRNPC2 MO was analyzed by radioactive, splicing-sensitive PCR (gels show triplicate samples) and quantified (right, fold change, rel. to CTRL_MO, student's unpaired t-test, mean ± SD, n = 3, ***p<0.001, ****p<0.0001). **C, D)** Validation of gene expression upon hnRNPC2-inducing MO (C2_MO) in HEK293 (C) and HeLa (D) cells. These data represent genes downregulated upon ΔhnRNPC2 knockout conditions (fold change, rel. to CTRL_MO, student's unpaired t-test, mean ± SD, n = 3, ns: non-significant, *p<0.05). **E, F)** Validation of gene expression upon hnRNPC2-inducing MO (C2_MO) in HEK293 (E) and HeLa (F) cells. These data represent genes upregulated upon ΔhnRNPC2 knockout conditions. Quantification as in C, D.

4.14. Phosphorylation of hnRNPC2 is required to induce IES

To further validate that phosphorylation of hnRNPC2 is required to induce IES, we mutated potential phosphorylation sites in hnRNPC2, including S115 (Fig. 27A) to alanine, creating non-phosphorylatable version of hnRNPC2. Additionally, two tyrosine residues located in close proximity to the amino acid fragment unique to hnRNPC2 isoforms were mutated to alanine. The cloning of the two hnRNPC2 versions into the pFLAG vector was performed by Dr. Debojit Bose. We co-expressed PKCθ along with either WT or mutant hnRNPC2 in HEK293 cells and assayed for IES after 0, 15, 30 and 150 minutes of PMA stimulation. As expected, we observed significantly stronger IES in *RPL10* and *eIF5A* upon 15 and 30 minutes upon PMA stimulation when expressing WT hnRNPC2 compared to the non-phosphorylatable version (Figs. 27B, C). Additionally, these results confirm that a specific phosphorylation site S115 in hnRNPC2 is responsible for observed IR events. We obtained similar results in Hela cells, further validating the hypothesis that phosphorylation of hnRNPC2 is required to mediate IES (Figs, 27D, E). As shown in Western Blot, we observed hnRNPC2 phosphorylation upon introducing hnRNPC_WT into HEK293 cells, even in non-stimulated samples (0 min time point), with phosphorylation levels further increased after PKCθ overexpression. Furthermore, the band for phosphorylated hnRNPC2 disappeared in samples with the mutated versions of hnRNPC2, regardless of the time frame of PMA stimulation used (Fig. 27F). These data provide evidence that PKCθ likely mediates IES through the phosphorylation of S115 on hnRNPC2.

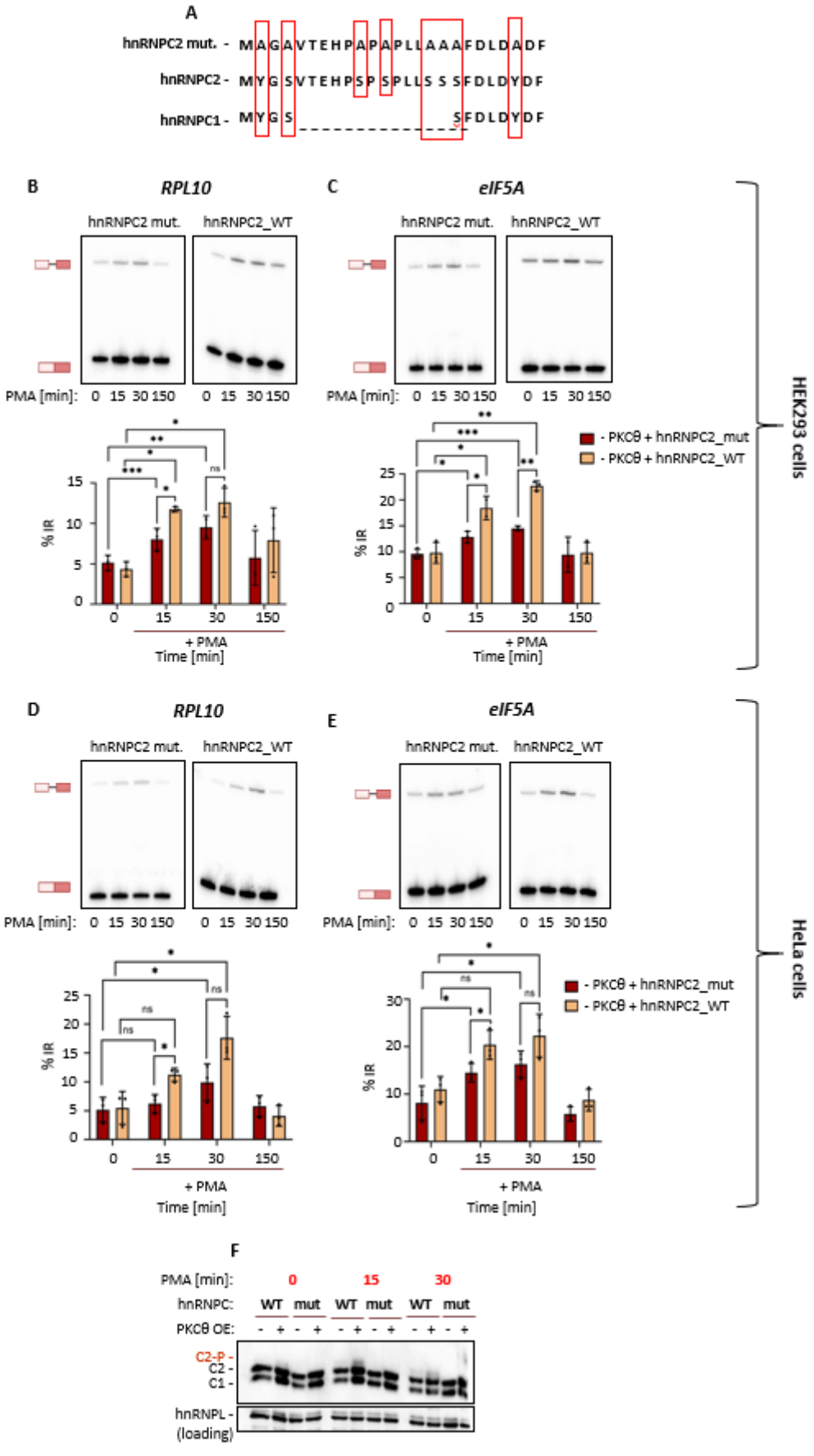
A
hnRNPC2 mut. - MAGAVTEHPAPAPLLAAAFDLDADF
hnRNPC2 - MYGSVTEHPSPSPLLSSSFDLDYDF
hnRNPC1 - MYGS SFDLDYDF
B
RPL10
hnRNPC2 mut.
hnRNPC2_WT
PMA [min]: 0 15 30 150 0 15 30 150
% IR
+ PMA
Time [min]
C
eIF5A
- PKCθ + hnRNPC2_mut
- PKCθ + hnRNPC2_WT
HEK293 cells
D
RPL10
E
eIF5A
HeLa cells
F
PMA [min]: 0 15 30
hnRNPC: WT mut WT mut WT mut
PKCθ OE: - + - + - + - + - + - +
C2-P -
C2 -
C1 -
hnRNPL -
(loading)

Figure 27: Phosphorylation of hnRNPC2 is required to induce IES. A) Alignment of hnRNPC1, hnRNPC2 and a non-phosphorylatable version of hnRNCP2. All potential phosphorylation sites in hnRNPC2, including S115 and some surrounding residues in hnRNPC1 were mutated. Mutated residues are highlighted in red. **B, C)** PKCθ-induced IES depends on hnRNPC2 phosphorylation. HEK293 cells were co-transfected with PKCθ and either hnRNPC2_WT or the nonphosphorylatable version. Representative gels of radioactive, splicing-sensitive RT-PCR (B) *RPL10* and C) *eIF5A*. Bottom: corresponding quantifications, %IR; student's unpaired t-test; mean ± SD, n = 3, ns: non-significant, **p<0.01, ***p<0.001). **D, E)** Experiments as in B, C using HeLa cells. **F)** PKCθ OE increases hnRNPC2 phosphorylation. HEK293 cells were co-transfected with PKCθ and either hnRNPC2_WT or the nonphosphorylatable version. After 48 hours of transfection, cells were stimulated with indicated time points, total protein was extracted, and Western Blot was performed. Representative graph (mean ± SD, n = 3).

4.15. hnRNPC plays role in *de novo* protein synthesis early after T cell activation

To explore the functionality of IES, we considered, based on GO term enrichment, a potential role in globally regulating translation efficiency upon T cell activation (Fig. 12G). As we observed IES in pre-mRNAs encoding components of the translation machinery, we suggested that IES may be involved in controlling *de novo* protein synthesis immediately after T cell activation. We first assessed *de novo* translation at different time points (from 0 to 24 hours) after PMA stimulation of Jurkat cells using both incorporation of puromycin followed by detection with an anti-puromycin antibody (a WB-SuNSET assay) and ^{35}S-methionine incorporation followed by autoradiography. These experiments revealed that the rate of translation is downregulated between the first 1h to 4h post-stimulation, then returns to (or slightly above) base line levels after 8 hours, and increases to a maximum level after 16 hours and 24 hours post stimulation (Figs. 28A, B). This data is consistent with previous studies showing that most changes in protein synthesis occur at later time points post-stimulation, while early-stage proteomic changes are processed, for instance, by altering the phosphorylation status of existing proteins [126]. The reduction of *de novo* protein synthesis is in line with the timeframe of hnRNPC2-controlled IES. To link these two phenomena, we downregulated hnRNPC using siRNA. In hnRNPC knockdown conditions, the initial reduction of translation upon PMA stimulation of Jurkat T cells was abolished (Fig. 28A, B), suggesting that hnRNPC-dependent IES may be involved in adjusting the efficiency of translation at early stages of T cell activation.

To further identify that the hnRNPC2 isoform is involved in controlling *de novo* translation, we used hnRNPC2-inducing MO that we used in previous experiments (Figs. 15, 26). With hnRNPC2- inducing MO we proved that hnRNPC2 isoform facilitates the accumulation of IES variants (Fig. 15). Based on a WB-SuNSET experiment, we observed an

even stronger reduction in *de novo* protein synthesis in Jurkat T cells with induced hnRNPC2 expression compared to control conditions, proving the involvement of the hnRNPC2 isoform in controlling translation upon early stages of T cell activation (Fig. 28C).

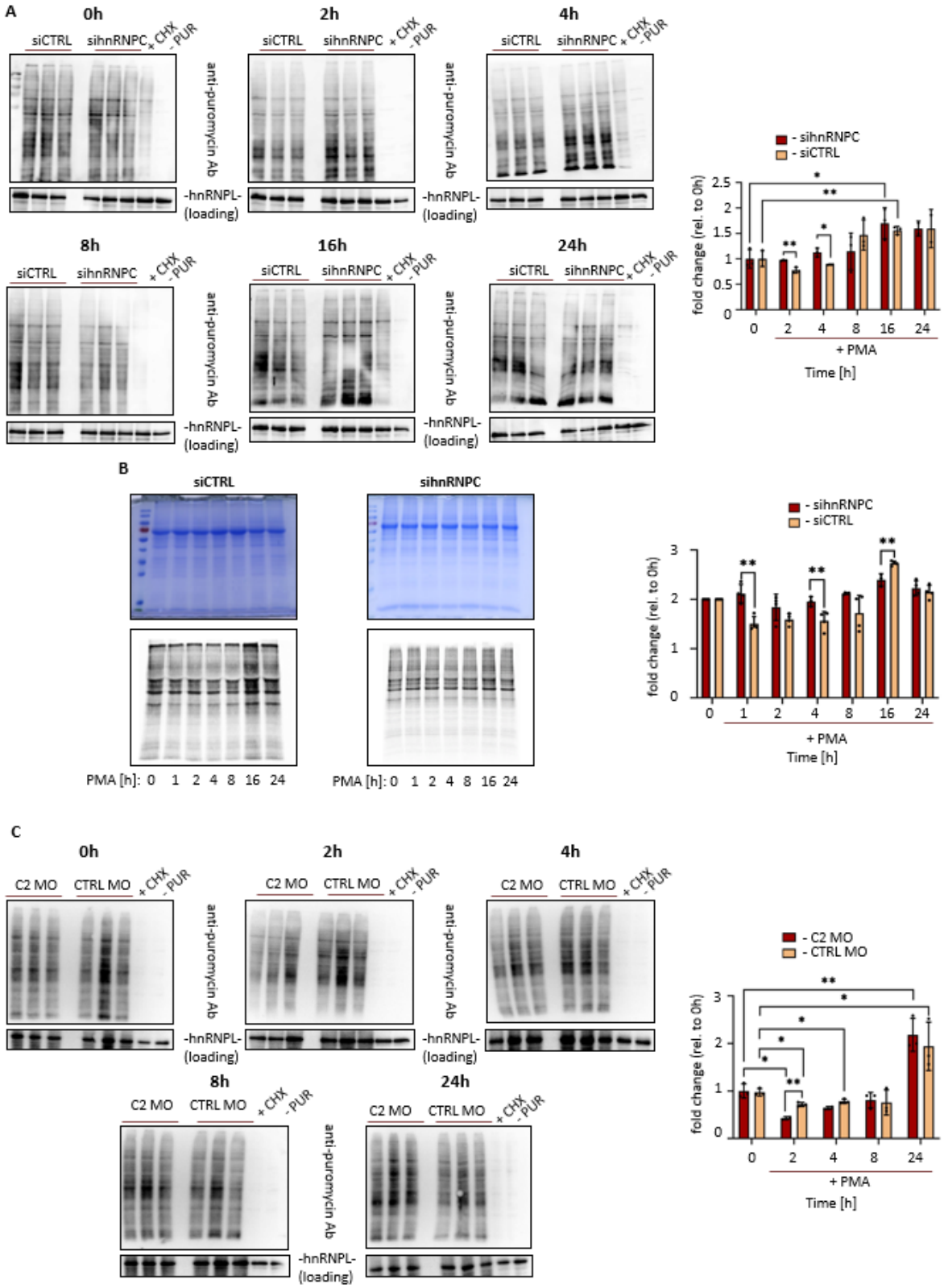

Figure 28: hnRNPC-mediated IES reduces global translation at early stages of T cell activation. A) *De novo* translation in Jurkat cells after PMA activation under control and hnRNPC knockdown conditions at the indicated time points. Cells were treated with 10 ug/ml of puromycin 10 minutes before harvesting. Total protein was extracted, and WB-SUnSET was performed. Upper panel: triplicate gels from the indicated time points showing decreased global translation at the early stages of T cell activation (0h vs. 2h/4h) only in siCTRL-electroporated cells. Cycloheximide was added 1 hour before harvesting as a control of treatment. -PUR – no puromycin treatment. hnRNPL serves as a loading control. Lower panel: Quantification of analysis from samples as shown on the left (fold change rel. to 0h; mean ± SD, n = 3, *p<0.05, ** - p<0.01). **B)** *De novo* translation in Jurkat cells after PMA activation in control and hnRNPC knockdown conditions at the indicated time points, analyzed using ^{35}S-Met incorporation. Upper gels show Coomassie-loading control for analyses, bottom gels show autoradiographs (representative gels). Bottom: Quantification of analysis from samples as shown below (n = 3, mean +/- SD). This experiment was performed by Dr. Debojit Bose. **C)** *De novo* translation in Jurkat cells after PMA activation in hnRNPC2- inducing MO (C2 MO) and CTRL MO conditions at the indicated time points. Cells were treated as in A. Upper panel: triplicate gels from the indicated time points showing decreased global translation at the early stages of T cell activation (0h vs. 2h) in C2 MO-electroporated cells. Lower panel (right): Quantification of analysis from samples as shown above and, on the left, (fold change rel. to 0h; mean ± SD, n = 3, *p<0.05, **p<0.01).

4.16. Intron-containing eIF5A reaches the cytoplasm for a short period during the early stages of T cell activation

We have identified a likely association between hnRNPC2-dependent IES and the regulation of *de novo* protein synthesis after T cell activation. First, we examined the consequences of retained introns in our target genes. We speculated that even a single protein coding IES isoform could directly control translation. This association may be amplified by the cumulative action of different IEGs containing retained introns during T cell activation. We selected eIF5A IR variant, as the retained intron lacks a stop codon that could target the mRNA to degradation pathways (Fig. 29A), unlike other analyzed target genes such as *RPL10* and *TRAF4* (Fig. 29B). The IES results in a different protein isoform containing 32 additional amino acids, which we termed eIF5A_IR. First, we addressed whether eIF5A_IR reaches the cytoplasm. Therefore, we stimulated Jurkat T cells with PMA at various time points (0, 15, 30, 60, 90, and 150 minutes) to determine if and when the IES product appears in the cytoplasmic RNA fraction. Cells were harvested, and cytoplasmic RNA was extracted. Upon analyzing cytoplasmic RNA, we detected the eIF5A_IR variant, confirming its export from the nucleus within a short time frame, with the highest peak observed 30 minutes after PMA stimulation (Fig. 29C). To validate these findings, we used splice-site blocking MOs, which bind complementary to intronic sequences and intron-exon boundaries, inducing retention of the targeted intron. We confirmed the increase of eIF5A_IR by introducing an intron-inducing eIF5A_MO into Jurkat T cells and performing radioactive, splicing-sensitive RT-PCR (Fig. 29D). Under these conditions, by

analyzing only the cytoplasmic RNA, we verified the presence of the intron-containing eIF5A isoform in the cytoplasm (Fig. 29E). As in this case, we detected both the endogenously occurring eIF5A_IR in the cytoplasm as well as experimentally induced IR by using eIF5A_MO, we observed even more mRNA exported to the cytoplasm. These findings collectively suggest that the intron-containing eIF5A is rapidly transported to the cytoplasm early during T cell activation, with significant cytoplasmic accumulation occurring as early as 15 to 30 minutes post-activation.

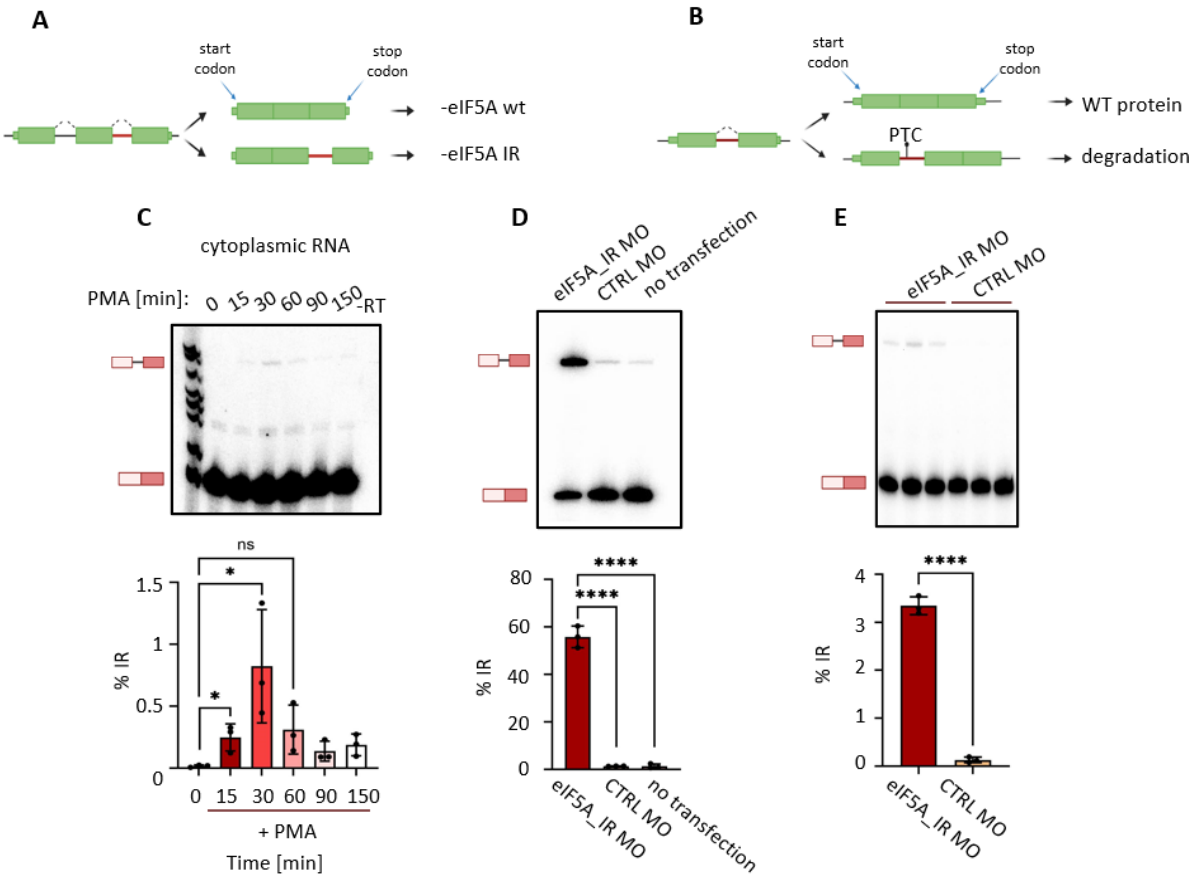

Figure 29: Individual IES products containing retained introns reach the cytoplasm during T cell activation. A) Schematic representation of eIF5A pre-mRNA with (eIF5A_IR) and without retained intron (eIF5A_WT). Green boxes represent exons, dashed lines represent introns. Red connecting line represents the IES event. Created with BioRender.com. **B)** Scheme as in A. Due to the presence of a PTC, IR likely induces NMD. **C)** Intron-containing eIF5A is exported to the cytoplasm. Jurkat cells were PMA-stimulated at the indicated time points and cytoplasmic RNA was extracted. Top: representative gel from radioactive, splicing-sensitive PCR showing IR events in cytoplasm after T cell activation. Bottom: corresponding quantification (%IR, mean ± SD). **D)** Jurkat cells were electroporated with either eIF5A_IR MO to induce intron retention or control MO for 48 hours. Cells were harvested and total RNA was extracted. Additionally, non-transfected cells were used as a negative control. Top: the efficiency of eIF5A_IR MO was analyzed by radioactive, splicing-sensitive PCR and quantified (bottom, % IR; student's unpaired t-test; mean ± SD, n = 3, ***p<0.001, ****p<0.0001). **E)** Jurkat cells were electroporated with either eIF5A_IR MO or CTRL MO as in D. Top: gel from radioactive, splicing-sensitive PCR showing IR events in cytoplasm after T cell activation. Gel shows triplicate samples. Bottom: corresponding quantification (% IR; student's unpaired t-test; mean ± SD, n = 3, ****p<0.0001).

4.17. Intron-containing eIF5A is involved in controlling the translation efficiency at early stages of T cell activation

To investigate the link between intron-containing eIF5A and the regulation of global translation, we first inserted a designed construct of eIF5A_IR into a pFLAG expression vector and transfected it into HEK293 cells. Additionally, we transfected WT construct of eIF5A lacking the retained intron. We performed WB and confirmed the successful introduction of both constructs into HEK293 cells (Fig 30A). We then used WB-SuNSET to address the direct impact of IES products on *de novo* protein synthesis. Overexpression of the eIF5A WT in HEK293 cells had no significant effect compared to the empty vector control. However, overexpression of the IES variant - eIF5A_IR - significantly decreased *de novo* protein synthesis (Fig. 30B). This result demonstrates that even a single IES variant, when overexpressed, can profoundly impact global *de novo* translation. To confirm these findings, we used eIF5A_MO to induce eIF5A intron retention in Jurkat T cells (as shown in Fig. 29D). WB-SuNSET showed reduced *de novo* protein synthesis in cells with increased eIF5A intron retention (Fig. 30C), with the reduction being more pronounced than with the introduction of the eIF5A_IR construct. Together, our data revealed that altering IES in a single event can globally control translation efficiency. We propose that the accumulating effect of several or many smaller IES changes in components of the translation machinery will have a similar overall effect, either by creating inhibiting protein variants (eIF5A) or by reducing the amount of expressed protein through inclusion of PTCs (as in *RPL10*, Fig. 29B). These findings support a model in which a coordinated IES switch, controlled by hnRNPC2, targets the translation machinery to transiently reduce *de novo* protein synthesis during the early hours after T cell activation.

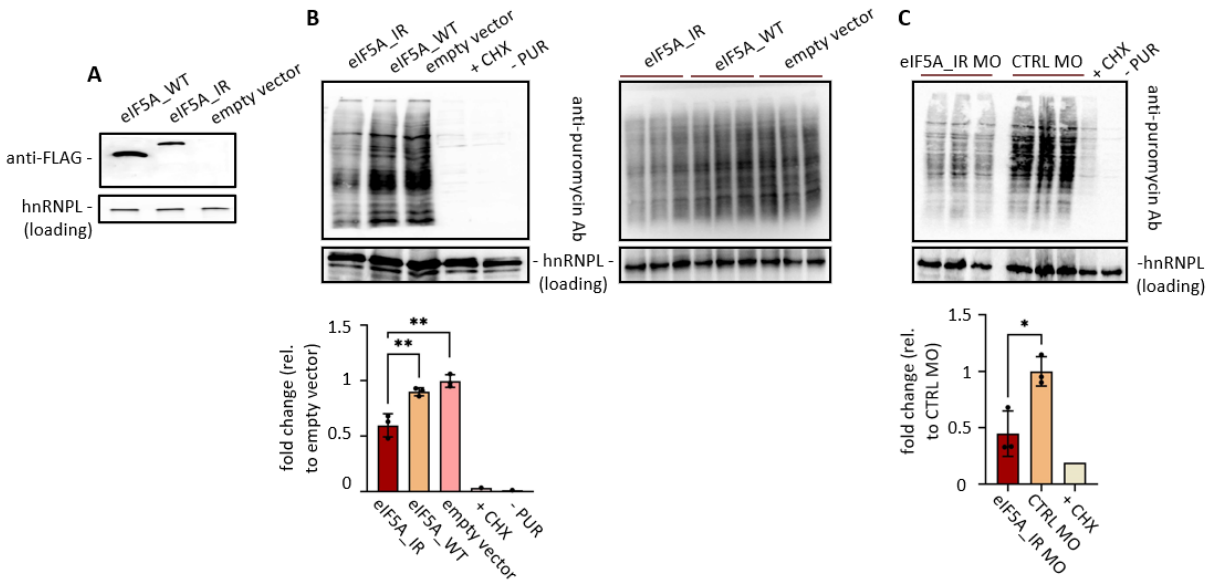

Figure 30: Intron-containing eIF5A reduces global *de novo* protein synthesis. A) HEK293 cells were transfected with eIF5A expression constructs (WT and IR). After 48hours, cells were harvested, and total protein was extracted. Western blot confirms overexpression with hnRNPL as a loading control. **B)** eIF5A_IR inhibits translation. HEK293 cells overexpressing eIF5A WT or IR variants for 48 hours were treated with 10ug/ml of puromycin 10 minutes before harvesting. Total protein was extracted. Left: A representative blot of the WB-SUnSET experiment. Cycloheximide (+ CHX) was added 1 hour before harvesting as a control. -PUR – no puromycin treatment. hnRNPL serves as a loading control. Right: Triplicate samples from the left. Bottom: Corresponding quantification (fold change normalized to empty vector; mean ± SD, n = 3, **p<0.01). **C)** Jurkat cells were electroporated with either eIF5A_IR MO to induce intron retention or control MO for 48 hours. WB-SUnSET was performed as in B. Top: A representative blot shows decreased global translation in Jurkat cells with electroporated eIF5A_IR MO. Bottom: Corresponding quantification; fold change normalized to CTRL MO; mean ± SD, n = 3, *p<0.05).

5. Discussion

The mechanism and functionality of immediate early genes (IEGs) have been analyzed for decades, and their essential role in establishing cellular responses to diverse stimuli is well established. Here, we demonstrated that one of the major signaling cascades controlling IEGs, MEK-ERK signaling, also targets splicing machinery. The response is a fast and transient splicing switch, independent of *de novo* protein synthesis, which we therefore termed immediate early splicing (IES). It has been commonly assumed that alternative splicing allows for a very rapid adaptation of the transcriptome in response to changes in the cellular environment. However, an immediate change in the splicing program and its ensuing functionality has remained unexplored.

5.1. The concept of immediate early splicing after PMA stimulation of T cells

5.1.1. Intron retention events

A substantial body of evidence supports the close coupling of splicing and transcription. Most alternative splicing events are linked to the progression of RNA Pol II. While the transcript is being spliced, it remains bound to RNA Pol II until it reaches the poly-A signal, at which point transcription stops, and the spliced mRNA is released from the chromatin [66]. However, several studies have demonstrated that splicing kinetics can vary for individual introns, with some introns undergoing slower processing and being spliced post-transcriptionally[70]. The goal of this project was to measure the efficiency and dynamics of co-transcriptional (alternative) splicing of nascent RNA immediate early splicing (IES). We aimed to determine whether this mechanism varies across three different time points (0, 30, and 150 minutes). To characterize the mechanistic basis and functionality of IES, we used Jurkat T cells stimulated with PMA as our research model. Detecting IES was only possible through RNA sequencing of chromatin-associated RNA, mimicking nascent RNA. Our bioinformatic analysis and subsequent validation revealed that the alternative splicing differs between 0 and 30 minutes, as well as between 30- and 150-minutes following PMA stimulation of Jurkat T cells. In contrast, co-transcriptional alternative splicing was similar between 0 and 150 minutes (Fig. 12). The changes in splicing patterns were 1) rapid, 2) transient, and 3) independent of *de novo* protein synthesis. These three criteria are required to categorize these AS modifications as IES. Interestingly, among all types of AS analyzed, the majority of splicing patterns were intron retention events (Figs 12 and 13). This type of AS is less frequently observed in human and

mouse muscle and embryonic stem cells, but is highly present in neural, adipose and immune cells[131]. IR contributes to the plasticity of the transcriptome and the regulation of gene expression, also those encoding ribosomal proteins[132]. It plays a role in cell development and differentiation and in response to cellular stress[133]. For instance, Ni et al., demonstrated that IR is prevalent in resting CD_{4+} T cells and dramatically decreases upon cell activation. Interestingly, they found that intron-retained transcripts are less stable, implying a potential linkage between IR and RNA degradation during T cell activation[134].

5.1.2. Consequences of intron-containing transcripts

Several sequencing studies have identified the presence of introns in 5-10% of fully transcribed RNAs[135]. A minor fraction of these IR events generates alternative transcripts where the intron-containing mRNAs code for distinct protein isoforms. In many cases, intron-containing transcripts carry premature termination codons (PTCs) as seen in *RPL10* or *TRAF4* – Fig. 29B), which likely triggers the degradation in the cytoplasm via non-sense-mediated decay (NMD). In contrast, when the retained intron is in frame of the gene, such as in *eIF5A* (Fig. 29A), the transcript is exported to the cytoplasm (Fig. 29C) and leads to the production of different protein isoforms. Another scenario involves detained intron (DI) transcripts, which remain in the nucleus rather than being exported to the cytoplasm. These DI transcripts are insensitive to NMD and can have half-lives exceeding an hour[70]. DI-containing transcripts may later be spliced to produce fully spliced mRNAs for nuclear export or be degraded in the nucleus by the exosome (Fig. 31). Recent studies have highlighted IR as a mechanism for regulating transcriptome dynamics, where certain intron-containing transcripts are intentionally retained in the nucleus for extended periods[27,131,133,136]. Therefore, IR events act to fine-tune mRNA levels by enabling their release into the cytosol upon signal-induced splicing completion.

Our study raises the open question of the fate of intron-containing transcripts after 30 minutes of Jurkat T cell activation. To experimentally address this question, we can track the processing of nascent RNA. One approach involves incorporating biotin into newly synthesized RNA, which can then be captured using streptavidin-based methods. It can be experimentally mediated by biotin-labeling of nucleotides added to nascent RNA by RNA Pol II [137.] Our experiments revealed that intron-containing eIF5A is exported to the cytoplasm upon T cell activation, with the highest peak occurring 30 minutes post-stimulation (Fig. 29C). However,

by biotinylating nascent RNA from T cells stimulated with PMA at different time points, we can determine the fate of intron-containing transcripts – whether they are degraded, spliced out later or translated (as in the case of IES product – eIF5A_IR). Furthermore, this approach will allow us to characterize the localization of these transcripts in different cellular compartments at various stages of T cell activation.

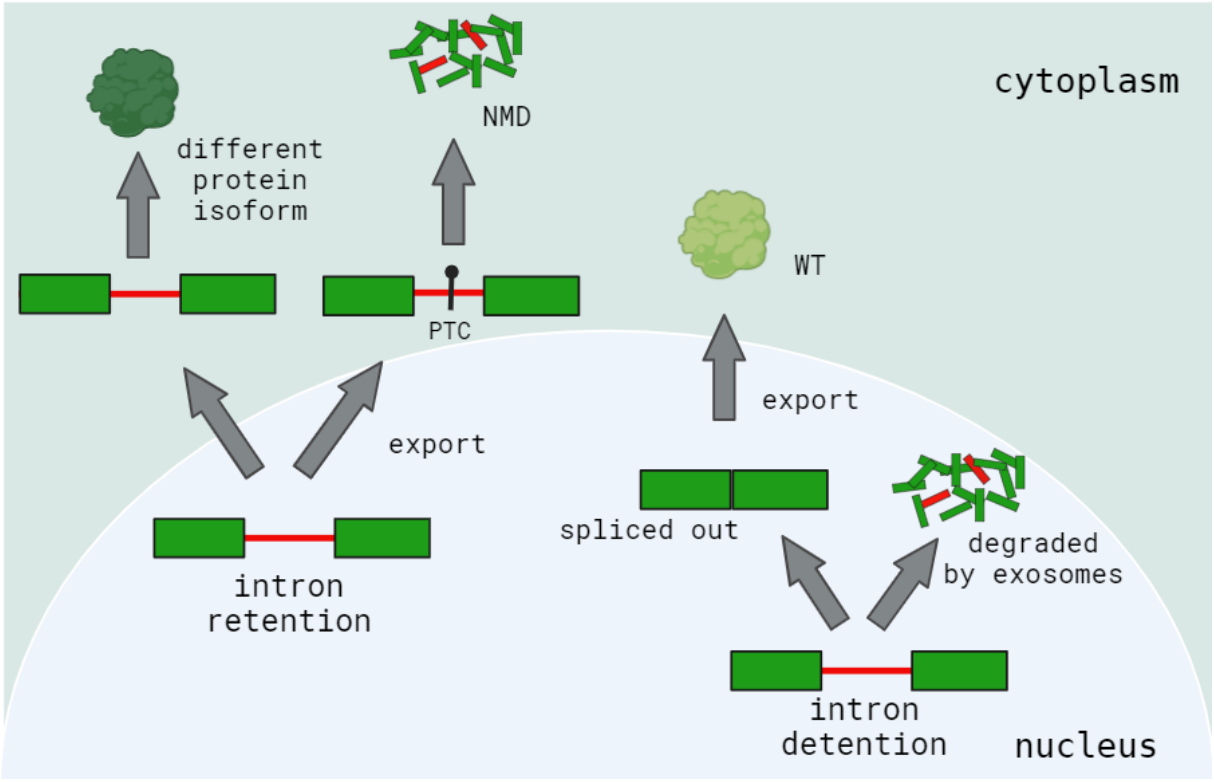

Figure 31. Two types of intron-containing transcripts. Retained introns can be exported to the cytoplasm, where they either undergo degradation via NMD, if they contain PTC, or they contribute to the synthesis of novel protein isoform. In contrast, detained introns remain in the nucleus, where they are either further spliced to produce fully spliced mRNAs for export or degraded by the exosome. Adapted from[138]. Created using Biorender.com

5.1.3. Intron length

Interestingly, we found that most of the retained introns were short, each having fewer than 100 nucleotides (Figs. 12, 13). This suggests that intron length may be a feature influencing the retention/detention in IEGs. This hypothesis could be further tested in future studies using minigene experiments to increase the length of these introns. It is already known that intron length affects the splicing efficiency, with introns shorter than 80 nts displaying a higher likelihood of reduced splicing efficiency[139]. The genome architecture influences how the spliceosome machinery binds to RNA. The minimal distance between 5'SS and BP is estimated to be 50nts; this length is required for efficient spliceosome assembly. Thus far, the

shortest naturally occurring intron with demonstrated efficient splicing is 43nts, found in the human *ESRP2* gene, encoding a splicing factor involved in splicing in epithelial cells [140].

Short introns are more commonly observed in the genomes of lower eukaryotes, where 87% of introns are shorter than 250nts. Intron length is the crucial factor to determine whether splice site recognition occurs across the intron or exon. Splice-site recognition across the intron, referred to as intron definition involves the spliceosome recognizing the splice sites within the intron. This process enhances the inclusion of exons, even when they have weak splice sites. Intron definition diminishes when intron size reaches a threshold length of >250 nts [141.] However, in the human genome, the vast majority of splice sites are recognized across the exon due to the presence of longer flanking introns[140]. Although the close proximity of splicing signals in short introns poses a challenge for the spliceosome, several studies have identified specific factors involved in recognizing short introns. For instance, Keiper et al, demonstrated that the splicing of short introns is controlled by two proteins, Smu1 and RED, which are involved in assembly of spliceosomal B complex assembly[142]. Silencing these proteins led to an increased intron retention rate. It is likely that during T cell activation, phosphorylated hnRNPC2, as other splicing factors including Smu1 and RED, play role in coordinating the fidelity of intron-defined splicing. hnRNPC2 may interact with intron-defined splicing machinery to modulate intron retention and ensure precise regulation of IES during immune response.

5.2. Immediate early splicing among target genes

Our GO term enrichment analysis revealed that retained introns after 30 minutes of PMA stimulation of Jurkat T cells were predominantly observed in genes involved in different steps of translation (Fig. 12G). This finding suggests that IES plays a role in regulating translation efficiency at early stages of T cell activation. We validated the retention of introns in several IEGs including those encoding ribosomal proteins (such as RPL10, RPL13, RPL7A), an RNA helicase – DDX39A, regulators of protein degradation (such as USP11, UBXN1), translation factor – eIF5A and regulator of protein translation – TRAF4 (Fig. 13). Many of these pre-mRNA with retained introns contain PTCs, altering the ORFs, that might thereby target these transcripts for degradation. However, IR event in *eIF5A* leads to the production of different protein isoform (Figs. 29 and 30).

5.2.1. Ribosomal proteins RPL

Components of ribosomal proteins RPL, including RPL10, RPL13 and RPL7A occupy neighboring positions in the 60S large subunit (LSU) of the ribosome. These proteins, along with 77 other ribosomal proteins and four ribosomal RNAs (rRNAs), are assembled to form a fully structured ribosome. Ribosomal proteins are composed of globular, surface-exposed RNA-binding domain that interacts with the rRNA core to stabilize the ribosome structure. Hence, they are involved in ribosome biogenesis and maintaining functional fidelity, acting as sensors of ribosomal activity[143]. The incorporation of RPL10 into the LSU is the final step in ribosome maturation. Without RPL10, the LSU is unable to bind to 40S small subunit (SSU) of the ribosome (SSU), preventing the formation of a functional ribosome [144]. IR in these genes could reduce the levels of functional proteins, impacting ribosome assembly and function. This could thereby result in a global decrease in protein synthesis, particularly affecting proteins critical for the immune response. This RPL10 deficiency could also slow down lymphocyte growth and effective proliferation, impairing cytokine secretion and cytotoxic activity.

5.2.2. TRAF4

TRAF4 (TNF receptor associated factor) plays a role in signaling pathways that govern inflammation, immunity, and cell survival. It interacts with signaling molecules involved in modulating translation efficiency. For instance, TRAF4 binds to phosphatidylinositol phosphate (PIP) lipids on cell membranes, which may facilitate the PI_3K kinase recruitment and the activation of downstream AKT/mTOR and ERK1/2 pathways. These two signaling cascades are involved in T cell growth and proliferation[145]. Furthermore, TRAF4 has been shown to increase NF-κB activation triggered by the glucocorticoid-induced TNF receptor, which is highly expressed in T cells, B cells and macrophages[90]. Preliminary data also indicated that TRAF4 promotes the JNK kinase activation, through the oligomerization of its intermediate factor – MEKK4[146]. These findings suggest that TRAF4 may influence translation indirectly by affecting the stability and activity of translation-related factors. IR in TRAF4 can lead to reduced levels of functional protein, impairing all mentioned-above signaling pathways involved in immune response. This can result in defective T cell activation, reduced cytokine production, impaired immune cell migration, and a weakened immune response.

5.2.3. Eukaryotic initiation factor 5a – eIF5A

Our analysis revealed that the IES product - eIF5A_IR does not contain a PTC, preventing its degradation. The retained intron leads to the production of a different protein isoform with additional 32 aa (Fig. 29A). The IES product was shown to be exported to the cytoplasm, as demonstrated by radioactive, splicing-sensitive RT-PCR, reflecting the endogenous conditions (Fig. 29C), and by using morpholinos that induce IR events in this mRNA (Fig. 29E).

eIF5A (eukaryotic initiation factor 5a) is a small (154aa) and ubiquitous protein highly conserved across eukaryotes. Its characteristic feature is a high abundance; there are more than 273 000 copies of eIF5A per cell, which is almost twice the number of ribosomes[147]. This high abundance can be explained by its crucial function during the elongation phase of protein synthesis. eIF5A accelerates peptidyl transfer at most sequences, especially those that are difficult to synthesize, such as consecutive proline codons (PPP), polyproline motifs, glycine residues, and charged amino acids. Furthermore, eIF5A stimulates the stabilization and hydrolysis of peptidyl-tRNA during translation termination[148]. A distinctive feature of eIF5A is a unique post-translational modification – hypusination. This modification involves the addition of conserved lysine residue (Nε-(4-amino-2-hydroxybutyl) lysine in Lys50 in humans) through the action of two enzymes: deoxyhypusine synthase (DHPS) and deoxyhypusine hydroxylase (DOHH). Hypusination allows for stronger and more efficient interaction of eIF5A with the ribosome. eIF5A localizes near the P-site tRNA, overlapping the E-site. More specifically, eIF5A prevents ribosome stalling at difficult-to-synthesize sequences by projecting the hypusine-containing domain toward the P-site to facilitate the transfer of the nascent chain from P-tRNA to A-tRNA[148]. Furthermore, eIF5A can be localized in the endoplasmic reticulum (ER), where it is associated with ribosomes bound to the ER membrane, and it seems to facilitate the co-translational translocation of certain proteins into the ER, such as collagen[149]. Several studies also indicated its involvement in operating the transport of newly generated mRNAs from the nucleus to the cytoplasm to maintain the balance of mRNA recruitment to the ribosome for translation and degradation[150]. Disruptions of *eIF5A* genes have been shown to cause growth arrest and strong anti-proliferative effects, including apoptosis[150].

IR in eIF5A may lead to reduced levels of functional eIF5A protein, impairing global translation elongation. This could decrease the synthesis of key proteins required for immune response, including cytokines, receptors and signaling molecules. Furthermore, it may hinder lymphocyte's ability to proliferate effectively after activation, attenuating the adaptive immune response. In this project, we identified a specific intron 5 in eIF5A that, instead of disrupting the synthesis of eIF5A WT, leads to the production of different protein isoform (IES product - eIF5A_IR). This protein isoform reduced *de novo* global translation (Fig. 30).

5.2.4.1. Structure of IES product – EIF5A_IR

eIF5A folds into a two-domain structure of predominantly β-sheet character, where the N - terminal region contains the hypusine residue (K50). This residue is located at the tip of an extended, unstructured, and exposed loop (hypusine loop) resembling a tRNA[151] (Fig. 30). Using the Alpha Fold database, we accurately overlapped the structures of two eIF5A protein isoforms. We aimed to predict whether the conformation of the IES product (EIF5A_IR) is altered due to the presence of an additional 32 amino acids resulting retained introns (Fig. 27A). The EIF5A_IR introduces a new helical stretch in the form of an α-helix, which could potentially interact with the P-site tRNA. The structure of IES product – EIF5A_IR was not shown in the literature yet. Therefore, IES product eIF5A may be associated with a regulation of translation machinery through its interactions with P-site. As we observed a reduction of *de novo* global translation (Fig. 28) associated with IES product, we hypothesize that intron-containing protein isoform of eIF5A may destabilize its interaction with the ribosome, thereby decreasing the efficiency of translation.

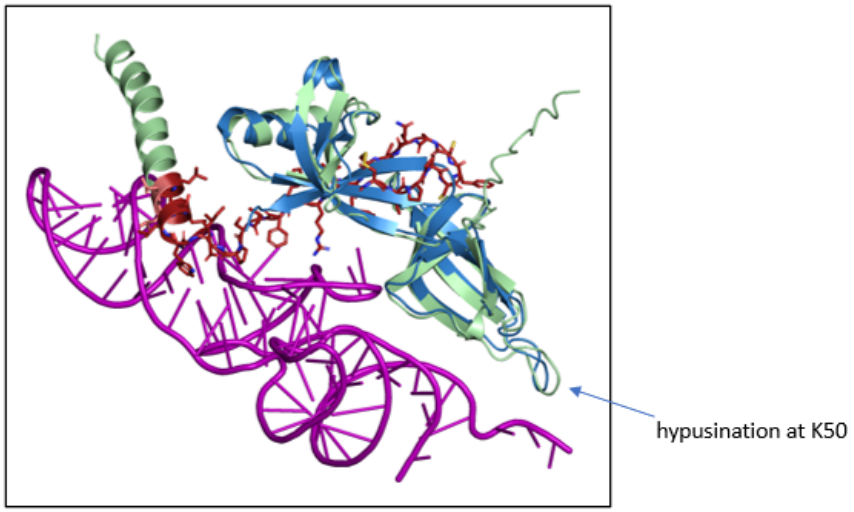

Figure 32: Overlaid structures of EIF5A_WT and IES product – EIF5A_IR. IES product alters the structure of EIF5A by the production of additional helical stretch in the form of an α-helix. The P-site tRNA is shown in violet, the IES product in green, with the additional amino acids highlighted in maroon sticks. EIF5A_WT is depicted in blue. The hypusination at K50 is indicated by an arrow. EIF5A_WT was shown in[152]; PDB: 3CPF; EIF5A_IR isoform is a predicted model. Created and analyzed together with Gopika Sasikumar (Prof. Markus Wahl's lab).

5.3. Phosphorylation as a strategy to influence AS

The impact of dynamic phosphorylation on coordinating splicing efficiency has been studied in detail for many different spliceosomal proteins and accessory splicing factors. Phosphorylation regulates the affinity of RNA: protein or protein: protein interactions[153]. For instance, the phosphorylation of SF1 and SRSF1 proteins enhances their ability to promote exon inclusion by facilitating their interactions with U1 snRNP and the U2AF65, respectively[154]. Additionally, phosphorylation can affect the subcellular localization of proteins[155]. For example, phosphorylation-dependent changes in localization can alter the recruitment of SR proteins from nuclear speckles, which serve as a storage sites for splicing factors, to nascent RNA during splicing, thereby influencing the recognition of splice sites. This modified SR localization is caused by enhanced interactions of phosphorylated SR proteins with their import receptor, transportin SR2[156]. Phosphorylation-dependent protein-protein interactions were also demonstrated in a study of Misteli et al. Upon stress stimuli such as osmotic shock or UV irradiation, hnRNPA1 was phosphorylated by MAPK p38, leading to its translocation to cytoplasmic stress granules (SGs). This nucleo-cytoplasmic transport modulates the nuclear ratio between hnRNPA1 and SR proteins, triggering changes in the AS of cellular genes, particularly at the A5SS[155]. Furthermore, Liu et al., found that phosphorylation affects the splicing activity of hnRNPL by reducing its interaction with U2AF65, leading to AS in the *slo1* gene, which is a main component of potassium channels[157].

5.3.1. Transient phosphorylation of hnRNPC affects IES upon T cell activation

As shown in Fig. 7, hnRNPC consists of two protein isoforms, hnRNPC1 and hnRNPC2, which differ from each other by the presence of an additional 13 aa in the hnRNPC2 isoform. Although hnRNPC2 contains several serine residues (Fig. 25A), our phosphoproteomic analysis showed that the transient phosphorylation of hnRNPC upon Jurkat T cell activation is located at specific residue, S115 (Fig. 14A). This residue is one of the 13 amino acids found only in C2 isoform. The transient, reversible hnRNPC2 phosphorylation was also confirmed by Western

Blot (Fig. 14C). The phosphorylation of hnRNPC2 increases after 15 and 30 minutes of PMA stimulation of Jurkat T cells, followed by a gradual return to baseline levels after 90 minutes. This result revealed that almost the entire hnRNPC2 population undergoes transient phosphorylation, which is an unusual observation. Typically, phosphorylation affects only a fraction of the protein population[158,159]. This selective phosphorylation often results in different behaviors of the protein, as observed in the case of hnRNPC2. Notably, hnRNPC forms a heterotetramer, with a macromolecular ratio C1:C2 = 3:1, as shown at the mRNA level (Fig. 14B). To find differences in functionality between hnRNPC1 and hnRNPC2, we performed RNA-sequencing with two opposite approaches: CRISPR/Cas9 ΔhnRNPC2 knockout (Fig. 24) and hnRNPC2-inducing MO (Fig. 26). The next goal was to experimentally validate these RNA-seq data (Figs. 25, 26). Although we observed significant changes in gene expression during the hnRNPC2 Δknockout (Figs. 24, 25), we were unable to replicate these results during validation using MO (Fig. 26). Altering the ratio between hnRNP1 and hnRNPC2 did not result in major changes in the transcriptome of HEK293 and HeLA cells. These results suggest that while hnRNPC2 may play a role in regulation, it does not appear to be directly associated with significant transcriptomic changes. Furthermore, the precise C1:C2 ratio in the hnRNPC tetramers is likely not critical for their functionality, at least when hnRNPC2 is present in its unphosphorylated stage.

By silencing hnRNPC in Jurkat T cells and HEK293 cells (Fig. 16), we observed an increase in IR events compared to control conditions, suggesting that hnRNPC is required for the efficient splicing of retained introns affected by IES. These findings were further supported by EMSA assays (Fig. 17), which showed that the phosphomimetic version of hnRNPC2 reduced binding affinity to target introns of analyzed genes, thereby reducing splicing efficiency. Furthermore, our results are consistent with data from experiments using hnRNPC2-inducing MO, where we manipulated the hnRNPC2:C1 ratio in favor of the hnRNPC2 isoform. Increased expression of hnRNPC2 due to MO treatment led to enhanced IR events in *RPL10* and *eIF5A* (Fig. 15D) and more phosphorylated hnRNPC2 was detected upon 15 and 30 minutes of T cell activation (Fig. 15E). The presence of more phosphorylated hnRNPC2 resulted in reduced binding to intronic regions, thus lowering splicing efficiency, which was evident from the increased IR events.

hnRNPC has been associated with reduced splicing efficiency, for example by competing with U2AF65 for binding to the polypyrimidine tract[53]. However, a splice-activating role of hnRNPC has also been described[160]. In recent years, Moon et al., showed that hnRNPC1 and hnRNPC2 promote the increase of exon 11 inclusion of *Ron* pre-mRNA. This change in AS was mediated through the activation of intron 10 splicing. The *Ron* proto-oncogene encodes a receptor for macrophage-stimulating protein (MSP), which is involved in macrophage activation, cell motility and epithelial cell migration. Upon binding of MSP to the *Ron* receptor, the receptor activates signaling pathways that promote cell proliferation, survival, and migration. Exon 11 skipping in the *Ron* gene leads to the formation of a truncated protein isoform lacking 49 aa, disrupting its ability to bind MSP[160]. Furthermore, our finding that hnRNPC2 phosphorylation attenuates efficient splicing is consistent with the study by Martino et al. hnRNPC phosphorylation was found to affect the AS of mRNAs involved in mechanotransduction and cardiovascular diseases, including Yes-associated protein 1 (*YAP1*). hnRNPC depletion led to exon 4 inclusion in the *YAP1* gene, which is associated with increased progression of heart failure. hnRNPC phosphorylation was mediated by PKC kinase upon pathological cardiac remodeling of extracellular matrix (ECM). Increased stress generated by cardiac ECM remodeling enhances the likelihood of hnRNPC relocation from the nucleus due to increased phosphorylation. Hence, the depletion of hnRNPC in the nucleus affects the AS of transcripts involved in the progression of heart failure, for example exon 4 inclusion in *YAP1* gene[161]. Moreover, this study presents the hypothesis worth exploring in our further studies to investigate the distribution of hnRNPC during T cell activation and determine whether phosphorylation affects the localization of this protein. Altogether, our data suggest that hnRNPC2 phosphorylation controls IES based on the direct affinity between these proteins and introns being retained in analyzed genes.

We demonstrated that the phosphorylation of hnRNPC2 is a key factor that alters its behavior and function during lymphocyte activation. Based on our findings, we developed a model that warrants further investigation. In resting T cells, transcripts of the analyzed genes are efficiently spliced by the splicing machinery, with hnRNPC1/2 playing a promoting role (as shown in every radioactive, splicing-sensitive RT-PCR). Upon 15 or 30 minutes of PMA stimulation, the increasing transient phosphorylation of hnRNPC2 reduces its binding to selected introns, thereby decreasing splicing efficiency, which is evident from the rise of IR events. As demonstrated by our example of eIF5A, partially spliced, intron-containing

transcripts generated within a short time, 15- or 30-minutes after T cell activation, can reach the cytoplasm to allow the translation of distinct protein isoforms. These introns are referred to as retained, rather than detained, since they pass through the nuclear pores to the cytoplasm and may be translated. Fully spliced transcripts, which are efficiently processed, are directly exported to the cytoplasm following transcription.

5.3. 2 Temporal phosphorylation of splicing factors other than hnRNPC

Our phosphoproteomic approach identified several splicing regulatory proteins that are phosphorylated upon T cell activation, including hnRNPC (Fig. 14A), U2AF35, and LARP1 (data not shown). We focused our analysis on hnRNPC due to its temporal phosphorylation, which aligned with IES. Additionally, knockdown experiments with different siRNAs abolished IES in hnRNPC knockdown, a result that was not observed with other splicing factors (Fig. 16B). The current understanding that hnRNPC binds to uridine-rich stretches of introns further supports our focus on this splicing factor[56]. In particular interesting is U2AF35, the protein that forms a heterodimer with U2AF65 and directly binds the AG dinucleotide at the 3' splice site and the polypyrimidine tract, respectively, during the spliceosome assembly[53]. A transient phosphorylation at a specific site, Ser61, on U2AF35 aligns with the kinetics of the alternative IES switch following T cell activation, suggesting its involvement in implementing of this switch. Consistent to our hypothesis, crystal structures of truncated U2AF1-U2AF2 complexes suggest that Ser61 phosphorylation may lead to conformational changes that alter the RNA-binding properties of the U2AF35 RRM[162]. However, the involvement of U2AF1 in IES requires further investigation. Furthermore, LA-related protein 1 (LARP1) is known to control ribosomal biogenesis as a phosphorylation-sensitive molecular switch dependent by mTOR pathway. Non-phosphorylated LARP1 interacts with 5' and 3'UTRs of mRNAs encoding ribosomal proteins and inhibits their translation. Upon LARP1 phosphorylation, this inhibitory activity is disrupted, leading to the translation of ribosomal proteins[163].

5.4. Signaling pathways involved in hnRNPC2-controlled IES -RAF/MEK/ERK

Signaling pathways involve the phosphorylation states of different kinases that regulate the activity of splicing factors. As shown in our study, ERK1/2 becomes phosphorylated upon PMA stimulation in Jurkat cells (Fig. 21F). This results in the activation of a signaling pathway that leads to temporal phosphorylation of hnRNPC2 and IES (Fig. 18). Consistency, the RAF/MEK/ERK1/2 signaling pathway has been found to phosphorylate

SAM68, which potentiates splicing of variable exons in *CD44*[164]. Furthermore, this pathway was found to phosphorylate hnRNPK, which results in its cytoplasmic accumulation under serum stimulation[165].

The expression of IEGs is rapidly and transiently "switched on" upon stimulation. Afterward, the expression returns to a steady-state, likely reaching pre-stimulation levels. We found that the phosphorylation of hnRNPC2 upon PMA stimulation, which triggers IES, is likely mediated by ERK1/2 kinase (Fig. 18). However, a key question remains: what intermediate factor "switches off" IES by reversing the transient phosphorylation of hnRNPC2? We observed transient phosphorylation of hnRNPC2 in Jurkat T cells at specific time points, with a quantitative shift in the entire population of hnRNPC2 when comparing resting T cells with those stimulated for 15, and 30 minutes after PMA stimulation (Fig. 14C). Given the significant peak of phosphorylation observed, it is unlikely that the entire protein population is degraded and replaced by a new hnRNPC2 isoform. Instead, it is more plausible that phosphatase activity mediates the dephosphorylation of hnRNPC2 at later time points, that affects IES, particularly beyond 30 minutes post-stimulation. The precise mechanism behind the “switching off” of IES induction remains to be further elucidated.

5.5. IES – specific to T and B cells or global effect?

Our study is the first to introduce the concept of IES. We uncovered a highly specific hnRNPC2-dependent mechanism that occurs in lymphocytes (T cells of human and mouse origin – Figs. 19A, B and B cells – Fig. 20) upon early stages of PMA stimulation. This concept may be expanded by using different cell lines and stimuli and targeting other genes. Furthermore, the phosphorylation of splicing factors other than hnRNPC can alter RNA affinity or binding specificity, potentially contributing to changes in splicing patterns. We did not observe hnRNPC2-mediated IES in neuroblastoma N2a cells in *RPL10* and *eIF5A* upon PMA or KCl stimulation for 0, 30, and 150 minutes (Figs. 19D, E). Similarly, no effects were seen following PMA or LPS treatment in macrophages RAW267.4 cells on the target genes (Figs 19F, G). Nevertheless, other targets regulated by different RBPs may contribute to controlling transcriptomic changes and cellular functionality in these settings. The immediate response to depolarization in neuronal cells (e.g. SH-SY5Y cells) is a model system that merits further studies. Several studies highlight the crucial role of IEGs in neurons, particularly in brain regions associated with learning, memory formation and synaptic plasticity[130]. To date, the

most studied IEG is *c-fos*, which has been shown to exhibit transient and rapidly changing expression following neuronal activation (Fig. 12A)[114]. Thus, it is likely that IES plays an essential role in controlling cellular responses under diverse conditions. However, further research is needed to fully understand the scope of IES and its functional consequences within cells.

5.6. The role of PKCθ kinase in hnRNPC2-controlled IES

Our observation that transient phosphorylation of hnRNPC2 leads to IES in T cells and B cells prompted us to search for additional kinases that might be responsible for this specificity. We focused on identifying proteins that are activated during lymphocyte activation but are not associated with other cell types. Through this approach, we identified various components of the PKC family that could induce IES by interacting with hnRNPC. We particularly focused on PKCθ, given its high expression in T cells as reported in the current literature. By performing RT-qPCR we confirmed the high expression of PKCθ in T cells of human and mouse origin (Jurkat and EL4 T cells – Figs. 21 A, B, respectively). Additionally, this kinase was barely or not expressed in any other tested cell lines. Interestingly, PKCθ was not expressed in Raji B cells and barely expressed in Ramos B cells, suggesting the involvement of different, independent mechanisms leading to hnRNPC2-dependent IES (Fig. 21A). This finding opens a potential new direction for further studies aimed at determining the upstream mechanisms leading to IES in B cells and the cooperative function of IES between T cells and B cells during their activation. It is likely that another PKC kinase, potentially PKCβ, may be involved in the hnRNPC2-controlled IES in B cells. It was shown that PKCβ is highly expressed in B cells and plays role in activating downstream signaling pathways crucial for the immune response[166].

First, we verified the consequences of PKCθ inhibition on IES and hnRNPC2 phosphorylation upon PMA stimulation in Jurkat T cells. Inhibition of PKCθ abrogated the IES switch and reduced hnRNPC2 phosphorylation (Figs. 21B, C, D). Furthermore, knockdown of PKCθ in Jurkat T cells also prevented IES and hnRNPC2 phosphorylation (Figs. 21F, G), further supporting our hypothesis of PKCθ-dependent IES.

Since we did not observe IR events upon PMA stimulation (Figs. 19A, B) or hnRNPC phosphorylation (Figs. 19C, D) in HEK293 and HeLa cells, we introduced the PKCθ kinase into these cells to determine whether the overexpression construct induces IES and increases

temporal hnRNPC2 phosphorylation in these cells. PKCθ overexpression was sufficient to induce IES in *RPL10* and *eIF5A* in both HEK293 and HeLa cells after 15 and 30 minutes of PMA stimulation (Figs. 22B, C, D, E).

To confirm our data and demonstrate that PKCθ acts through hnRNPC to mediate IES, we co-expressed this kinase along with hnRNPC2 WT and a non-phosphorylable version of hnRNPC2, where all serine and tyrosine residues in the sequence specific to hnRNPC2 isoform were mutated to alanine (Fig. 27). Notably, we observed significantly stronger IES when expressing WT hnRNPC2 as compared to the non-phosphorylatable version, suggesting interactions between hnRNPC2 and PKCθ. This data also supports the finding that hnRNPC2, likely through S115, mediates the IES switch. All these results suggest that PKCθ acts as an additional intermediate, differentiating the signaling pathways between T cells and those in other tested cell lines. However, the exact position of PKCθ within the signaling pathways leading to IES, and its direct targets, remain to be fully elucidated.

One potential model is that PKCθ initiates the priming phosphorylation of hnRNPC2, which then recruits RAF/MEK/ERK signaling pathway to allow temporal phosphorylation of S115 in hnRNPC2, leading to the IES. This hypothesis could be tested using knockdown, overexpression and pharmacological inhibition of PKCθ and then mass spectrometry (MS) to assess the phosphorylation status of hnRNPC2 under both basal and PMA-stimulated conditions. Additionally, we can introduce a kinase-dead version of PKCθ to determine whether PKCθ acts as a scaffolding kinase. This form of the kinase involves mutations in at least one amino acid, that disrupt its catalytic activity, preventing it from transferring phosphate groups to target molecules. They function antagonistically to the WT kinases and exhibit dominant-negative effects[167]. If the kinase-dead PKCθ still enables ERK1/2-mediated phosphorylation of hnRNPC2, it would suggest that PKCθ acts as a scaffold independent of its catalytic activity, rather than mediating the priming phosphorylation of hnRNPC2. Moreover, to analyze the phosphorylation sites of hnRNPC that are targets of PKCθ*, in vitro* kinase assays could be performed. This approach would involve recombinant hnRNPC2 fragments and a commercially available PKCθ enzyme. We also cannot rule out the possibility that PKCθ phosphorylates additional targets involved in hnRNPC2-depedent IES. Several studies indicate that PKC proteins are regulated by their phosphorylation status, which is crucial for protecting PKC from degradation; unphosphorylated proteins are rapidly degraded. PMA-induced

binding of PKC to the cellular membrane converts PKC into its dephosphorylated state, and the addition of PKC inhibitors can protect PKC from dephosphorylation[168]. Therefore, using MS to assess the phosphorylation status of PKCθ under both basal and PMA-stimulated conditions is also worth considering.

5.7. The role of reduction of *de novo* protein synthesis during T cell activation

Upon receiving the appropriate signals, resting T cells are transformed from a quiescent state to an active proliferation state, inducing a battery of genes involved in T cell activation. This process necessitates major transcriptomic and proteomic adaptations to facilitate fundamental changes in cellular functionality. Many studies have analyzed different phases of T cell activation at different levels, from signaling cascades initiated within seconds of T cell receptor engagement to the formation of long-lasting memory T cells upon infection in *in vivo* models[169–172]. AS acts largely independent of changes in *de novo* transcription to induce transcriptomic changes upon T cell activation[173]. While activation induced AS has been analyzed at later timepoints upon stimulation, i.e. 24h or 48h post-induction[174], its role in the early phases of T cell activation has remained elusive. Immediately upon T cell activation, phosphorylation cascades alter the activity of existing proteins that prepare the cell for long term functional changes. For example, T cell activation induces IEGs that then contribute to fundamentally altering the transcriptome at later stages of activation. At the same time, *de novo* protein synthesis is reduced in the hours following T cell activation. This likely is a coordinated reaction to allow faster protein turnover and the formation of an 'activated proteome'. The preexisting mRNAs from the resting phase are translated with reduced efficiency and only once major transcriptomic changes have been made (16h-24h post-stimulation), the translation efficiency is strongly increased[175,176].These findings are consistent with our data from the ^{35}S-methionine incorporation assay and WB-SUnSET analysis, which show that during the early stages of T cell activation, global *de novo* protein synthesis is reduced within the first four hours. However, after eight hours of PMA stimulation, protein synthesis returns to baseline levels or even increases, indicating a surge in global translation (Fig. 28). Simultaneously carrying out energy-demanding processes such as translation and degradation would be highly challenging for lymphocyte metabolism during its early stages of activation. Therefore, T cells must carefully manage their energy expenditure to balance various needs. The observed reduction of translation in the first hours of T cell activation

allows the maintenance of lymphocyte homeostasis. It also prevents the excessive synthesis of proteins that are unnecessary at the onset of activation but may become critical at later stages of lymphocyte activation. Moreover, we have demonstrated that this drop of translation efficiency is abolished when hnRNPC is silenced, indicating that hnRNPC is essential for this decrease during lymphocyte activation. This result is further supported by experiment using hnRNPC2-inducing MO, which increases the levels of the hnRNPC2 isoform. We observed an even stronger reduction in *de novo* protein synthesis (Fig. 28C). Furthermore, this result suggests that IES that is controlled by minor hnRNPC2 isoform may directly lead to altered global *de novo* protein synthesis.

To link IES with reduced global *de novo* translation, we focused on eIF5A, as the retained intron produces different protein isoform with 32 more amino acids. When we introduced IES product - EIF5A_IR overexpression construct into HEK293 cells and performed WB-SUnSET, we observed a significant reduction of translation efficiency. In contrast, there was no change in translation efficiency between HEK293 cells transfected with eIF5A WT construct (eIF5A _WT) and those transfected with an empty vector (Fig. 30B). Furthermore, the IES event in eIF5A alone is sufficient to reduce translation efficiency when manipulated using an antisense morpholino (MO) (Fig. 30C). This suggests that this mRNA variant is translated into a protein that acts to globally reduce translation. Although the level of intron retention (IR) achieved using the MO approach is higher than what is observed during T cell activation, we propose that coordinated IES events across multiple components of the translation machinery could have a similar inhibitory effect on *de novo* translation. This result aligns with recent studies suggesting that retained introns are involved in fine-tuning the transcriptome by eliminating physiologically irrelevant transcripts and/or preventing the production of unwanted gene products during development and differentiation[70,138].

6. Conclusion

We have introduced the concept of immediate early splicing (IES) that occurs during the early stages of T cell activation. IES involves intron retention events that are directly regulated by transient phosphorylation of hnRNPC2, a minor isoform of hnRNPC. This temporal phosphorylation of hnRNPC2 is mediated by the RAF/MERK/ERK signaling pathway and involves the recruitment of PKCθ following T cell activation While hnRNPC2-controlled IES is also observed in B cells, the mechanism appears to involve different kinases. Intron-containing transcripts that lack the PTC, as in the case of eIF5A, lead to the production of different protein isoform, that contain additional 32 amino acids. This IES product results in a reduction in *de novo* protein synthesis during the first four hours of T cell activation (Fig. 31). Therefore, in this project, we generated a new conceptual framework for splicing regulation in the rapid tuning of translation following lymphocyte activation.

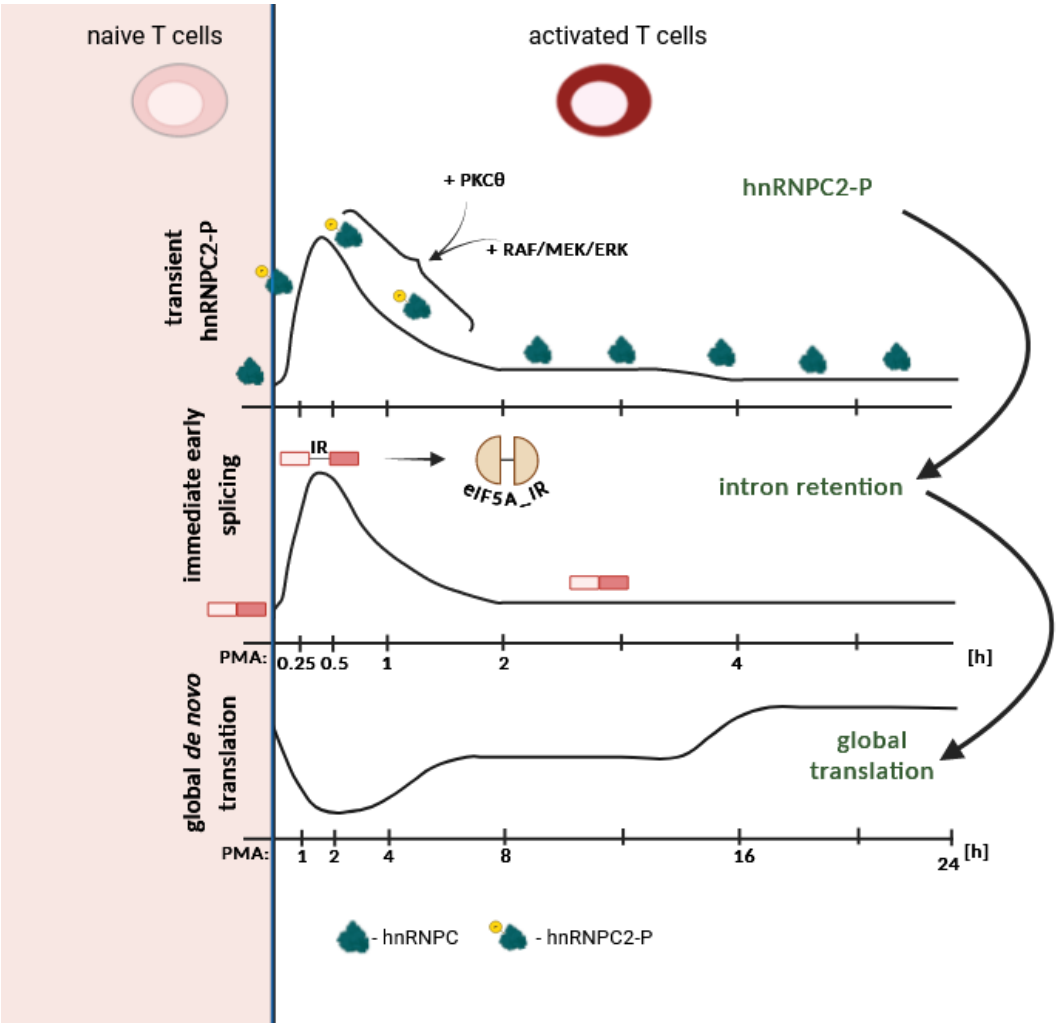

Figure 33. The scheme combining all our findings

7. Appendix

7.1. Abbreviation

3’SS	3‘splice site
5’SS	5‘splice site
Δ	depletion/mutant
A	adenine
A3SS	alternative 3’SS
A5SS	alternative 5’SS
aa	amino acid
Ab	antibody
AD	Alzheimer’s disease
AKT1/2/3	protein kinase B
ALS	amyotrophic lateral sclerosis
AP	alkaline phosphatase
AP-1	activator protein-1
AS	alternative splicing
APC	antigen-presenting cells
APS	ammonium peroxydisulfate
ATCC	American Type Culture Collection
ATP	adenosine triphosphate
BCR	B cell receptor
bp	base pair
BR	basic region
BSA	bovine serum albumin
°C	degree Celsius
C	cytosine
C1	hnRNPC1
C2	hnRNPC2
C2-P	phosphorylated hnRNPC2-P
Ca	calcium
cDNA	complementary DNA
CO_2	carbon dioxide
cSMAC	central supramolecular activation cluster
CTD	carboxy-terminal domain

CTLA-4	cytotoxic T-lymphocyte antigen 4
CTRL	control
Da	dalton
DAG	diacylglycerol
DDX39A	DExD-box helicase 39A
DI	detained introns
DMEM	Dulbecco’s modified eagle's medium
DMSO	dimethyl sulfoxide
DNA	deoxyribonucleic acid
DOHH	deoxyhypusine hydroxylase
dNTP	deoxynucleotide triphosphates
DPHS	deoxyhypusine synthase
dSMAC	distal supramolecular activation cluster
DTT	dithiothreitol
EDTA	ethylenediaminetetraacetate
EGF	epidermal growth factor
eIF5A	eukaryotic initiation factor 5A
EMSA	electrophoretic mobility shift assay
ER	endoplasmic reticulum
ERK1/2	extracellular-signal-regulated kinases
ESE	exonic splicing enhancer
ESS	exonic splicing silencer
F	farad
FBS	fetal bovine serum
FDR	false discovery rate
FL	full length
FOXP3	forkhead box protein P3
g	gram / centrifugal force
G	guanine
GAPDH	glyceraldehyde-3-phosphate dehydrogenase
GATA3	GATA-binding protein 3
GFP	green fluorescent protein
GO	gene ontology
h	hour
H_2O	water

HCC	hepatocellular carcinoma
HCl	hydrochloric Acid
HIV	human immunodeficiency virus
HMMR	hyaluronan-mediated motility receptor
hnRNP	heterogeneous nuclear ribonucleoprotein
HS	high salt
ICAM-1	intercellular adhesion molecule -1
iCLIP	individual-nucleotide resolution crosslinking-immunoprecipitation
IEG	immediate early gene
IES	immediate early splicing
IKK	IκB kinase
IL-2	interleukin - 2
IL-4	interleukin – 4
IL-6	interleukin – 6
IL-7	interleukin – 7
IP_3	inositol triphosphate
IR	intron retention
IRES	internal ribosome entry site
IS	immunological synapse
ISE	intronic splicing enhancer
ISS	intronic splicing silencer
JAK1/2	janus kinase
JNK1/2/3	c-Jun N-terminal protein kinase
kDa	kilodalton
KCl	potassium chloride
KOH	potassium hydroxide
L	liter
LAT	linker for activated T cells
LEF1	lymphocyte enhancer factor 1
LFA-1	lymphocyte Function-associated Antigen 1
LPS	lipopolysaccharide
LS	low salt
LSU	large subunit
M	molar
µ	micro

m7G	7-methylguanosine
MAPK	mitogen-activated protein kinases
MEK1/2	mitogen-activated protein kinase kinase
MHC	major histocompatibility complex
min	minutes
$MgCl_2$	magnesium chloride
ml	milliliter
mM	millimolar
MO	morpholino
mRNA	messenger RNA
MSP	macrophage-stimulating protein
n	nano
NaCl	sodium chloride
NaOH	sodium hydroxide
NF-κB	nuclear factor kappa-light-chain-enhancer of activated B cells
NFAT	nuclear factor of activated T cells
NMD	Nonsense-mediated decay
NP-40	nonidet P-40
NPS	nuclear pore complex
NRS	nuclear retention sequence
OD	oligomerization domain
OH	hydroxyl group
ORF	open reading frame
PAGE	polyacrylamide gel-electrophoresis
PBS	phosphate buffered saline
PCA	principal component analysis
PCI	phenol-chloroform-isoamyl alcohol
PCR	polymerase chain reaction
PDGF	platelet-derived growth factor
pH	potential of hydrogen
PI	phosphatidylinositol
PKC	protein kinase C
PMA	phorbol myristate acetate
PMSF	phenylmethylsulphonyl fluoride
Pol	polymerase

PPT	polypyrimidine tract
pre-mRNA	precursor-mRNA
PSI	percentage spliced in
pSMAC	peripheral supramolecular activation cluster
PTC	Premature termination stop codon
PTK	protein tyrosine kinase
PTM	post-translational modification
%	percent
RBM	RNA-binding motif
RIPA	radioimmunoprecipitation assay buffer
RNA	ribonucleic acid
RPL7A	ribosomal protein L7A
RPL10	ribosomal protein L10
RPL13	ribosomal protein L13
rpm	Revolutions per minute
RPMI	roswell Park Memorial Institute Medium
RT	room temperature/ Reverse transcription
s	second
SAPK	stress-activated protein kinases
SDS	sodium dodecyl sulfate
SE	exon skipping
sgRNA	single guide RNA
siRNA	small interfering RNA
SMA	spinal muscular atrophy
SMAC	supramolecular activation cluster
sp.	species
SR	serine/arginine-rich protein
SSU	small subunit
T	thymine
TAE	buffer solution containing **T**ris base, **a**cetic acid and **E**DTA
TBE	buffer solution containing **T**ris base, **b**oric acid and **E**DTA.
TBST	buffer solution containing **t**ris-**b**uffered **s**aline (TRS) and **T**ween 20.
Tc	cytotoxic T cell
TCR	T cell receptor
TCR-MC	TCR microclusters

Th	helper T cell
TEMED	N, N, N’, N’-tetraacetylethylenediamine
TRAF4	TNF Receptor Associated Factor 4
Tris	Tris-(hydroxymethyl)-aminomethane
U	Uracil/unit
U2AF	U2-auxiliary factor
UBXN1	UBX domain protein 1
USP11	ubiquitin-Specific Peptidase 11
UV	ultraviolet
WB	Western Blot
V	Volt
Vol	Volume
ZAP70	zeta-chain-associated protein kinase 70

7.2. References

1. CRICK F. Central Dogma of Molecular Biology. *Nature*. 1970;227(5258):561-563. doi:10.1038/227561a0

2. Watson JD, Crick FHC. Molecular structure of nucleic acids; a structure for deoxyribose nucleic acid. *Nature*. 1953;171(4356):737-738. doi:10.1038/171737A0

3. Costa dos Santos G, Renovato-Martins M, de Brito NM. The remodel of the "central dogma": a metabolomics interaction perspective. *Metabolomics*. 2021;17(5):48. doi:10.1007/s11306-021-01800-8

4. Verwilt J, Mestdagh P, Vandesompele J. Artifacts and biases of the reverse transcription reaction in RNA sequencing. *RNA*. 2023;29(7):889-897. doi:10.1261/rna.079623.123

5. Zudaire I, Napal Fraile M. Exploring the Conceptual Challenges of Integrating Epigenetics in Secondary-Level Science Teaching. *Res Sci Educ*. 2021;51(4):957-974. doi:10.1007/s11165-019-09899-5

6. Boreikaitė V, Passmore LA. 3'-End Processing of Eukaryotic mRNA: Machinery, Regulation, and Impact on Gene Expression. *Annu Rev Biochem*. 2023;92(1):199-225. doi:10.1146/annurev-biochem-052521-012445

7. Berget SM, Moore C, Sharp PA. Spliced segments at the 5' terminus of adenovirus 2 late mRNA. *Proceedings of the National Academy of Sciences*. 1977;74(8):3171-3175. doi:10.1073/pnas.74.8.3171

8. Suran M. Finding the tail end: The discovery of RNA splicing. *Proceedings of the National Academy of Sciences*. 2020;117(4):1829-1832. doi:10.1073/pnas.1919416116

9. Mokry M, Feitsma H, Nijman IJ, et al. Accurate SNP and mutation detection by targeted custom microarray-based genomic enrichment of short-fragment sequencing libraries. *Nucleic Acids Res*. 2010;38(10):e116-e116. doi:10.1093/nar/gkq072

10. Lee Y, Rio DC. Mechanisms and Regulation of Alternative Pre-mRNA Splicing. *Annu Rev Biochem*. 2015;84(1):291-323. doi:10.1146/annurev-biochem-060614-034316

11. Gao K, Masuda A, Matsuura T, Ohno K. Human branch point consensus sequence is yUnAy. *Nucleic Acids Res*. 2008;36(7):2257-2267. doi:10.1093/nar/gkn073

12. Ruskin B, Krainer AR, Maniatis T, Green MR. Excision of an intact intron as a novel lariat structure during pre-mRNA splicing in vitro. *Cell*. 1984;38(1):317-331. doi:10.1016/0092-8674(84)90553-1

13. Green MR. PRE-mRNA SPLICING. *Annu Rev Genet*. 1986;20(1):671-708. doi:10.1146/annurev.ge.20.120186.003323

14. Fleckner J, Zhang M, Valcárcel J, Green MR. U2AF65 recruits a novel human DEAD box protein required for the U2 snRNP-branchpoint interaction. *Genes Dev*. 1997;11(14):1864-1872. doi:10.1101/gad.11.14.1864

15. Nelson KK, Green MR. Mammalian U2 snRNP has a sequence-specific RNA-binding activity. *Genes Dev*. 1989;3(10):1562-1571. doi:10.1101/gad.3.10.1562

16. Yan C, Wan R, Shi Y. Molecular Mechanisms of pre-mRNA Splicing through Structural Biology of the Spliceosome. *Cold Spring Harb Perspect Biol*. 2019;11(1):a032409. doi:10.1101/cshperspect.a032409

17. Zamore PD, Green MR. Identification, purification, and biochemical characterization of U2 small nuclear ribonucleoprotein auxiliary factor. *Proceedings of the National Academy of Sciences*. 1989;86(23):9243-9247. doi:10.1073/pnas.86.23.9243

18. Wahl MC, Will CL, Lührmann R. The Spliceosome: Design Principles of a Dynamic RNP Machine. *Cell*. 2009;136(4):701-718. doi:10.1016/j.cell.2009.02.009

19. Haltenhof T, Kotte A, De Bortoli F, et al. A Conserved Kinase-Based Body-Temperature Sensor Globally Controls Alternative Splicing and Gene Expression. *Mol Cell*. 2020;78(1):57-69.e4. doi:10.1016/j.molcel.2020.01.028

20. Los B, Preußner M, Eschke K, et al. Body temperature variation controls pre-mRNA processing and transcription of antiviral genes and SARS-CoV-2 replication. *Nucleic Acids Res*. 2022;50(12):6769-6785. doi:10.1093/nar/gkac513

21. Preußner M, Wilhelmi I, Schultz AS, et al. Rhythmic U2af26 Alternative Splicing Controls PERIOD1 Stability and the Circadian Clock in Mice. *Mol Cell*. 2014;54(4):651-662. doi:10.1016/j.molcel.2014.04.015

22. Liao KC, Garcia-Blanco MA. Role of Alternative Splicing in Regulating Host Response to Viral Infection. *Cells*. 2021;10(7):1720. doi:10.3390/cells10071720

23. Liu Q, Fang L, Wu C. Alternative Splicing and Isoforms: From Mechanisms to Diseases. *Genes (Basel)*. 2022;13(3):401. doi:10.3390/genes13030401

24. Black DL. Mechanisms of Alternative Pre-Messenger RNA Splicing. *Annu Rev Biochem*. 2003;72(1):291-336. doi:10.1146/annurev.biochem.72.121801.161720

25. Sammeth M, Foissac S, Guigó R. A General Definition and Nomenclature for Alternative Splicing Events. *PLoS Comput Biol*. 2008;4(8):e1000147. doi:10.1371/journal.pcbi.1000147

26. Sammeth M. Complete Alternative Splicing Events Are Bubbles in Splicing Graphs. *Journal of Computational Biology*. 2009;16(8):1117-1140. doi:10.1089/cmb.2009.0108

27. Sakabe N, de Souza S. Sequence features responsible for intron retention in human. *BMC Genomics*. 2007;8(1):59. doi:10.1186/1471-2164-8-59

28. Jaillon O, Bouhouche K, Gout JF, et al. Translational control of intron splicing in eukaryotes. *Nature*. 2008;451(7176):359-362. doi:10.1038/nature06495

29. GRAVELEY BR. Sorting out the complexity of SR protein functions. *RNA*. 2000;6(9):S1355838200000960. doi:10.1017/S1355838200000960

30. Marasco LE, Kornblihtt AR. The physiology of alternative splicing. *Nat Rev Mol Cell Biol*. 2023;24(4):242-254. doi:10.1038/s41580-022-00545-z

31. Rossbach O, Hung LH, Khrameeva E, et al. Crosslinking-immunoprecipitation (iCLIP) analysis reveals global regulatory roles of hnRNP L. *RNA Biol*. 2014;11(2):146-155. doi:10.4161/rna.27991

32. Caputi M. SR proteins and hnRNP H regulate the splicing of the HIV-1 tev-specific exon 6D. *EMBO J*. 2002;21(4):845-855. doi:10.1093/emboj/21.4.845

33. Gillentine MA, Wang T, Hoekzema K, et al. Rare deleterious mutations of HNRNP genes result in shared neurodevelopmental disorders. *Genome Med*. 2021;13(1):63. doi:10.1186/s13073-021-00870-6

34. Han SP, Tang YH, Smith R. Functional diversity of the hnRNPs: past, present and perspectives. *Biochemical Journal*. 2010;430(3):379-392. doi:10.1042/BJ20100396

35. Geuens T, Bouhy D, Timmerman V. The hnRNP family: insights into their role in health and disease. *Hum Genet*. 2016;135(8):851-867. doi:10.1007/s00439-016-1683-5

36. Huelga SC, Vu AQ, Arnold JD, et al. Integrative Genome-wide Analysis Reveals Cooperative Regulation of Alternative Splicing by hnRNP Proteins. *Cell Rep*. 2012;1(2):167-178. doi:10.1016/j.celrep.2012.02.001

37. Paradis C, Cloutier P, Shkreta L, Toutant J, Klarskov K, Chabot B. hnRNP I/PTB can antagonize the splicing repressor activity of SRp30c. *RNA*. 2007;13(8):1287-1300. doi:10.1261/rna.403607

38. Xu H, Li P, Wang X, Zhuang H, Hua ZC. Emerging roles of hnRNP A2B1 in cancer and inflammation. *Int J Biol Macromol*. 2022;221:1077-1092. doi:10.1016/j.ijbiomac.2022.09.104

39. Nadal M, Anton R, Dorca-Arévalo J, Estébanez-Perpiñá E, Tizzano EF, Fuentes-Prior P. Structure and function analysis of Sam68 and <scp>hnRNP A1</scp> synergy in the exclusion of exon 7 from <scp> *SMN2* </scp> transcripts. *Protein Science*. 2023;32(4). doi:10.1002/pro.4553

40. Purice MD, Taylor JP. Linking hnRNP Function to ALS and FTD Pathology. *Front Neurosci*. 2018;12. doi:10.3389/fnins.2018.00326

41. Jiang L, Lin W, Zhang C, et al. Interaction of tau with HNRNPA2B1 and N6-methyladenosine RNA mediates the progression of tauopathy. *Mol Cell*. 2021;81(20):4209-4227.e12. doi:10.1016/j.molcel.2021.07.038

42. Christian KJ, Lang MA, Raffalli-Mathieu F. Interaction of Heterogeneous Nuclear Ribonucleoprotein C1/C2 with a Novel *cis* -Regulatory Element within p53 mRNA as a Response to Cytostatic Drug Treatment. *Mol Pharmacol*. 2008;73(5):1558-1567. doi:10.1124/mol.107.042507

43. Whitson SR, LeStourgeon WM, Krezel AM. Solution Structure of the Symmetric Coiled Coil Tetramer Formed by the Oligomerization Domain of hnRNP C: Implications for Biological Function. *J Mol Biol*. 2005;350(2):319-337. doi:10.1016/j.jmb.2005.05.002

44. König J, Zarnack K, Rot G, et al. iCLIP reveals the function of hnRNP particles in splicing at individual nucleotide resolution. *Nat Struct Mol Biol*. 2010;17(7):909-915. doi:10.1038/nsmb.1838

45. Cieniková Z, Damberger FF, Hall J, Allain FHT, Maris C. Structural and Mechanistic Insights into Poly(uridine) Tract Recognition by the hnRNP C RNA Recognition Motif. *J Am Chem Soc*. 2014;136(41):14536-14544. doi:10.1021/ja507690d

46. Mo L, Meng L, Huang Z, Yi L, Yang N, Li G. An analysis of the role of HnRNP C dysregulation in cancers. *Biomark Res*. 2022;10(1):19. doi:10.1186/s40364-022-00366-4

47. McAfee JG, Soltaninassab SR, Lindsay ME, LeStourgeon WM. Proteins C1 and C2 of Heterogeneous Nuclear Ribonucleoprotein Complexes Bind RNA in a Highly Cooperative Fashion: Support for Their Contiguous Deposition on Pre-mRNA during Transcription. *Biochemistry*. 1996;35(4):1212-1222. doi:10.1021/bi951974k

48. Huang M, Rech JE, Northington SJ, et al. The C-protein tetramer binds 230 to 240 nucleotides of pre-mRNA and nucleates the assembly of 40S heterogeneous nuclear ribonucleoprotein particles. *Mol Cell Biol*. 1994;14(1):518-533. doi:10.1128/MCB.14.1.518

49. Barnett SF, Theiry TA, Lestourgeon WM. The Core Proteins A2 and B1 Exist as $(A2)_3$ B1 Tetramers in 40S Nuclear Ribonucleoprotein Particles. *Mol Cell Biol*. 1991;11(2):864-871. doi:10.1128/mcb.11.2.864-871.1991

50. Nakielny S, Dreyfuss G. The hnRNP C proteins contain a nuclear retention sequence that can override nuclear export signals. *J Cell Biol*. 1996;134(6):1365-1373. doi:10.1083/jcb.134.6.1365

51. Buratti E, Chivers M, Královičová J, et al. Aberrant 5′ splice sites in human disease genes: mutation pattern, nucleotide structure and comparison of computational tools that predict their utilization. *Nucleic Acids Res*. 2007;35(13):4250-4263. doi:10.1093/nar/gkm402

52. Vořechovský I. Aberrant 3′ splice sites in human disease genes: mutation pattern, nucleotide structure and comparison of computational tools that predict their utilization. *Nucleic Acids Res*. 2006;34(16):4630-4641. doi:10.1093/nar/gkl535

53. Zarnack K, König J, Tajnik M, et al. Direct Competition between hnRNP C and U2AF65 Protects the Transcriptome from the Exonization of Alu Elements. *Cell*. 2013;152(3):453-466. doi:10.1016/j.cell.2012.12.023

54. Godet AC, David F, Hantelys F, et al. IRES Trans-Acting Factors, Key Actors of the Stress Response. *Int J Mol Sci*. 2019;20(4):924. doi:10.3390/ijms20040924

55. Kim JH, Paek KY, Choi K, et al. Heterogeneous Nuclear Ribonucleoprotein C Modulates Translation of c- *myc* mRNA in a Cell Cycle Phase-Dependent Manner. *Mol Cell Biol*. 2003;23(2):708-720. doi:10.1128/MCB.23.2.708-720.2003

56. Sella O, Gerlitz G, Le SY, Elroy-Stein O. Differentiation-Induced Internal Translation of c- *sis* mRNA: Analysis of the *cis* Elements and Their Differentiation-Linked Binding to the hnRNP C Protein. *Mol Cell Biol*. 1999;19(8):5429-5440. doi:10.1128/MCB.19.8.5429

57. Schepens B, Tinton SA, Bruynooghe Y, et al. A role for hnRNP C1/C2 and Unr in internal initiation of translation during mitosis. *EMBO J*. 2007;26(1):158-169. doi:10.1038/sj.emboj.7601468

58. Holčík M, Gordon BW, Korneluk RG. The Internal Ribosome Entry Site-Mediated Translation of Antiapoptotic Protein XIAP Is Modulated by the Heterogeneous Nuclear Ribonucleoproteins C1 and C2. *Mol Cell Biol*. 2003;23(1):280-288. doi:10.1128/MCB.23.1.280-288.2003

59. Dai B, Sun F, Cai X, Li C, Liu H, Shang Y. Significance of RNA N6-Methyladenosine Regulators in the Diagnosis and Subtype Classification of Childhood Asthma Using the Gene Expression Omnibus Database. *Front Genet*. 2021;12. doi:10.3389/fgene.2021.634162

60. Wang X, Zhao BS, Roundtree IA, et al. N6-methyladenosine Modulates Messenger RNA Translation Efficiency. *Cell*. 2015;161(6):1388-1399. doi:10.1016/j.cell.2015.05.014

61. Liu D, Luo X, Xie M, et al. HNRNPC downregulation inhibits IL-6/STAT3-mediated HCC metastasis by decreasing HIF1A expression. *Cancer Sci*. 2022;113(10):3347-3361. doi:10.1111/cas.15494

62. Park YM, Hwang SJ, Masuda K, et al. Heterogeneous Nuclear Ribonucleoprotein C1/C2 Controls the Metastatic Potential of Glioblastoma by Regulating PDCD4. *Mol Cell Biol*. 2012;32(20):4237-4244. doi:10.1128/MCB.00443-12

63. Wu Y, Zhao W, Liu Y, et al. Function of HNRNPC in breast cancer cells by controlling the dsRNA-induced interferon response. *EMBO J*. 2018;37(23). doi:10.15252/embj.201899017

64. Guo E, Mao X, Wang X, et al. Alternatively spliced ANLN isoforms synergistically contribute to the progression of head and neck squamous cell carcinoma. *Cell Death Dis*. 2021;12(8):764. doi:10.1038/s41419-021-04063-2

65. Niggl E, Bouman A, Briere LC, et al. HNRNPC haploinsufficiency affects alternative splicing of intellectual disability-associated genes and causes a neurodevelopmental disorder. *The American Journal of Human Genetics*. 2023;110(8):1414-1435. doi:10.1016/j.ajhg.2023.07.005

66. Merkhofer EC, Hu P, Johnson TL. Introduction to Cotranscriptional RNA Splicing. In: ; 2014:83-96. doi:10.1007/978-1-62703-980-2_6

67. de la Mata M, Kornblihtt AR. RNA polymerase II C-terminal domain mediates regulation of alternative splicing by SRp20. *Nat Struct Mol Biol*. 2006;13(11):973-980. doi:10.1038/nsmb1155

68. David CJ, Boyne AR, Millhouse SR, Manley JL. The RNA polymerase II C-terminal domain promotes splicing activation through recruitment of a U2AF65–Prp19 complex. *Genes Dev*. 2011;25(9):972-983. doi:10.1101/gad.2038011

69. Andersson R, Enroth S, Rada-Iglesias A, Wadelius C, Komorowski J. Nucleosomes are well positioned in exons and carry characteristic histone modifications. *Genome Res*. 2009;19(10):1732-1741. doi:10.1101/gr.092353.109

70. Boutz PL, Bhutkar A, Sharp PA. Detained introns are a novel, widespread class of post-transcriptionally spliced introns. *Genes Dev*. 2015;29(1):63-80. doi:10.1101/gad.247361.114

71. Rahhal R, Seto E. Emerging roles of histone modifications and HDACs in RNA splicing. *Nucleic Acids Res*. 2019;47(10):4911-4926. doi:10.1093/nar/gkz292

72. Crotty S. A brief history of T cell help to B cells. *Nat Rev Immunol*. 2015;15(3):185-189. doi:10.1038/nri3803

73. Bach FH, Bach ML, Sondel PM. Differential function of major histocompatibility complex antigens in T-lymphocyte activation. *Nature*. 1976;259(5541):273-281. doi:10.1038/259273a0

74. Cantor H, Boyse EA. Regulation of Cellular and Humoral Immune Responses by T-cell Subclasses. *Cold Spring Harb Symp Quant Biol*. 1977;41(0):23-32. doi:10.1101/SQB.1977.041.01.006

75. Lam WY, Bhattacharya D. Metabolic Links between Plasma Cell Survival, Secretion, and Stress. *Trends Immunol*. 2018;39(1):19-27. doi:10.1016/j.it.2017.08.007

76. Roche B, Arcangioli B, Martienssen R. Transcriptional reprogramming in cellular quiescence. *RNA Biol*. 2017;14(7):843-853. doi:10.1080/15476286.2017.1327510

77. Zetterberg A, Larsson O. Coordination between Cell Growth and Cell Cycle Transit in Animal Cells. *Cold Spring Harb Symp Quant Biol*. 1991;56(0):137-147. doi:10.1101/SQB.1991.056.01.018

78. Lea NC, Orr SJ, Stoeber K, et al. Commitment Point during $G_0 \rightarrow G_1$ That Controls Entry into the Cell Cycle. *Mol Cell Biol*. 2003;23(7):2351-2361. doi:10.1128/MCB.23.7.2351-2361.2003

79. Xia F, Qian CR, Xun Z, et al. TCR and CD28 Concomitant Stimulation Elicits a Distinctive Calcium Response in Naive T Cells. *Front Immunol*. 2018;9. doi:10.3389/fimmu.2018.02864

80. Dustin ML. The Immunological Synapse. *Cancer Immunol Res*. 2014;2(11):1023-1033. doi:10.1158/2326-6066.CIR-14-0161

81. Yokosuka T, Saito T. The Immunological Synapse, TCR Microclusters, and T Cell Activation. In: ; 2010:81-107. doi:10.1007/978-3-642-03858-7_5

82. Newton AC. Regulation of protein kinase C. *Curr Opin Cell Biol*. 1997;9(2):161-167. doi:10.1016/S0955-0674(97)80058-0

83. Krishna S, Xie D, Gorentla B, Shin J, Gao J, Zhong XP. Chronic Activation of the Kinase IKKβ Impairs T Cell Function and Survival. *The Journal of Immunology*. 2012;189(3):1209-1219. doi:10.4049/jimmunol.1102429

84. Capitani N, Baldari CT. The Immunological Synapse: An Emerging Target for Immune Evasion by Bacterial Pathogens. *Front Immunol*. 2022;13. doi:10.3389/fimmu.2022.943344

85. Sun Y, Dandekar RD, Mao YS, Yin HL, Wülfing C. Phosphatidylinositol (4,5) Bisphosphate Controls T Cell Activation by Regulating T Cell Rigidity and Organization. *PLoS One*. 2011;6(11):e27227. doi:10.1371/journal.pone.0027227

86. Hünig T, Tiefenthaler G, zum Büschenfelde KHM, Meuer SC. Alternative pathway activation of T cells by binding of CD2 to its cell-surface ligand. *Nature*. 1987;326(6110):298-301. doi:10.1038/326298a0

87. Zhong X, Guo R, Zhou H, Liu C, Wan C. Diacylglycerol kinases in immune cell function and self-tolerance. *Immunol Rev*. 2008;224(1):249-264. doi:10.1111/j.1600-065X.2008.00647.x

88. Szamel M, Resch K. T-Cell Antigen Receptor-Induced Signal-Transduction Pathways. Activation and Function of Protein Kinases C in T Lymphocytes. *Eur J Biochem*. 1995;228(1):1-15. doi:10.1111/j.1432-1033.1995.tb20221.x

89. Schulze-Luehrmann J, Ghosh S. Antigen-Receptor Signaling to Nuclear Factor κB. *Immunity*. 2006;25(5):701-715. doi:10.1016/j.immuni.2006.10.010

90. Esparza EM, Arch RH. TRAF4 functions as an intermediate of GITR-induced NF-?B activation. *Cellular and Molecular Life Sciences*. 2004;61(24):3087-3092. doi:10.1007/s00018-004-4417-0

91. Lu HY, Bauman BM, Arjunaraja S, et al. The CBM-opathies—A Rapidly Expanding Spectrum of Human Inborn Errors of Immunity Caused by Mutations in the CARD11-BCL10-MALT1 Complex. *Front Immunol*. 2018;9. doi:10.3389/fimmu.2018.02078

92. Veh J, Mangold C, Felsen A, et al. Phorbol-12-myristate-13-acetate is a potent enhancer of B cells with a granzyme B+ regulatory phenotype. *Front Immunol*. 2023;14. doi:10.3389/fimmu.2023.1194880

93. Schaub A, Glasmacher E. Splicing in immune cells—mechanistic insights and emerging topics. *Int Immunol*. 2017;29(4):173-181. doi:10.1093/intimm/dxx026

94. Butte MJ, Lee SJ, Jesneck J, Keir ME, Haining WN, Sharpe AH. CD28 Costimulation Regulates Genome-Wide Effects on Alternative Splicing. *PLoS One*. 2012;7(6):e40032. doi:10.1371/journal.pone.0040032

95. Prochazka L, Tesarik R, Turanek J. Regulation of alternative splicing of CD44 in cancer. *Cell Signal*. 2014;26(10):2234-2239. doi:10.1016/j.cellsig.2014.07.011

96. Hermiston ML, Xu Z, Weiss A. CD45: A Critical Regulator of Signaling Thresholds in Immune Cells. *Annu Rev Immunol*. 2003;21(1):107-137. doi:10.1146/annurev.immunol.21.120601.140946

97. Gu M, Kakoulidou M, Giscombe R, et al. Identification of CTLA-4 isoforms produced by alternative splicing and their association with myasthenia gravis. *Clinical Immunology*. 2008;128(3):374-381. doi:10.1016/j.clim.2008.05.006

98. Castro MAA, Oliveira MI, Nunes RJ, et al. Extracellular Isoforms of CD6 Generated by Alternative Splicing Regulate Targeting of CD6 to the Immunological Synapse. *The Journal of Immunology*. 2007;178(7):4351-4361. doi:10.4049/jimmunol.178.7.4351

99. Ogiya D, Chyra Z, Verselis SJ, et al. Identification of disease-related aberrantly spliced transcripts in myeloma and strategies to target these alterations by RNA-based therapeutics. *Blood Cancer J*. 2023;13(1):23. doi:10.1038/s41408-023-00791-0

100. Davidson D, Viallet J, Veillette A. Unique Catalytic Properties Dictate the Enhanced Function of $p59^{fynT}$, the Hemopoietic Cell-Specific Isoform of the Fyn Tyrosine Protein Kinase, in T cells. *Mol Cell Biol*. 1994;14(7):4554-4564. doi:10.1128/mcb.14.7.4554-4564.1994

101. Tanaka Y, Nagai Y, Okumura M, Greene MI, Kambayashi T. PRMT5 Is Required for T Cell Survival and Proliferation by Maintaining Cytokine Signaling. *Front Immunol*. 2020;11. doi:10.3389/fimmu.2020.00621

102. Luzina IG, Lockatell V, Todd NW, Keegan AD, Hasday JD, Atamas SP. Splice isoforms of human interleukin-4 are functionally active in mice in vivo. *Immunology*. 2011;132(3):385-393. doi:10.1111/j.1365-2567.2010.03393.x

103. Rincón M, Anguita J, Nakamura T, Fikrig E, Flavell RA. Interleukin (IL)-6 Directs the Differentiation of IL-4–producing CD4+ T Cells. *J Exp Med*. 1997;185(3):461-470. doi:10.1084/jem.185.3.461

104. Galarza-Muñoz G, Briggs FBS, Evsyukova I, et al. Human Epistatic Interaction Controls IL7R Splicing and Increases Multiple Sclerosis Risk. *Cell*. 2017;169(1):72-84.e13. doi:10.1016/j.cell.2017.03.007

105. Kaur G, Goodall JC, Jarvis LB, Hill Gaston JS. Characterisation of Foxp3 splice variants in human CD4+ and CD8+ T cells—Identification of Foxp3Δ7 in human regulatory T cells. *Mol Immunol*. 2010;48(1-3):321-332. doi:10.1016/j.molimm.2010.07.008

106. Amsen D, Antov A, Jankovic D, et al. Direct Regulation of Gata3 Expression Determines the T Helper Differentiation Potential of Notch. *Immunity*. 2007;27(1):89-99. doi:10.1016/j.immuni.2007.05.021

107. Mallory MJ, Jackson J, Weber B, Chi A, Heyd F, Lynch KW. Signal- and Development-Dependent Alternative Splicing of LEF1 in T Cells Is Controlled by CELF2. *Mol Cell Biol*. 2011;31(11):2184-2195. doi:10.1128/MCB.05170-11

108. Bahrami S, Drabløs F. Gene regulation in the immediate-early response process. *Adv Biol Regul*. 2016;62:37-49. doi:10.1016/j.jbior.2016.05.001

109. Li CY, Hofmann HA, Harris ML, Earley RL. Real or fake? Natural and artificial social stimuli elicit divergent behavioural and neural responses in mangrove rivulus, *Kryptolebias marmoratus*. *Proceedings of the Royal Society B: Biological Sciences*. 2018;285(1891):20181610. doi:10.1098/rspb.2018.1610

110. Morgan JI, Curran T. Stimulus-Transcription Coupling in the Nervous System: Involvement of the Inducible Proto-Oncogenes *fos* and *jun*. *Annu Rev Neurosci*. 1991;14(1):421-451. doi:10.1146/annurev.ne.14.030191.002225

111. Bisagno V, Cadet JL. Histone Deacetylases and Immediate Early Genes: Key Players in Psychostimulant-Induced Neuronal Plasticity. *Neurotox Res*. 2021;39(6):2134-2140. doi:10.1007/s12640-021-00420-3

112. Cochran BH, Zullo J, Verma IM, Stiles CD. Expression of the c- *fos* Gene and of an *fos* -Related Gene Is Stimulated by Platelet-Derived Growth Factor. *Science (1979)*. 1984;226(4678):1080-1082. doi:10.1126/science.6093261

113. Miao GG, Curran T. Cell transformation by c-fos requires an extended period of expression and is independent of the cell cycle. *Mol Cell Biol*. 1994;14(6):4295-4310. doi:10.1128/MCB.14.6.4295

114. Cruz-Mendoza F, Jauregui-Huerta F, Aguilar-Delgadillo A, García-Estrada J, Luquin S. Immediate Early Gene c-fos in the Brain: Focus on Glial Cells. *Brain Sci*. 2022;12(6):687. doi:10.3390/brainsci12060687

115. Roskoski R. ERK1/2 MAP kinases: Structure, function, and regulation. *Pharmacol Res*. 2012;66(2):105-143. doi:10.1016/j.phrs.2012.04.005

116. Lake D, Corrêa SAL, Müller J. Negative feedback regulation of the ERK1/2 MAPK pathway. *Cellular and Molecular Life Sciences*. 2016;73(23):4397-4413. doi:10.1007/s00018-016-2297-8

117. Greenberg ME, Ziff EB. Stimulation of 3T3 cells induces transcription of the c-fos proto-oncogene. *Nature*. 1984;311(5985):433-438. doi:10.1038/311433a0

118. Ginty DD, Kornhauser JM, Thompson MA, et al. Regulation of CREB Phosphorylation in the Suprachiasmatic Nucleus by Light and a Circadian Clock. *Science (1979)*. 1993;260(5105):238-241. doi:10.1126/science.8097062

119. Gallo FT, Katche C, Morici JF, Medina JH, Weisstaub N V. Immediate Early Genes, Memory and Psychiatric Disorders: Focus on c-Fos, Egr1 and Arc. *Front Behav Neurosci*. 2018;12. doi:10.3389/fnbeh.2018.00079

120. Blake D, Radens CM, Ferretti MB, Gazzara MR, Lynch KW. Alternative splicing of apoptosis genes promotes human T cell survival. *Elife*. 2022;11. doi:10.7554/eLife.80953

121. Ip JY, Tong A, Pan Q, Topp JD, Blencowe BJ, Lynch KW. Global analysis of alternative splicing during T-cell activation. *RNA*. 2007;13(4):563-572. doi:10.1261/rna.457207

122. Martinez NM, Lynch KW. Control of alternative splicing in immune responses: many regulators, many predictions, much still to learn. *Immunol Rev*. 2013;253(1):216-236. doi:10.1111/imr.12047

123. Rade M, Böhlen S, Neuhaus V, et al. A time-resolved meta-analysis of consensus gene expression profiles during human T-cell activation. *Genome Biol*. 2023;24(1):287. doi:10.1186/s13059-023-03120-7

124. Chapman NM, Boothby MR, Chi H. Metabolic coordination of T cell quiescence and activation. *Nat Rev Immunol*. 2020;20(1):55-70. doi:10.1038/s41577-019-0203-y

125. Sprent J, Surh CD. Normal T cell homeostasis: the conversion of naive cells into memory-phenotype cells. *Nat Immunol*. 2011;12(6):478-484. doi:10.1038/ni.2018

126. Tan H, Yang K, Li Y, et al. Integrative Proteomics and Phosphoproteomics Profiling Reveals Dynamic Signaling Networks and Bioenergetics Pathways Underlying T Cell Activation. *Immunity*. 2017;46(3):488-503. doi:10.1016/j.immuni.2017.02.010

127. Ran FA, Hsu PD, Wright J, Agarwala V, Scott DA, Zhang F. Genome engineering using the CRISPR-Cas9 system. *Nat Protoc*. 2013;8(11):2281-2308. doi:10.1038/nprot.2013.143

128. Zhang J, Zhang D, McQuade JS, Behbehani M, Tsien JZ, Xu M. c-fos regulates neuronal excitability and survival. *Nat Genet*. 2002;30(4):416-420. doi:10.1038/ng859

129. Bilbrough T, Piemontese E, Seitz O. Dissecting the role of protein phosphorylation: a chemical biology toolbox. *Chem Soc Rev*. 2022;51(13):5691-5730. doi:10.1039/D1CS00991E

130. Minatohara K, Akiyoshi M, Okuno H. Role of Immediate-Early Genes in Synaptic Plasticity and Neuronal Ensembles Underlying the Memory Trace. *Front Mol Neurosci*. 2015;8(JAN2016):78. doi:10.3389/FNMOL.2015.00078

131. Braunschweig U, Barbosa-Morais NL, Pan Q, et al. Widespread intron retention in mammals functionally tunes transcriptomes. *Genome Res*. 2014;24(11):1774-1786. doi:10.1101/gr.177790.114

132. Parenteau J, Durand M, Morin G, et al. Introns within Ribosomal Protein Genes Regulate the Production and Function of Yeast Ribosomes. *Cell*. 2011;147(2):320-331. doi:10.1016/j.cell.2011.08.044

133. Wong JJL, Schmitz U. Intron retention: importance, challenges, and opportunities. *Trends in Genetics*. 2022;38(8):789-792. doi:10.1016/j.tig.2022.03.017

134. Ni T, Yang W, Han M, et al. Global intron retention mediated gene regulation during CD4 $^{+}$ T cell activation. *Nucleic Acids Res*. 2016;44(14):6817-6829. doi:10.1093/nar/gkw591

135. Braunschweig U, Gueroussov S, Plocik AM, Graveley BR, Blencowe BJ. Dynamic Integration of Splicing within Gene Regulatory Pathways. *Cell*. 2013;152(6):1252-1269. doi:10.1016/j.cell.2013.02.034

136. Mauger O, Lemoine F, Scheiffele P. Targeted Intron Retention and Excision for Rapid Gene Regulation in Response to Neuronal Activity. *Neuron*. 2016;92(6):1266-1278. doi:10.1016/j.neuron.2016.11.032

137. Moritz B, Wahle E. Simple methods for the 3' biotinylation of RNA. *RNA*. 2014;20(3):421-427. doi:10.1261/rna.042986.113

138. Fu XD. Exploiting the Hidden Treasure of Detained Introns. *Cancer Cell*. 2017;32(4):393-395. doi:10.1016/j.ccell.2017.09.005

139. Ruskin B, Greene JM, Green MR. Cryptic branch point activation allows accurate in vitro splicing of human β-globin intron mutants. *Cell*. 1985;41(3):833-844. doi:10.1016/S0092-8674(85)80064-7

140. Hubé F, Francastel C. Mammalian Introns: When the Junk Generates Molecular Diversity. *Int J Mol Sci*. 2015;16(3):4429-4452. doi:10.3390/ijms16034429

141. Jo BS, Choi SS. Introns: The Functional Benefits of Introns in Genomes. *Genomics Inform*. 2015;13(4):112. doi:10.5808/GI.2015.13.4.112

142. Keiper S, Papasaikas P, Will CL, Valcárcel J, Girard C, Lührmann R. Smu1 and RED are required for activation of spliceosomal B complexes assembled on short introns. *Nat Commun*. 2019;10(1):3639. doi:10.1038/s41467-019-11293-8

143. Pollutri D, Penzo M. Ribosomal Protein L10: From Function to Dysfunction. *Cells*. 2020;9(11):2503. doi:10.3390/cells9112503

144. Bussiere C, Hashem Y, Arora S, Frank J, Johnson AW. Integrity of the P-site is probed during maturation of the 60S ribosomal subunit. *Journal of Cell Biology*. 2012;197(6):747-759. doi:10.1083/jcb.201112131

145. Xiao J, Chen X, Liu W, et al. TRAF4 is crucial for ST2+ memory Th2 cell expansion in IL-33–driven airway inflammation. *JCI Insight*. 2023;8(18). doi:10.1172/jci.insight.169736

146. Abell AN, Johnson GL. MEKK4 Is an Effector of the Embryonic TRAF4 for JNK Activation. *Journal of Biological Chemistry*. 2005;280(43):35793-35796. doi:10.1074/jbc.C500260200

147. Kulak NA, Pichler G, Paron I, Nagaraj N, Mann M. Minimal, encapsulated proteomic-sample processing applied to copy-number estimation in eukaryotic cells. *Nat Methods*. 2014;11(3):319-324. doi:10.1038/nmeth.2834

148. Saini P, Eyler DE, Green R, Dever TE. Hypusine-containing protein eIF5A promotes translation elongation. *Nature*. 2009;459(7243):118-121. doi:10.1038/nature08034

149. Rossi D, Galvão FC, Bellato HM, et al. eIF5A has a function in the cotranslational translocation of proteins into the ER. *Amino Acids*. 2014;46(3):645-653. doi:10.1007/s00726-013-1618-6

150. Schrader R, Young C, Kozian D, Hoffmann R, Lottspeich F. Temperature-sensitive eIF5A Mutant Accumulates Transcripts Targeted to the Nonsense-mediated Decay Pathway. *Journal of Biological Chemistry*. 2006;281(46):35336-35346. doi:10.1074/jbc.M601460200

151. Tong Y, Park I, Hong B, Nedyalkova L, Tempel W, Park H. Crystal structure of human eIF5A1: Insight into functional similarity of human eIF5A1 and eIF5A2. *Proteins: Structure, Function, and Bioinformatics*. 2009;75(4):1040-1045. doi:10.1002/prot.22378

152. Tong Y, Park I, Hong B, Nedyalkova L, Tempel W, Park H. Crystal structure of human eIF5A1: Insight into functional similarity of human eIF5A1 and eIF5A2. *Proteins: Structure, Function, and Bioinformatics*. 2009;75(4):1040-1045. doi:10.1002/prot.22378

153. Kretova M, Selicky T, Cipakova I, Cipak L. Regulation of Pre-mRNA Splicing: Indispensable Role of Post-Translational Modifications of Splicing Factors. *Life*. 2023;13(3):604. doi:10.3390/life13030604

154. Manceau V, Swenson M, Le Caer J, Sobel A, Kielkopf CL, Maucuer A. Major phosphorylation of SF1 on adjacent Ser-Pro motifs enhances interaction with U2AF ^{65}. *FEBS J*. 2006;273(3):577-587. doi:10.1111/j.1742-4658.2005.05091.x

155. Misteli T, Cáceres JF, Clement JQ, Krainer AR, Wilkinson MF, Spector DL. Serine Phosphorylation of SR Proteins Is Required for Their Recruitment to Sites of Transcription In Vivo. *J Cell Biol*. 1998;143(2):297-307. doi:10.1083/jcb.143.2.297

156. Lai MC, Lin RI, Tarn WY. Transportin-SR2 mediates nuclear import of phosphorylated SR proteins. *Proceedings of the National Academy of Sciences*. 2001;98(18):10154-10159. doi:10.1073/pnas.181354098

157. Liu G, Razanau A, Hai Y, et al. A Conserved Serine of Heterogeneous Nuclear Ribonucleoprotein L (hnRNP L) Mediates Depolarization-regulated Alternative Splicing of Potassium Channels. *Journal of Biological Chemistry*. 2012;287(27):22709-22716. doi:10.1074/jbc.M112.357343

158. Nishi H, Shaytan A, Panchenko AR. Physicochemical mechanisms of protein regulation by phosphorylation. *Front Genet*. 2014;5(AUG). doi:10.3389/FGENE.2014.00270

159. Zhang T, Keele GR, Gyuricza IG, et al. Multi-omics analysis identifies drivers of protein phosphorylation. *Genome Biol*. 2023;24(1). doi:10.1186/S13059-023-02892-2

160. Moon H, Jang HN, Liu Y, et al. RRM but not the Asp/Glu domain of hnRNP C_1/C_2 is required for splicing regulation of Ron exon 11 pre-mRNA. *BMB Rep*. 2019;52(11):641-646. doi:10.5483/BMBRep.2019.52.11.080

161. Martino F, Varadarajan NM, Perestrelo AR, et al. The mechanical regulation of RNA binding protein hnRNPC in the failing heart. *Sci Transl Med*. 2022;14(672). doi:10.1126/scitranslmed.abo5715

162. Kielkopf CL, Rodionova NA, Green MR, Burley SK. A Novel Peptide Recognition Mode Revealed by the X-Ray Structure of a Core U2AF35/U2AF65 Heterodimer. *Cell*. 2001;106(5):595-605. doi:10.1016/S0092-8674(01)00480-9

163. Hong S, Freeberg MA, Han T, et al. LARP1 functions as a molecular switch for mTORC1-mediated translation of an essential class of mRNAs. *Elife*. 2017;6. doi:10.7554/eLife.25237

164. Tisserant A, König H. Signal-Regulated Pre-mRNA Occupancy by the General Splicing Factor U2AF. *PLoS One*. 2008;3(1):e1418. doi:10.1371/journal.pone.0001418

165. Habelhah H, Shah K, Huang L, et al. ERK phosphorylation drives cytoplasmic accumulation of hnRNP-K and inhibition of mRNA translation. *Nat Cell Biol*. 2001;3(3):325-330. doi:10.1038/35060131

166. Su TT, Guo B, Kawakami Y, et al. PKC-β controls IκB kinase lipid raft recruitment and activation in response to BCR signaling. *Nat Immunol*. 2002;3(8):780-786. doi:10.1038/ni823

167. Madaro L, Marrocco V, Fiore P, et al. PKCθ signaling is required for myoblast fusion by regulating the expression of caveolin-3 and β1D integrin upstream focal adhesion kinase. *Mol Biol Cell*. 2011;22(8):1409-1419. doi:10.1091/mbc.e10-10-0821

168. Gould CM, Antal CE, Reyes G, et al. Active Site Inhibitors Protect Protein Kinase C from Dephosphorylation and Stabilize Its Mature Form. *Journal of Biological Chemistry*. 2011;286(33):28922-28930. doi:10.1074/jbc.M111.272526

169. Hwang JR, Byeon Y, Kim D, Park SG. Recent insights of T cell receptor-mediated signaling pathways for T cell activation and development. *Exp Mol Med*. 2020;52(5):750-761. doi:10.1038/s12276-020-0435-8

170. Jankowska KI, Williamson EK, Roy NH, et al. Integrins Modulate T Cell Receptor Signaling by Constraining Actin Flow at the Immunological Synapse. *Front Immunol*. 2018;9. doi:10.3389/fimmu.2018.00025

171. Hope JL, Stairiker CJ, Bae EA, Otero DC, Bradley LM. Striking a Balance—Cellular and Molecular Drivers of Memory T Cell Development and Responses to Chronic Stimulation. *Front Immunol*. 2019;10. doi:10.3389/fimmu.2019.01595

172. Sánchez-Escabias E, Guerrero-Martínez JA, Reyes JC. Co-transcriptional splicing efficiency is a gene-specific feature that can be regulated by TGFβ. *Commun Biol*. 2022;5(1). doi:10.1038/S42003-022-03224-Z

173. Ip JY, Tong A, Pan Q, Topp JD, Blencowe BJ, Lynch KW. Global analysis of alternative splicing during T-cell activation. *RNA*. 2007;13(4):563-572. doi:10.1261/rna.457207

174. Martinez NM, Lynch KW. Control of alternative splicing in immune responses: many regulators, many predictions, much still to learn. *Immunol Rev*. 2013;253(1):216-236. doi:10.1111/imr.12047

175. Rade M, Böhlen S, Neuhaus V, et al. A time-resolved meta-analysis of consensus gene expression profiles during human T-cell activation. *Genome Biol*. 2023;24(1). doi:10.1186/S13059-023-03120-7

176. Tan H, Yang K, Li Y, et al. Integrative Proteomics and Phosphoproteomics Profiling Reveals Dynamic Signaling Networks and Bioenergetics Pathways Underlying T Cell Activation. *Immunity*. 2017;46(3):488-503. doi:10.1016/J.IMMUNI.2017.02.010

7.3. Figures

7.4. Tables